

**Appendix B1**  
**Water Supply Sub-Team Members**

---



# Appendix B1—Water Supply Sub-Team Members

The information presented in the Water Supply Assessment Technical Report is the outcome of a collaborative process involving representatives of numerous organizations.

A list of Water Supply Sub-Team members and their affiliations is presented below.

- Carly Jerla, Bureau of Reclamation
- Armin Munévar, CH2M HILL
- Jerry Zimmerman, Colorado River Board of California
- John Whipple, New Mexico Interstate Stream Commission
- Robert Kirk, Navajo Nation
- John Gerstle, Trout Unlimited
- Chuck Cullom, Central Arizona Project
- Robert King, Utah Division of Natural Resources
- Mike Roberts, The Nature Conservancy
- Steve Cullinan, U.S. Fish and Wildlife Service
- Tapash Das, CH2M HILL

Additional support in the form of supplemental analysis, review, and information was provided by those listed below.

- Jim Prairie, Bureau of Reclamation
- Ken Nowak, Bureau of Reclamation
- Subhrendu Gangopadhyay, Bureau of Reclamation's Technical Service Center
- Levi Brekke, Bureau of Reclamation's Technical Service Center
- Tom Pruitt, Bureau of Reclamation's Technical Service Center
- Joe Barsugli, University of Colorado and the National Oceanic and Atmospheric Administration
- Ben Harding, AMEC Earth & Environmental



**Appendix B2**  
**Supplemental Water Supply Data and Methods**

---



# Appendix B2—Supplemental Water Supply Data and Methods

This appendix provides supplemental information related to the water supply data and methods discussed in the Technical Report. As discussed in the Technical Report, the assessment of historical and future supply conditions focused on four main groups of water supply indicators: climate, hydrologic processes, climate teleconnections, and streamflow. Although the primary indicator of water supply in the Colorado River Basin (Basin) is streamflow, a fundamental understanding of the processes that influence the quantity, location, and timing of streamflow is beneficial. Additional detail on the methods used to assess these indicators for water supply is supplied in this appendix.

Table B2-1 summarizes the water supply indicators evaluated as part of the water supply assessment. In addition, the table provides the relevance of the particular parameter for this study, temporal and spatial scales considered, and analysis methods. Table B2-2 summarizes the data sources considered in the evaluation of each of the water supply indicators. The subsequent sections provide further detail on the data and methods under each of the four water supply indicator groups.

**TABLE B2-1**  
Summary of the Water Supply Indicators for the Water Supply Assessment

<b>Water Supply Indicator</b>	<b>Relevance</b>	<b>Temporal Scale</b>	<b>Spatial Scale</b>	<b>Method of Analysis</b>	<b>Method of Display</b>
<b>CLIMATE</b>					
Temperature	Identification of trends in climate patterns	Monthly, Seasonal, Annual, Decadal	Grid cell, Select Watersheds, and Basin-wide	Statistical analysis of trends and variability	Spatial analysis and visualization
Precipitation	Identification of trends in climate patterns	Monthly, Seasonal, Annual, Decadal	Grid cell, Select Watersheds, and Basin-wide	Statistical analysis of trends and variability	Spatial analysis and visualization
<b>HYDROLOGIC PROCESSES</b>					
Runoff	Identification of changes in runoff processes; identification of "productive" watersheds	Monthly, Seasonal, Annual, Decadal	Grid cell, Select Watersheds, and Basin-wide	Calculated as unit runoff; statistics to be generated	Spatial analysis and visualization
Evapotranspiration (ET)	Identification of changes in natural losses; identification of "water stressed" watersheds	Monthly, Seasonal, Annual, Decadal	Grid cell, Select Watersheds, and Basin-wide	Calculated as unit actual ET; statistics to be generated	Spatial analysis and visualization
Snowpack Accumulation and Snowmelt	Identification of spatial changes in snowpack development and timing of melt	Monthly, Seasonal, Annual, Decadal	Grid cell, Select Watersheds, and Basin-wide	Calculated as unit snow water equivalent (SWE); peak and timing	Spatial analysis and visualization
Soil Moisture	Identification of causes of drought and severe drying conditions; identification of watersheds most impacted	Monthly, Seasonal, Annual, Decadal	Grid cell, Select Watersheds, and Basin-wide	Calculated as percentage of maximum	Spatial analysis and visualization
<b>CLIMATE TELECONNECTIONS</b>					
El Niño – Southern Oscillation (ENSO)	Identify changes in teleconnections and influence on regional climate; identify relationship between long-term and shorter-term climate indices	Season, Annual, Decadal	Global/ Regional	Statistical analysis of correlation between indicator and streamflow	Correlation plots and statistics
Pacific Decadal Oscillation (PDO)	Identify changes in teleconnections and influence on regional climate; identify relationship between long-term and shorter-term climate indices	Annual, Decadal	Global/ Regional	Statistical analysis of correlation between indicator and streamflow	Correlation plots and statistics
Atlantic Multi-decadal Oscillation	Identify changes in teleconnections and influence on regional	Annual, Decadal	Global/ Regional	Qualitative discussion	Qualitative discussion

TABLE B2-1  
Summary of the Water Supply Indicators for the Water Supply Assessment

<b>Water Supply Indicator</b>	<b>Relevance</b>	<b>Temporal Scale</b>	<b>Spatial Scale</b>	<b>Method of Analysis</b>	<b>Method of Display</b>
(AMO)	climate; identify relationship between long-term and shorter-term climate indices				
<b>STREAMFLOW</b>					
Intervening and Total Natural Flows at 29 Basin Locations	Identification of changes in streamflow trends and variability	Monthly, Annual, 1-, 3-, 5-, 10-year, and multi-decadal	Accumulated Flow at Point	Statistical analysis of trends and variability; drought and surplus statistics	Table and box-whisker of statistics, Basin-scale maps

TABLE B2-2  
Sources of Data Used for the Water Supply Assessment

Parameter	Description	Data Source
<b>CLIMATE INDICATORS</b>		
Historical Temperature and Precipitation	Historical gridded temperature and precipitation at 1/8 <sup>th</sup> -degree resolution for the period of 1950 to 1999. Extension through 2005 is not documented.	Maurer et al., 2002 ( <a href="http://www.engr.scu.edu/~emaurer/data.shtml">http://www.engr.scu.edu/~emaurer/data.shtml</a> )
Future Temperature and Precipitation Projections	112 future monthly temperature and precipitation projections based on Intergovernmental Panel on Climate Change Fourth Assessment Report emission scenarios and subsequently bias corrected and statistically downscaled to 1/8 <sup>th</sup> -degree resolution for the period of 1950 to 2099.	Maurer et al., 2007 ( <a href="http://gdo-dcp.ucllnl.org/downscaled_cmip3_projections/">http://gdo-dcp.ucllnl.org/downscaled_cmip3_projections/</a> )
<b>HYDROLOGIC PROCESS INDICATORS</b>		
ET, Runoff, SWE, Soil Moisture	Variable Infiltration Capacity (VIC)-simulated hydrologic fluxes and grid cell storage terms driven by observed climatology (1950–2005) and 112 future climate projections (1950–2099)	Reclamation, 2011
Snowpack	Point snow water equivalent from late 1970s to present from the snow-telemetry (SNOTEL) network	National Resources Conservation Service, 2010 ( <a href="http://www.wcc.nrcs.usda.gov/snow/">http://www.wcc.nrcs.usda.gov/snow/</a> )
<b>TELECONNECTION INDICATORS</b>		
ENSO	Monthly Southern Oscillation index for January 1866 through March 2010	University of East Anglia Climatic Research Unit, 2010 ( <a href="http://www.cru.uea.ac.uk/cru/data/soi/">http://www.cru.uea.ac.uk/cru/data/soi/</a> )
PDO	Monthly PDO indices for January 1900 through January 2010	Joint Institute for the Study of the Atmosphere and Ocean, 2010 ( <a href="http://jisao.washington.edu/pdo/">http://jisao.washington.edu/pdo/</a> )
<b>STREAMFLOW INDICATORS</b>		
Observed Streamflow used in the Observed Resampled Scenario	Natural streamflow for the period of 1906–2007 for the 29 streamflow locations commonly used for U.S. Bureau of Reclamation (Reclamation) planning.	Prairie and Callejo, 2005; Reclamation, 2010
Paleo Reconstructed Streamflow used in the Paleo Resampled Scenario	Reconstructed natural streamflows for the period 762–2005 at 29 locations derived from ecologically contrasting tree-ring sites in the southern Colorado Plateau during the past 2 millennia.	Reclamation, 2010; Meko et al., 2007
Paleo Conditioned Streamflow used in the Paleo Conditioned Scenario	Blended paleo streamflow states with observed streamflow magnitudes at 29 locations.	Prairie et al., 2008
Future Streamflow Projections used in the Downscaled General Circulation Model (GCM) Projected Scenario	VIC-simulated runoff and routed streamflow at 29 locations driven by 112 future climate projections for the period 1950–2099.	Reclamation, 2011

## 1.0 Climate

### 1.1 Historical Climate

Gridded observed climate data for the period from 1950 to 1999, as developed by Maurer et al. (2002), were downloaded via the Internet from Santa Clara University (<http://www.engr.scu.edu/~emaurer/data.shtml>). The data are stored in network common data format (netCDF) at 1/8<sup>th</sup>-degree resolution and contain daily temperature (min and max), precipitation, and wind speed values for the contiguous United States. Subsequent to the Maurer et al. (2002) data, the gridded dataset was extended to 2005 using identical methods. The temperature and precipitation data were processed into monthly average temperature and monthly total precipitation to facilitate comparisons. The monthly, seasonal, and annual statistics were computed for each parameter and for each grid cell for the period 1971–2000 to facilitate comparisons to projected future conditions. This 1971–2000 historical base period was selected as the most current 30-year climatological period at the time of the Colorado River Basin Water Supply and Demand Study (Study), as described by the National Oceanic and Atmospheric Administration (NOAA, 2010) and is used as the basis for comparing to future climate projections<sup>1</sup>.

### 1.2 Projections of Future Climate

Future climate change projections are made primarily on the basis of General Circulation Model (GCM) simulations under a range of future emission scenarios. A total of 112 future climate projections used in the Intergovernmental Panel on Climate Change (IPCC) Fourth Assessment Report (AR4), subsequently bias corrected and spatially downscaled (BCSD), were obtained from the Lawrence Livermore National Laboratory under the World Climate Research Program's (WCRP's) Coupled Model Intercomparison Project Phase 3 (CMIP3). This archive contains climate projections generated from 16 different GCMs developed by national climate centers and for *Special Report on Emissions Scenarios* (SRES) Emission Scenarios A2, A1B, and B1. These projections have been bias corrected and spatially downscaled to 1/8<sup>th</sup>-degree (~12-kilometer) resolution over the contiguous United States through methods described in detail in Wood et al. (2002), Wood et al. (2004), and Maurer (2007).

#### 1.2.1 Emission Scenarios

In 2000, IPCC published the SRES scenarios that described a family of six emission scenarios to condition GCMs (IPCC, 2000). The emissions scenarios are defined by alternative future development pathways, covering a wide range of demographic, economic, and technological driving forces and resulting GHG emissions. The GHG emissions associated with each scenario are shown in figure B2-1.

---

<sup>1</sup> A new 30-year historical base period (1981–2010) was issued by NOAA on July 1, 2011.

**FIGURE B2-1**

Scenarios for GHG Emissions from 2000 to 2100 in the Absence of Additional Climate Policies  
 Units on the y-axis are billion tons of total annual emissions in equivalent carbon dioxide units.

Source: IPCC 2007

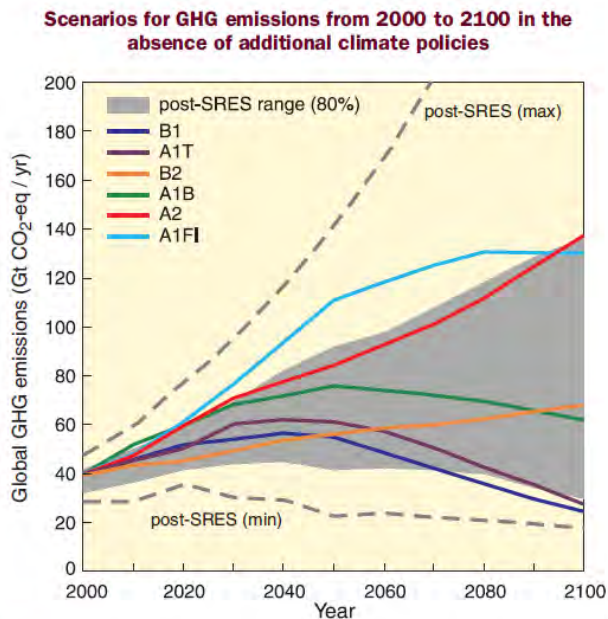


**Figure 3.1.** Global GHG emissions (in GtCO<sub>2</sub>-eq per year) in the absence of additional climate policies: six illustrative SRES marker scenarios (coloured lines) and 80<sup>th</sup> percentile range of recent scenarios published since SRES (post-SRES) (gray shaded area). Dashed lines show the full range of post-SRES scenarios. The emissions include CO<sub>2</sub>, CH<sub>4</sub>, N<sub>2</sub>O and F-gases. [WGIII 1.3, 3.2, Figure SPM.4]

Of the six emission scenarios included in the IPCC AR4, three were selected to drive the CMIP3 multi-model dataset—A2 (high), A1B (medium), and B1 (low). The A2 scenario is representative of high population growth, slow economic development, and slow technological change. It is characterized by a continuously increasing rate of GHG emissions and features the highest annual emissions rates of any scenario by the end of the 21st Century. The A1B scenario features a global population that peaks mid-century and rapid introduction of new and more-efficient technologies balanced across both fossil- and non-fossil-intensive energy sources. As a result, GHG emissions in the A1B scenario peak around mid-century. Lastly, the B1 scenario describes a world with rapid changes in economic structures toward a service and information economy. GHG emission rates in this scenario peak prior to mid-century and are generally the lowest of the scenarios. The best estimates of global temperature change during the 21st Century for each of the A2, A1B, and B1 scenarios are 3.4 °C, 2.8 °C, and 1.8 °C, respectively<sup>2</sup> (IPCC, 2007).

<sup>2</sup> Temperature change reflects the difference between the global average in the 2090–2099 period relative to the global average in the 1980–1999 period.

FIGURE B2-2

Projections of Surface Temperatures for the Selected GHG Emissions Scenarios from 2000 to 2100

Source: IPCC 2007

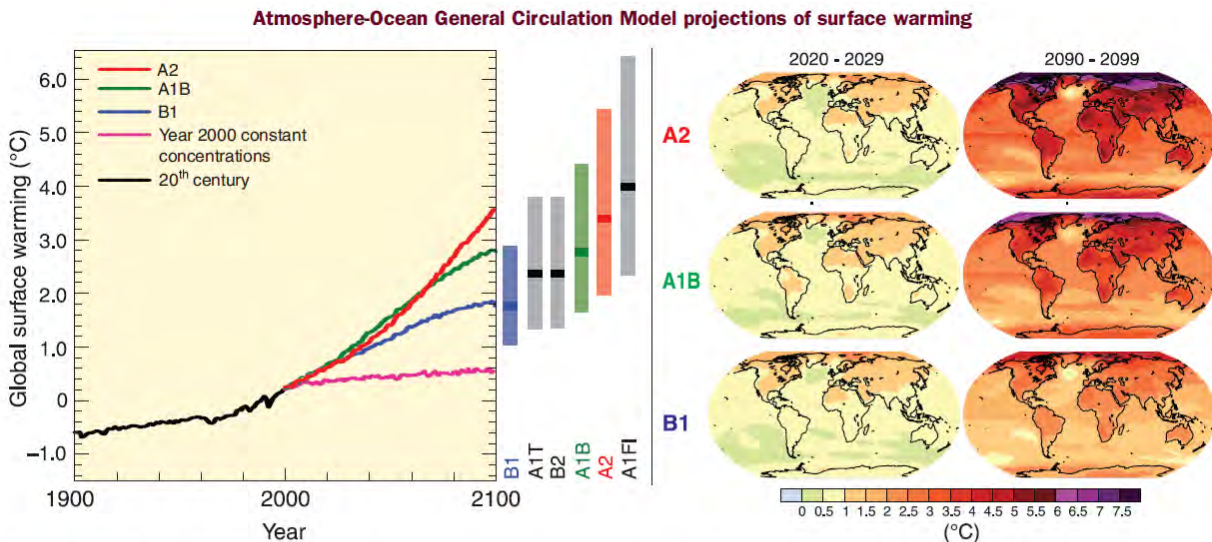


**Figure 3.2.** Left panel: Solid lines are multi-model global averages of surface warming (relative to 1980-1999) for the SRES scenarios A2, A1B and B1, shown as continuations of the 20<sup>th</sup> century simulations. The orange line is for the experiment where concentrations were held constant at year 2000 values. The bars in the middle of the figure indicate the best estimate (solid line within each bar) and the likely range assessed for the six SRES marker scenarios at 2090-2099 relative to 1980-1999. The assessment of the best estimate and likely ranges in the bars includes the Atmosphere-Ocean General Circulation Models (AOGCMs) in the left part of the figure, as well as results from a hierarchy of independent models and observational constraints. Right panels: Projected surface temperature changes for the early and late 21<sup>st</sup> century relative to the period 1980-1999. The panels show the multi-AOGCM average projections for the A2 (top), A1B (middle) and B1 (bottom) SRES scenarios averaged over decades 2020-2029 (left) and 2090-2099 (right). [WGI 10.4, 10.8, Figures 10.28, 10.29, SPM]

## 1.2.2 General Circulation Models

The CMIP3 multi-model dataset consists of 112 unique climate projections. Sixteen GCMs were coupled with the three emissions scenarios described previously to generate these projections. Many of the GCMs were simulated multiple times for the same emission scenario due to differences in starting climate system state or initial conditions, so the number of available projections is greater than simply the product of GCMs and emission scenarios. Table B2-3 summarizes the GCMs, initial conditions (specified by the run numbers in the A2, A1B, and B1 columns), and emissions scenario combinations (A2, A1B, and B1) featured in the CMIP3 dataset. Initial conditions (initial atmosphere and ocean conditions used in a GCM simulation) for the 21<sup>st</sup> Century are defined by the 20<sup>th</sup> Century “control” simulation. A description of the 20<sup>th</sup> Century “control” simulations corresponding to each GCM simulation in table B2-3 can be found at [http://www-pcmdi.llnl.gov/ipcc/standard\\_output.html#Experiments](http://www-pcmdi.llnl.gov/ipcc/standard_output.html#Experiments).

**TABLE B2-3**  
 WCRP CMIP3 Multi-Model Dataset GCMs, Initial Conditions, and Emissions Scenarios  
 Source: Maurer et al., 2007.

<b>Modeling Group, Country</b>	<b>WCRP CMIP3 I.D.</b>	<b>A2</b>	<b>A1B</b>	<b>B1</b>	<b>Primary Reference</b>
Bjerknes Center for Climate Research, Norway	BCCR-BCM2.0	1	1	1	Furevik et al., 2003
Canadian Center for Climate Modeling & Analysis, Canada	CGCM3.1 (T47)	1...5	1...5	1...5	Flato and Boer, 2001
Meteo-France/Center National de Recherches Meteorologiques, France	CNRM-CM3	1	1	1	Salas-Melia et al., 2005
CSIRO Atmospheric Research, Australia	CSIRO-Mk3.0	1	1	1	Gordon et al., 2002
U.S. Dept. of Commerce/NOAA/Geophysical Fluid Dynamics Laboratory, United States	GFDL-CM2.0	1	1	1	Delworth et al., 2006
U.S. Dept. of Commerce/NOAA/Geophysical Fluid Dynamics Laboratory, United States	GFDL-CM2.1	1	1	1	Delworth et al., 2006
National Aeronautics and Space Administration /Goddard Institute for Space Studies, United States	GISS-ER	1	2, 4	1	Russell et al., 2000
Institute for Numerical Mathematics, Russia	INM-CM3.0	1	1	1	Diansky and Volodin, 2002
Institut Pierre Simon Laplace, France	IPSL-CM4	1	1	1	IPSL, 2005
Center for Climate System Research (The University of Tokyo), National Institute for Environmental Studies, and Frontier Research Center for Global Change, Japan	MIROC3.2 (medres)	1...3	1...3	1...3	K-1 model developers, 2004
Meteorological Institute of the University of Bonn, Germany and Institute of Korea Meteorological Administration, Korea	ECHO-G	1...3	1...3	1...3	Legutke and Voss, 1999
Max Planck Institute for Meteorology, Germany	ECHAM5/ MPI-OM	1...3	1...3	1...3	Jungclaus et al., 2006
Meteorological Research Institute, Japan	MRI-CGCM2.3.2	1...5	1...5	1...5	Yukimoto et al., 2001
National Center for Atmospheric Research, United States	CCSM3	1...4	1...3, 5...7	1...7	Collins et al., 2006
National Center for Atmospheric Research, United States	PCM	1...4	1...4	2...3	Washington et al., 2000
Hadley Center for Climate Prediction and Research/Met Office, United Kingdom	UKMO-HadCM3	1	1	1	Gordon et al., 2000
<b>Total Number of Climate Projections</b>		<b>36</b>	<b>39</b>	<b>37</b>	

### **1.2.3 Bias Correction and Spatial Downscaling**

The CMIP3 climate projections have undergone BCSD to 1/8<sup>th</sup>-degree (~12-kilometer) resolution through methods described in detail in Wood et al. (2002), Wood et al. (2004), and Maurer (2007). The purpose of this bias correction is to adjust a given climate projection for inconsistencies between the simulated historical climate data and observed historical climate data, which are the result of GCM bias. In the BCSD approach, projections are bias corrected using a quantile mapping technique at 2-degree (~200-kilometer) spatial resolution. Following bias correction, the adjusted climate projection data are statistically consistent on a monthly basis with the observed climate data for the historical overlap period, which is 1950–1999 in the Study. Beyond the historical overlap period (2000–2099), the adjusted climate projection data reflect the same relative changes in mean, variance, and other statistics between the projected (2000–2099) and historical periods (1950–1999) as was present in the unadjusted dataset, but the adjusted climate projection data are mapped onto the observed dataset variance. Note that this methodology assumes that the GCM biases have the same structure during the 20th and 21st Century simulations.

Downscaling spatially translates bias corrected climate data from the coarse, 2-degree (~200-kilometer), spatial resolution typical of climate models to a basin-relevant resolution of 1/8<sup>th</sup>-degree (12 kilometers), which is more useful for hydrology and other applications. The spatial downscaling process generally preserves observed spatial relationships between large- and fine-scale climates. This approach assumes that the topographic and climatic features that determine the fine-scale distribution of the large-scale climate will be the same in the future as in the historical period.

### **1.2.4 Weather Generation (Temporal Disaggregation)**

The resulting BCSD climate projections provide a representation of future monthly temperature and precipitation through 2099. However, to be useful for hydrologic modeling, this information is required on a daily temporal scale. The monthly downscaled data was temporally disaggregated to a daily temporal scale to create realistic weather patterns using the sampling methods described in Wood et al. (2002) with extensions of this approach as applied by Salathé (2005) and Mote and Salathé (2010). To generate daily values, for each month in the simulation a month is randomly selected from the historic record for the same month (e.g., for the month of January, a January is selected from the 1950–1999 period). The daily precipitation and temperature from the historic record are then adjusted (rescaled precipitation and shifted temperature) such that the monthly average matches the simulated monthly value. The same historic month is used throughout the domain to preserve plausible spatial structure to daily storms (Mote and Salathé 2010). The results of the temporal disaggregation are daily weather sequences that preserve the monthly values from the downscaled climate projections. Some uncertainties can be introduced depending on the method employed to produce the daily data from the monthly climate values. A comparative analysis of two available methods to generate daily weather patterns for this Study favored the use of the method employed by Salathé (2005) and incorporated in the SECURE Report (Reclamation, 2011) to produce the daily downscaled data. Additional detail of the comparative analysis of two daily weather generation (temporal disaggregation) methods is presented in appendix B3 Section3, Comparison of Daily Weather Generation (Temporal Disaggregation) Methods.

## 2.0 Hydrologic Processes

The primary sources for hydrologic process data are derived from the VIC-simulated conditions driven by either observed historical climatology (1950–2005) or projected climate (1950–2099). VIC simulates all major moisture fluxes at the grid cell using physically based methods. These moisture fluxes are not generally measured at the spatial resolution necessary for Basin assessments; thus the VIC-derived patterns are considered the most suitable source. For example, while station-specific SWE, precipitation, and temperature are available from the National Resources Conservation Service SNOTEL network at 800 stations in 11 western states and Alaska (<http://www.wcc.nrcs.usda.gov/snow/>), the spatial representativeness of the SNOTEL data is uncertain (Daly et al., 2000). In preliminary results, Molotch et al. (2001) showed that SWE can begin to vary significantly beyond 500 meters from a SNOTEL site, due to terrain impacts on snow ablation, as well as small-scale depositional variations. A variety of methods have been used to distribute point measurements to spatial grids. The methods used are complex and beyond the scope of the Study; therefore, site-specific SNOTEL data were not processed to independently validate the SWE fields derived from the VIC model for this study. However, Mote et al. (2008) found correlation of better than 0.75 between VIC-simulated SWE and measured SWE for the Rockies. Other parameters such as ET and soil moisture are not routinely measured, nor at scales which permit validation with the VIC-simulated fields. Thus, the use of VIC-simulated historical fluxes enables a consistent comparison of change when considering simulated fluxes under future climate.

Both the climate and hydrologic data from VIC simulations are stored in formatted text files known as “flux files.” One flux file is produced for every grid cell of the model domain, and each file contains values for the specified parameters at every time step of the simulation. Gridded climate and hydrologic parameter data generated by the VIC model for the historical and projected periods were converted from daily to monthly values and stored in a specialized format (netCDF). This data conversion allows for statistical and spatial analysis of the data and enables a better understanding of the primary factors, both climatological and hydrological, that drive projected changes in streamflows relative to historical conditions. In addition to the primary VIC outputs of air temperature, precipitation, ET, runoff, and baseflow, total runoff (sum of baseflow and runoff) and runoff efficiency were computed at each grid cell and added to the netCDF files. Runoff efficiency is defined as the fraction of total runoff to the total precipitation. The complete list of hydroclimatic variables compiled are included in table B2-4.

One netCDF file was produced for each climate projection and for the historical observed, for a total of 113 netCDF files. As with the climate data, monthly, seasonal, and annual statistics were derived for the hydrologic process information for the historical period 1971–2000 and three future 30-year climatological periods: 2011–2040, 2041–2070, and 2066–2095. The historical period 1971–2000 is selected as the reference climate because it was the most current 30-year climatological period as described by NOAA (2010) at the time this Study was initiated. Representative statistics were generated on monthly, seasonal, and annual bases. In this analysis, the seasons are defined as follows: Fall: October, November, and December; Winter: January, February, and March; Spring: April, May, and June; and Summer: July, August, and September.

TABLE B2-4  
Climate and Hydrologic Parameters

VIC Parameter	Units
Average air temperature	degrees Celsius (°C)
Precipitation	millimeters (mm)
ET	Mm
Runoff (surface)	Mm
Baseflow (subsurface)	Mm
Total runoff	Mm
Soil moisture (in each of three soil layers)	Mm
Soil moisture fraction	percent
SWE	Mm
Runoff efficiency (total runoff/total precipitation)	fraction

The statistical analysis was conducted on both grid cell and watershed bases. The results of the grid cell analysis produce the most informative map graphics and clearly show spatial variation at the greatest resolution possible. At this spatial scale, the statistics for each grid cell are developed independently. The resulting statistics are stored in netCDF files. Monthly time series data were extracted from these files to characterize patterns of change in hydrologic parameters.

Finally, “change metrics” are generated for each parameter, in which the difference between future period statistics and historical period statistics are calculated on both absolute and percent change bases. These results are again stored in netCDF files, with two files generated for each future period—one for grid cell data and one for watershed data. The format of these files is identical to those containing the results of the statistical analysis.

### 3.0 Climate Teleconnections

During the past 30 years, the understanding of the climatic importance of the oceans, particularly ocean temperature, has steadily improved (U.S. Department of Interior, 2004). Initial research focused on the distant effects of the recurrent warming of the equatorial Pacific Ocean referred to as El Niño, which South American fishermen have long known to have an adverse effect on the coastal fisheries in Peru. El Niño is the warm phase of the sea-surface temperature component of a coupled ocean-atmosphere process, ENSO, which spans the equatorial Pacific Ocean. The atmospheric component, the Southern Oscillation, refers to a “seesaw” effect in sea-level pressure between the tropical Pacific and Indian Oceans. Reduced sea-level pressure in the Pacific Ocean, combined with increased sea-level pressure in the Indian Ocean, leads to a weakening in the trade winds over the eastern Pacific. This weakening enables warm water from the central equatorial Pacific to spread eastward and southward along the west coast of South America, creating the classic El Niño condition. Conversely, and about as frequently, the sea-level pressure in the Pacific Ocean increases while pressure in the Indian Ocean decreases, which causes trade winds to intensify over the eastern Pacific. When this occurs, equatorial upwelling

of deep, cold water, as well as cold water from the West Coast of South America, are pulled northward and westward from the coast into the eastern and central Pacific, producing La Niña. Thus, El Niño and La Niña are, respectively, the warm and cold phases of the coupled ENSO system.

ENSO events typically last from 6 to 18 months and, therefore, are the single most important factor affecting inter-annual climatic variability on a global scale (Diaz and Kiladis, 1992). ENSO has been linked to the occurrence of flooding in the Lower Basin (Webb and Betancourt, 1992) and to both floods and droughts across the western United States (Cayan et al., 1999). Warm winter storms have been enhanced during El Niño, causing above-average runoff and floods in the Southwest, such as during 1982 and 1983. However, not all El Niño events lead to increased runoff in the Southwest. For example, during the 2002–2003 warm episode, runoff was below average in the Basin. Similarly, La Niña is frequently, though not always, associated with below-average flow in the Colorado River. As a result, although ENSO exerts a strong influence in modulating wet versus dry conditions in many parts of the United States, the effect is not always the same in any given region. Some condition other than ENSO must also be influencing weather and climate patterns affecting the Colorado River.

In the mid-1990s, scientists identified another ocean temperature pattern, this one occurring in the extratropical Pacific Ocean north of 20 °N (Mantua and Hare, 2002), the PDO. The PDO varies or oscillates on a decadal scale of 30 to 50 years for the total cycle; that is, much of the North Pacific Ocean will be predominantly though not uniformly warm (or cool) for periods of about 15 to 25 years. During the 20th Century, the PDO exhibited several phases—warmer along coastal southeastern Alaska from 1923 to 1943 and again from 1976 to 1998, and cooler from 1944 to 1975. Since 1999, the PDO has exhibited higher-frequency fluctuations, varying from cool (1999–2001) to warm (2002–2004). Currently, the causes of the variations in the PDO are unknown and its potential predictability is uncertain. Recent research indicates that the PDO phase may be associated with decadal-length periods of above- and below-average precipitation and streamflow in the Basin (Hidalgo, 2004) but, as with ENSO, such associations are not always consistent.

Climate teleconnections were first analyzed by selecting indices that could have potential influence in streamflow changes for the Basin. Published research (Redmond and Koch 1991, Webb and Betancourt 1992, Cayan et al. 1999, Mo et al. 2009, and others) indicates that the strongest correlations with Basin flows were observed with the PDO and ENSO indices. For ENSO, data were collected for both the ocean component (sea surface temperature anomalies) and the atmospheric component. The two components are highly correlated and combined describe ENSO. The Southern Oscillation Index (SOI), the atmospheric component, was the primary dataset used in the Study due to the longer availability of information. Therefore, the quantitative teleconnections analysis was based on the PDO index and the SOI. Only a qualitative discussion of the AMO is included in the Technical Report.

Annual averages of the PDO on a water-year basis were calculated and compared with the same water year annual flows. Annual average values for the SOI were computed, using different annual windows. The average SOI index presented in the Study refers to the June–November period, which was identified as a strong indicator of ENSO events (Redmond and Koch, 1991). Once the SOI averages were computed, ENSO events were determined by years when the averaged SOI was below -1 (classified as an El Niño year) or above 1 (classified as a La Niña year). A warm PDO was defined as a PDO value greater than or equal to 0.0, and a cold PDO

was a PDO value less than 0.0. AMO research by Mo et al. (2009) indicates that the direct influence of the AMO on drought is small. The major influence of the AMO is to modulate the impact of ENSO on drought. The influence is large when the sea surface temperature anomalies in the tropical Pacific and in the North Atlantic are opposite in phase. A cold (warm) event in a positive (negative) AMO phase amplifies the impact of the cold (warm) ENSO on drought. The ENSO influence on drought is much weaker when the sea surface temperature anomalies in the tropical Pacific and in the North Atlantic are in phase. Because the AMO cycle is approximately 70 years, AMO research is constrained by the observed data record of approximately 150 years. AMO research continues in this area using indirect observations of tree rings and sedimentary layers.

There are also other climate teleconnections that appear to influence the characteristics of seasonal precipitation (e.g., Madden-Julian Oscillation and Arctic Oscillation) (Becker et al., 2011; Bond and Vecchi, 2003; Hu and Feng, 2010). However, the understanding of the influence of these teleconnections on the Colorado River precipitation, and their usefulness as an indicator, is still evolving.

## 4.0 Streamflow

Streamflow was analyzed through the use of two historical data sets (observed period and a longer paleo-reconstructed period) and projections of future streamflow based on climate models. Using information from the recent past, more distant past, and projections of the future enabled a robust assessment of plausible future conditions.

Two historical streamflow data sets—the observed record spanning the period 1906–2007 and the paleo-reconstructed record spanning the period 762–2005—were used in the Study to characterize historical streamflow patterns and variability. Period comparisons are made between the full extent of the data and a more recent period. For the observed dataset spanning 1906 to 2007, the second comparison period (1978–2007) was selected as the most recent (based on available natural flow records) 30-year period because it captures the recent drought period and the apparent climate shift after 1977 (IPCC 2007). For the Paleo dataset spanning 762 to 2005, the second comparison period selected was 1906–2005 so that direct comparisons could be made of the observed and paleo timeframes. Annual flows and moving averages for 3, 5, 10, 20, and 30 years were computed for the two time periods so that differences in mean flows and variability of flows could be accessed. Annual flows and moving averages were also used to evaluate minimum and maximum streamflows. Exceedance probability plots were used to evaluate the likelihood of annual flows to exceed a specified streamflow value.

One future streamflow projection data set was represented in the Downscaled GCM Projected scenario. In this scenario, the routed streamflow from the VIC simulations driven by 112 climate projections for the period 1950–2099 were used to characterize natural flows at each of the 29 flow locations. VIC-simulated runoff from each grid cell was routed to the outlet of each watershed (the 29 flow locations) using VIC's offline routing tool (Lohmann et al. 1996; 1998). The routing tool processed individual cell runoff and baseflow terms and routed the flow based on flow direction and flow accumulation inputs derived from digital elevation models. Flows were output in both daily and monthly time steps. Only the monthly flows were used in the analysis for the Study. It is important to note that VIC routed flows are considered “natural flows” in that they do not include effects of diversions, imports, storage, or other human

management of the water resource. Bias-correction was applied to the VIC-simulated flows to account for any systematic bias in the hydrology model or data sets.

Annual streamflows for both the historical analysis and future water supply scenarios were analyzed to provide an estimate of the inter-annual variability, or deficit and surplus conditions. Definitions of “drought” are often subjective in water planning. In general, droughts are defined as periods of prolonged dryness. The inter-annual variability of the climate and hydrology of the Southwest imply basins may be in frequent states of drought. As part of the analysis conducted for this report, different averaging periods for determining and measuring deficits (cumulative volume below some reference) were considered. The definition used in the Technical Report is the following: a deficit occurs whenever the 2-year average flow falls below the long-term mean annual flow of 1906–2007. The use of a 1-year averaging period was discarded because it implied that any 1 year above the 15 million acre-feet (maf) Lees Ferry natural flow would break a multi-year deficit. The use of a 2-year averaging period implies that it may take 2 consecutive above-normal years (or 1 extreme wet year) to end a drought. For a basin with sizable reservoir storage in comparison to its mean flow such as the Colorado River, it may take several years to alleviate storage deficits. Averaging periods of 1 to 10 years were evaluated, following research by Timilsena et al. (2007). The 2-year averaging period appeared to produce similar deficits as the longer-averaging periods, and was thus selected as useful indicator.

A summary of the streamflow data sources used in each of the water supply scenarios is included below.

#### 4.1 Observed Natural Streamflows used in the Observed Resampled Scenario

The natural streamflows were obtained for the 1906–2007 period at the 29 flow locations commonly used by the Bureau of Reclamation (Reclamation) for planning. Reclamation uses data collected from the U.S. Geological Survey (USGS) and other gage sites, consumptive use records, records of reservoir releases, and other data to compute monthly natural flows at 29 locations throughout the Basin: 20 locations upstream of and including the Lees Ferry gaging station in Arizona, and 9 locations below the Lees Ferry gaging station (Prairie and Callejo, 2005).

Natural flow for the Upper Basin is computed as follows:

$$\text{Natural Flow} = \text{Historic Flow} + \text{Consumptive Uses and Losses} \pm \text{Reservoir Regulation}$$

Historical streamflow data were obtained from USGS web pages. Total depletions in the form of consumptive uses and losses include the following: irrigated agriculture, reservoir evaporation, stockponds, livestock, thermal power, minerals, municipal and industrial, and exports/imports. Reservoir regulation includes mainstem reservoirs and non-mainstem reservoirs.

Natural flows for the Lower Basin comprise computed gains and losses (on the mainstem) and historical flows (on the tributaries). Computed gains and losses consider the following consumptive uses and losses: decree accounting reports (<http://www.usbr.gov/lc/region/g4000/wtracct.html>), evaporation (from Lakes Mead, Mohave, and Havasu), and phreatophytes. Reservoir regulation includes change in reservoir storage and change in bank storage. Historical flows on the tributaries (Paria, Virgin, Little Colorado, and Bill Williams Rivers) have not had the historical depletions added back to the gaged flow due to the state of current methods and processes. Thus, most Lower Basin flows should not be considered natural. See *Technical Report C – Water Demand Assessment, Appendix C5*,

*Modeling of Lower Basin Tributaries in the Colorado River Simulation System*, for more detail on the treatment of the Lower Basin tributaries.

Monthly intervening and total natural flow for the 29 locations are available. “Intervening” flows represent the flow generated between two locations, but do not include the cumulative contribution of the locations upstream. “Total” flows, on the other hand, included the local intervening flow and all upstream flows from that location.

Additional information, documentation, and the natural flow data are available at <http://www.usbr.gov/lc/region/g4000/NaturalFlow/Index.html>.

#### **4.2 Paleo Reconstructed Streamflow used in the Paleo Resampled Scenario**

The natural streamflows in the Paleo Resampled Scenario were derived from streamflow reconstructions at Lees Ferry from tree-ring chronologies for the period of 762-2005. The reconstructed streamflows at Lees Ferry were derived from ecologically contrasting tree-ring sites in the southern Colorado Plateau during the past 2 millennia (Meko et al., 2007). Streamflow values were disaggregated, spatially, and temporally, to the 29 locations by Reclamation (Prairie and Rajagopalan 2007; Prairie et al. 2008).

#### **4.3 Paleo Conditioned Streamflow used in the Paleo Conditioned Scenario**

The Paleo Conditioned scenario blends the observed historical record and Paleo-reconstructed record to generate future inflow scenarios that comprise magnitudes of the historical record and state information from the Paleo record provided by Reclamation (Prairie and Rajagopalan 2007; Prairie et al. 2008).

#### **4.4 Future Streamflow Projections used in the Downscaled GCM Projected Scenario**

The Downscaled GCM Projected scenario includes VIC hydrologic model traces of future streamflows for the 1950–2099 period from 112 GCM realizations for the 29 streamflow locations within the Basin. VIC model results were provided by Reclamation from work conducted for the Westwide Climate Risk Assessment (Reclamation 2011).

## **5.0 References**

- Cayan, D.R., Redmond, K.T., Riddle, L.G. 1999. ENSO and Hydrologic Extremes in the Western United States. *Journal of Climate*, 12: 2881-2893.
- Collins, W.D., Bitz, C.M., Blackmon, M.L., Bonan, G.B., Bretherton, C.S., Carton, J.A., Chang, P., Doney, S.C., Hack, J.J., Henderson, T.B., Kiehl, J.T., Large, W.G., McKenna, D.S., Santer, B.D., Smith, R.D. 2006. The Community Climate System Model Version 3 (CCSM3). *J Climate*, 19(11):2122-2143.
- Daly, C., G.H. Taylor, W. P. Gibson, T.W. Parzybok, G. L. Johnson, P. Pasteris. 2000. High-quality spatial climate data sets for the United States and beyond. *Transactions of the American Society of Agricultural Engineers*, 43: 1957-1962.
- Diaz, H.F., Kiladis, G.N. 1992. Atmospheric Teleconnections Associated with the Extreme Phases of the Southern Oscillation, Diaz, H.F., and Markgraf, V.A. (eds.), *El Niño: Historical and Paleoclimatic Aspects of the Southern Oscillation*. Cambridge, Cambridge University Press, p. 7-28.

- Delworth, T.L. et al. 2006. GFDL's CM2 global coupled climate models part 1: formulation and simulation characteristics. *J Climate* 19:643-674.
- Diansky, N.A., Volodin, E.M. 2002. Simulation of present-day climate with a coupled atmosphere-ocean general circulation model. *Izv Atmos Ocean Phys (Engl Transl)* 38(6):732-747.
- Furevik, T., Bentsen, M., Drange, H., Kindem, I.K.T., Kvamstø, N. G., Sorteberg, A. 2003. Description and evaluation of the bergen climate model: ARPEGE coupled with MICOM. *Clim Dyn* 21:27-51.
- Flato, G.M., Boer, G.J. 2001. Warming Asymmetry in Climate Change Simulations. *Geophys. Res. Lett.*, 28:195-198.
- Gordon C., Cooper, C., Senior, C.A., Banks, H.T., Gregory, J.M., Johns, T.C., Mitchell, J.F.B., Wood, R.A. 2000. The simulation of SST, sea ice extents and ocean heat transports in a version of the Hadley Centre coupled model without flux adjustments. *Clim Dyn* 16:147-168.
- Hidalgo, H. G. 2004. Climate precursors of multi-decadal drought variability in the western United States, *Water Resour. Res.*, 40, W12504, doi:10.1029/2004WR003350.
- Intergovernmental Panel on Climate Change. 2000. Emissions Scenarios. Special Report of the Intergovernmental Panel on Climate Change [Nakicenovic, N., and Swart, R., (eds.)], Cambridge University Press, Cambridge, United Kingdom and New York, 570 pp.
- Intergovernmental Panel on Climate Change. 2007. Climate Change 2007: The Physical Science Basis. Contribution of Working Group I to the Fourth Assessment Report of the Intergovernmental Panel on Climate Change [Solomon, S., Quin, D., Manning, M., Chen, Z., Marquis, M., Averyt, K.B., Tignor, M., Miller, H.L. (eds.)], Cambridge University Press, Cambridge, United Kingdom and New York, 996 pp.
- IPSL. 2005. The new IPSL climate system model: IPSL-CM4. Institut Pierre Simon Laplace des Sciences de l'Environnement Global, Paris, France, p 73.
- Joint Institute for the Study of the Atmosphere and Ocean, 2010 (<http://jisao.washington.edu/pdo/>; accessed March 30, 2011).
- Jungclaus, J.H., Botzet, M., Haak, H., Keenlyside, N., Luo, J-J, Latif, M., Marotzke, J., Mikolajewicz, U., Roeckner, E. 2006. Ocean circulation and tropical variability in the AOGCM ECHAM5/MPI-OM. *J Climate* 19:3952-3972.
- K-1 model developers. 2004. K-1 coupled model (MIROC) description, K-1 technical report, 1. In: Hasumi H, Emori S (eds) Center for Climate System Research, University of Tokyo, 34 pp.
- Legutke, S., Voss, R. 1999. The Hamburg Atmosphere-Ocean Coupled Circulation Model ECHO-G. Technical report, No. 18, German Climate Computer Centre (DKRZ), Hamburg, 62 pp.
- Lohmann, D., Nolte-Holube, R., Raschke, E. 1996. A large-scale horizontal routing model to be coupled to land surface parameterization schemes. *Tellus*, 48: 708-721
- Lohmann, D., Raschke, E., Nijssen, B., Lettenmaier, D. P. 1998. Regional Scale Hydrology: I. Formulation of the VIC-2L Model Coupled to a Routing Model. *Hydrological Sciences Journal*, 43, 131-141.
- Mantua, N.J., Hare, S.R. 2002. The Pacific Decadal Oscillation, *Journal of Ocean*, 58: 35-42.
- Maurer, E.P. 2007. Uncertainty in hydrologic impacts of climate change in the Sierra Nevada, California under two emissions scenarios, *Climatic Change*, Vol. 82, No. 3-4, 309-325, DOI: 10.1007/s10584-006-9180-9

- Maurer, E. P., Brekke, L., Pruitt, T., Duffy, P.B. 2007. Fine-Resolution Climate Projections Enhance Regional Climate Change Impact Studies, *Eos, Transactions, American Geophysical Union*, 88 (47), 504
- Maurer, E.P., Wood, A.W., Adam, J.C., Lettenmaier, D.P., Nijssen, B. 2002. A Long-Term Hydrologically-Based Data Set of Land Surface Fluxes and States for the Conterminous United States, *Journal of Climate*, 15(22), 3237-3251.
- Meko, D.M., Woodhouse, C.A., Baisan, C.A., Knight, T., Lukas, J.J., Hughs, M.K., Salzer, M.W. 2007. Medieval Drought in the Upper Colorado River Basin. *Geophysical Research Letters*, 34(5), L10705, doi: 10.1029/2007GL029988.
- Mo, K.C., Schemm, J.E., Yoo, S. 2009. Influence of ENSO and the Atlantic Multi-Decadal Oscillation on Drought over the United States. *Journal of Climate*, 22(22), 5962-5982. DOI:10.1175/2009JCLI2966.1.
- Mote, P., Clark, M., Hamlet, A. 2008. Variability and Trends in Mountain Snowpack in Western North America. 20th Conference on Climate Variability and Change. American Meteorological Society. New Orleans, Louisiana.
- Mote P.W., Salathé, E.P. 2010. Future climate in the Pacific Northwest. *Climatic Change*, 102, 29–50. DOI 10.1007/s10584-010-9848-z.
- Molotch, N. P., Fassnacht, S. R., Colee, M. T., Bardsley, T., Bales, R. C. 2001. A comparison of spatial statistical techniques for the development of a validation dataset for mesoscale modeling of snow water equivalence. *Eos Trans. AGU*, 82(47), Fall Meet. Suppl., F553.
- National Oceanic and Atmospheric Administration 2011. <http://www.ncdc.noaa.gov/oa/climate/normal/usnormals.html> (accessed June 30, 2011).
- National Resource Conservation Service 2011. <http://www.wcc.nrcs.usda.gov/snow/> (accessed June 30, 2011).
- NOAA, 2010. <http://www.ncdc.noaa.gov/oa/climate/normal/usnormalsprods.html>
- Prairie, J, Callejo, R. 2005. Natural Flow and Salt Computation Methods, Calendar Years 1971-1995. U.S. Department of the Interior, Upper Colorado and Lower Colorado Regional Offices, Technical Services and Dams Division, Boulder Canyon Operations Office, Water Quality Group, River Operations Group, Salt Lake City, Utah, Boulder City, Nevada. pp 1-122.
- Prairie, J., Rajagopalan, B. 2007. "[Stochastic Streamflow Generation Incorporating Paleo-Reconstruction.](#)" Proceedings of the World Environmental & Water Resources Congress, Tampa, FL.
- Prairie, J., Nowak, K., Rajagopalan, B., Lall, U., Fulp, T. 2008. A Stochastic Nonparametric Approach for Streamflow Generation Combining Observational and Paleoreconstructed Data. *Water Resources Research* Volume 44, W06423, DOI: 10.1029/2007WR006684.
- Reclamation, 2010. Colorado River Natural Flow and Salt Data (<http://www.usbr.gov/lc/region/g4000/NaturalFlow/supportNF.html>, accessed December 2010).
- Reclamation, 2011. West-Wide Climate Risk Assessments: Bias-Corrected and Spatially Downscaled Surface Water Projections, Technical Memorandum No. 86-68210-2011-01, prepared by the U.S. Department of the Interior, Bureau of Reclamation, Technical Services Center, Denver, Colorado. 138pp.
- Russell, G.L., Miller, J.R., Rind, D., Ruedy, R.A., Schmidt, G.A., Sheth, S. 2000. Comparison of model and observed regional temperature changes during the past 40 years. *J Geophys Res* 105:14891-14898.

- Redmond, K.T., Koch, R.W. 1991. Surface Climate and Streamflow Variability in the Western United States and Their Relationship to Large-Scale Circulation Indices. *Water Resources Research*, 27, 2381–2399.
- Salathé, E.P. 2005. Downscaling simulations of future global climate with application to hydrologic modeling. *Int J Climatol*, 25, 419–436.
- Salas-Mélia, D., Chauvin, F., Déqué, M., Douville, H., Gueremy, J.F., Mareut, P., Planton, S., Royer, J.F., Tyteca, S. 2005. Description and validation of the CNRM-CM3 global coupled model, CNRM working note 103.
- Timilsena J., Piechota T., Tootle G. and Singh A. 2009. Associations of interdecadal/interannual climate variability and long-term Colorado River Basin streamflow. *J. Hydrol.* 365(3-4), 289-301, DOI:10.1016/j.jhydrol.2008.11.
- U.S. Department of the Interior. 2004. Climatic Fluctuations, Drought, and Flow in the Colorado River Basin, U.S. Geological Survey, USGS Fact Sheet 2004-3062, version 2.
- University of East Anglia Climatic Research Unit 2010 (<http://www.cru.uea.ac.uk/cru/data/soi/>; accessed March 30, 2011).
- Webb, R.H., Betancourt, J.L. 1992. Climatic Variability and Flood Frequency of the Santa Cruz River, Pima County, Arizona: U.S. Geological Survey. *Water-Supply Paper* 2379, 40 p.
- Wood, A.W., E.P. Maurer, A. Kumar, and D.P. Lettenmaier. 2002. Long-range experimental hydrologic forecasting for the Eastern United States, *J. Geophysical Research-Atmospheres*, 107(D20), 4429, DOI:10.1029/2001JD000659.
- Wood, A.W., L.R. Leung, V. Sridhar, and D.P. Lettenmaier. 2004. Hydrologic implications of dynamical and statistical approaches to downscaling climate model outputs, *Climatic Change*, 15, 189–216.

**Appendix B3**  
**Supplemental Analysis of Future Climate Data**

---



# Appendix B3—Supplemental Analysis of Future Climate Data

During the development of the hydrologic simulations under historical and projected climate forcings as part of the Water Supply Assessment, biases were observed for the overlapping period of 1950–1999 as compared to the natural flow data set. These biases are due to differences between the General Circulation Model (GCM)-simulated historical climate and observed climate data, differences in hydrology model inputs and parameterization, and differences between the Variable Infiltration Capacity (VIC)-simulated hydrologic responses and observed watershed responses implied in the natural flows. This appendix describes analysis that was conducted to determine the effect of bias in climate forcings used to simulate streamflows and whether choice of the daily weather generation (temporal disaggregation) method significantly affects this bias.

While it was expected that biases would exist due to the hydrology model and historical gridded climate, it was believed that these biases would be similar (same magnitude and direction) when comparing to simulations of GCM-simulated historical climate. However, the biases were found to be substantially different when comparing three representations of the historical period (1950–1999) streamflow: (1) natural flows derived from gauge measurements; (2) VIC simulated flows when forced with observed (derived) historical climate; and (3) VIC simulated flows when forced with GCM-simulated historical climate. For example, the VIC simulation using observed historical climate for 1950–1999 suggested an over-estimation of flows in the Colorado River at Lees Ferry, Arizona. However, the same VIC model, when forced with GCM-simulated historical climate, produced an under-estimation of flow. Without a robust streamflow bias correction method, it is possible that the effects of climate change could be overstated.

Several potential causes of streamflow bias were investigated to support the use of the downscaled climate projections on a daily scale and to support the development of a streamflow bias correction method. The biases were investigated through various separate analyses using the historical climate forcings and VIC model simulations for the period of 1950–1999. The following areas related to climate forcing bias were investigated:

1. ***Bias due to 2-degree climate forcings.*** The projected climate forcings are bias corrected through the bias correction and spatial downscaling (BCSD) process at a common 2-degree scale. The forcings are corrected for each month, but residual bias at seasonal, annual, and multi-year scales are possible.
2. ***Bias due to 1/8<sup>th</sup>-degree spatial downscaling.*** Since the BCSD process corrects for month-specific bias at the 2-degree scale, it is possible that residual bias exists after performing spatial downscaling to the 1/8<sup>th</sup>-degree scale.
3. ***Bias due to daily weather generation method.*** Two data sets were available using slightly different methods to temporally disaggregate monthly climate data into daily weather inputs. It is possible that the choice of method could affect the resulting streamflow bias.

The evaluation of each of the potential causes of bias is discussed further in the following sections. In each of these evaluations, GCM-simulated historical climate was compared to historical observed climate from Maurer et al. (2002) for the period of 1950–1999. While any of the 112 downscaled climate projections could have been used, we selected one particular projection (Trace 44 – sresa2.ccma\_cgcm3\_1.4) for presentation of results. Biases were found to be relatively consistent across the range of projections.

Analyses were performed for precipitation at representative grid cells at the following locations in the Colorado River Basin (Basin) (table B3-1). However, results are shown for the grid cell at the Colorado River at the Glenwood Springs, Colorado location.

TABLE B3-1  
Locations where evaluation of biases was performed (decimal latitude and longitude).

No.	Location	Nearest Grid Cell (lat, lon)
1	Colorado River at Lees Ferry, Arizona	36.4375, -112.0625
2	Green River at Green River, Utah	38.8125, -111.3125
3	San Juan River near Bluff, Utah	35.5625, -110.6875
4	Colorado River near Cisco, Utah	38.6875, -109.6875
5	Colorado River above Imperial Dam, Arizona	32.9375, -114.8125
6	Colorado River at Glenwood Springs, Colorado	39.3125, -107.5625
7	Colorado River below Fontenelle Res, Wyoming	42.0625, -110.8125
8	San Juan River near Archuleta, New Mexico	36.6875, -107.8125
9	Colorado River below Davis Dam, Arizona-Nevada	35.1875, -115.0625
10	Taylor River below Taylor Park Reservoir, Colorado	38.8125, -106.5625

## 1.0 Bias Due to 2-degree Climate Forcings

The BCSD method adjusts monthly biases in climate projections at the 2-degree spatial scale. By construction, the method preserves monthly precipitation and temperature statistics to the observed for the overlapping 1950–1999 period at the 2-degree spatial scale. However, since hydrologic responses are dependent on seasonal, annual, and sometimes multi-year sequences of precipitation and temperature, the bias was evaluated for longer temporal scales.

Figures B3-1A and B3-1B show the observed, raw GCM, and the bias corrected GCM monthly precipitation for grid cell at the Colorado River at Glenwood Springs location. As can be seen from the figures, the raw GCM results need to be bias corrected to achieve similar statistics to the observed in the overlapping period. The raw GCM biases appear to be largest in the December and January months. However, after bias correction, the monthly statistics are preserved for all months as compared to the observed (BC line is same as Obs line).

Figure B3-2 shows the same information for the seasonal and annual time scales. As shown in this figure, despite monthly bias correction, residual bias exists at seasonal and annual scales as compared to the observed. The 2-degree bias corrected GCM precipitation appears to underestimate the periods of high seasonal precipitation. The underestimation of high seasonal precipitation appears to be caused by differences in sequences of wet months within the season between the GCM-simulated historical climate and the observed climate. The seasonal bias is

largest during the winter (January, February, and March) and fall (October, November, and December) and relatively small in other seasons. However, small bias continues to persist at annual scales as shown in the bottom panel of the figure. Figure B3-3 also indicates that GCM-simulated historical climate (after bias correction) retains bias at multi-year scales. In almost all multi-year averaging periods the observed precipitation is larger than the bias corrected GCM precipitation, although the magnitude of this impact has not been isolated.

The temperature biases (not shown) are significantly less than precipitation biases at all time scales and are not believed to represent a significant source of bias to streamflow assessments.

FIGURE B3-1A

Comparison of monthly precipitation non-exceedance probability using 2-degree raw GCM (raw), 2-degree bias corrected GCM using Trace 44 - sresa2.cccma\_cgcm3\_1.4 (BC) with 2-degree spatially aggregated precipitation from observation taken from Maurer et al. (2002) (Obs), for a GCM grid cell at the Colorado River at Glenwood Springs, Colorado location. January–June shown.

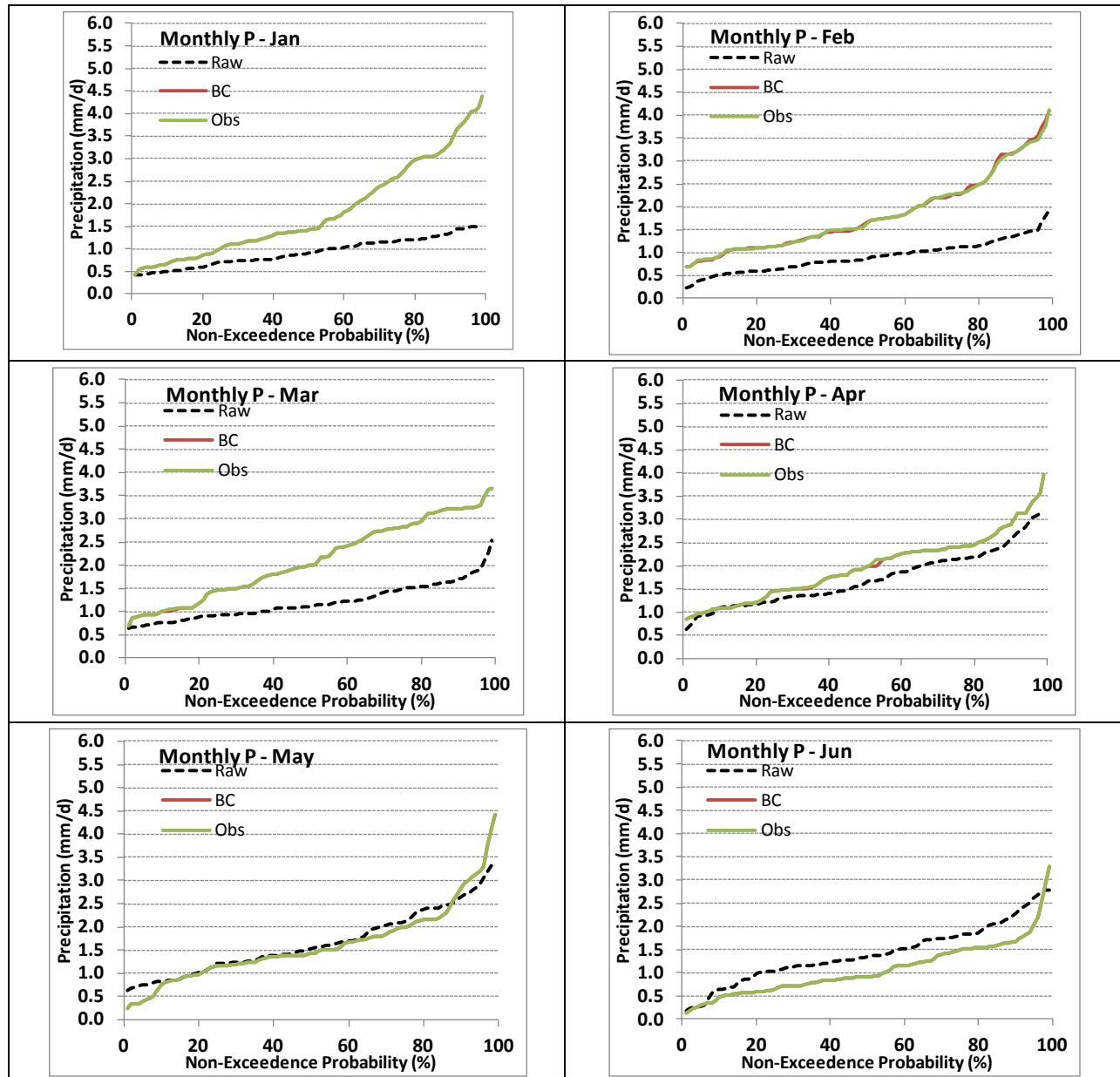


FIGURE B3-1B

Comparison of monthly precipitation non-exceedance probability using 2-degree raw GCM (raw), 2-degree bias corrected GCM using Trace 44 - sresa2.cccma\_cgcm3\_1.4 (BC) with 2-degree spatially aggregated precipitation from observation taken from Maurer et al. (2002) (Obs), for a GCM grid cell at the Colorado River at Glenwood Springs, Colorado location. July–December shown.

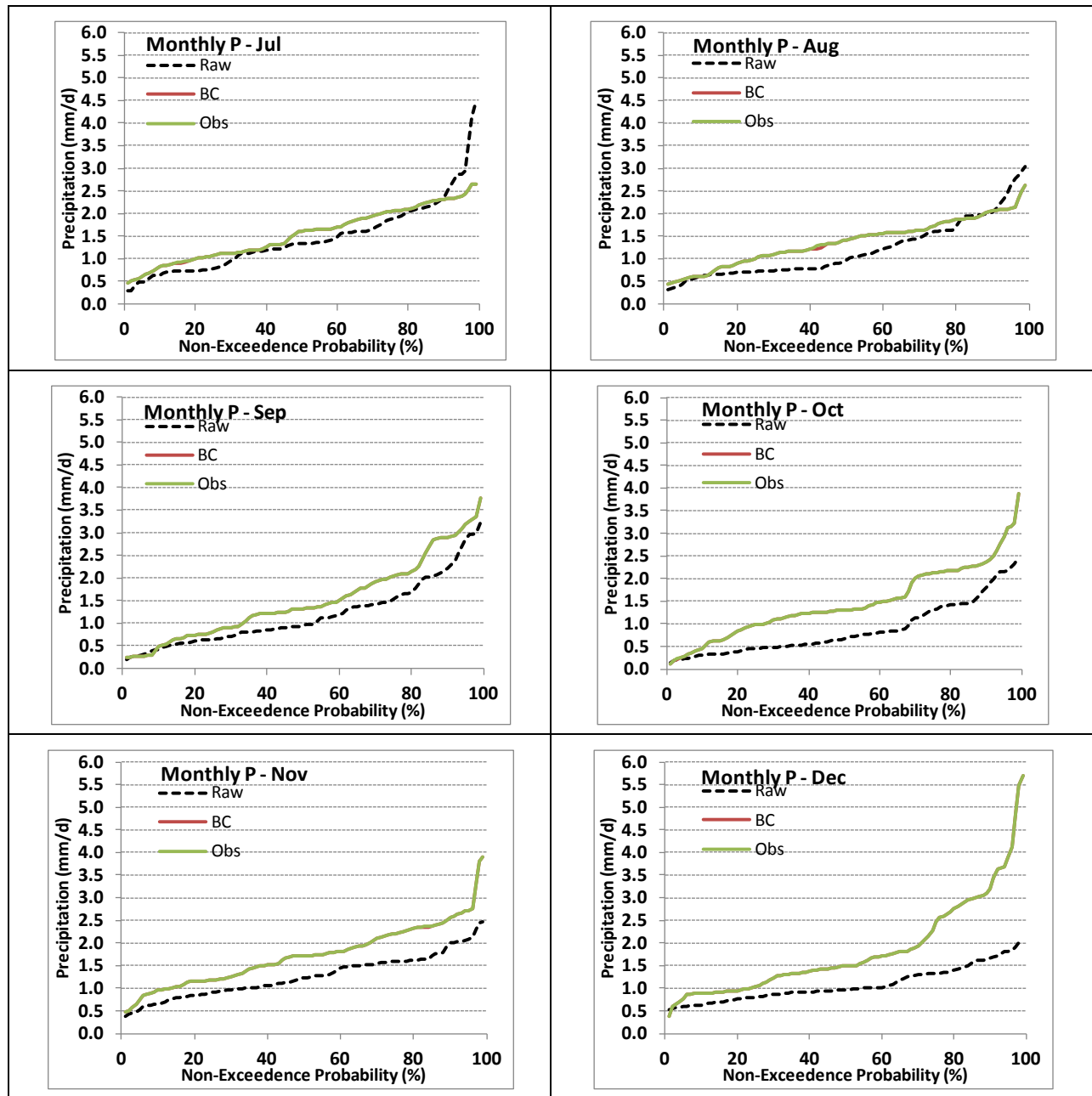


FIGURE B3-2

Comparison of seasonal and annual precipitation non-exceedance probability using 2-degree raw GCM (raw), 2-degree bias corrected GCM using Trace 44 - sresa2.cccma\_cgcm3\_1.4 (BC) with 2-degree spatially aggregated precipitation from observation taken from Maurer et al. (2002) (Obs), for a GCM grid cell at the Colorado River at Glenwood Springs, Colorado location.

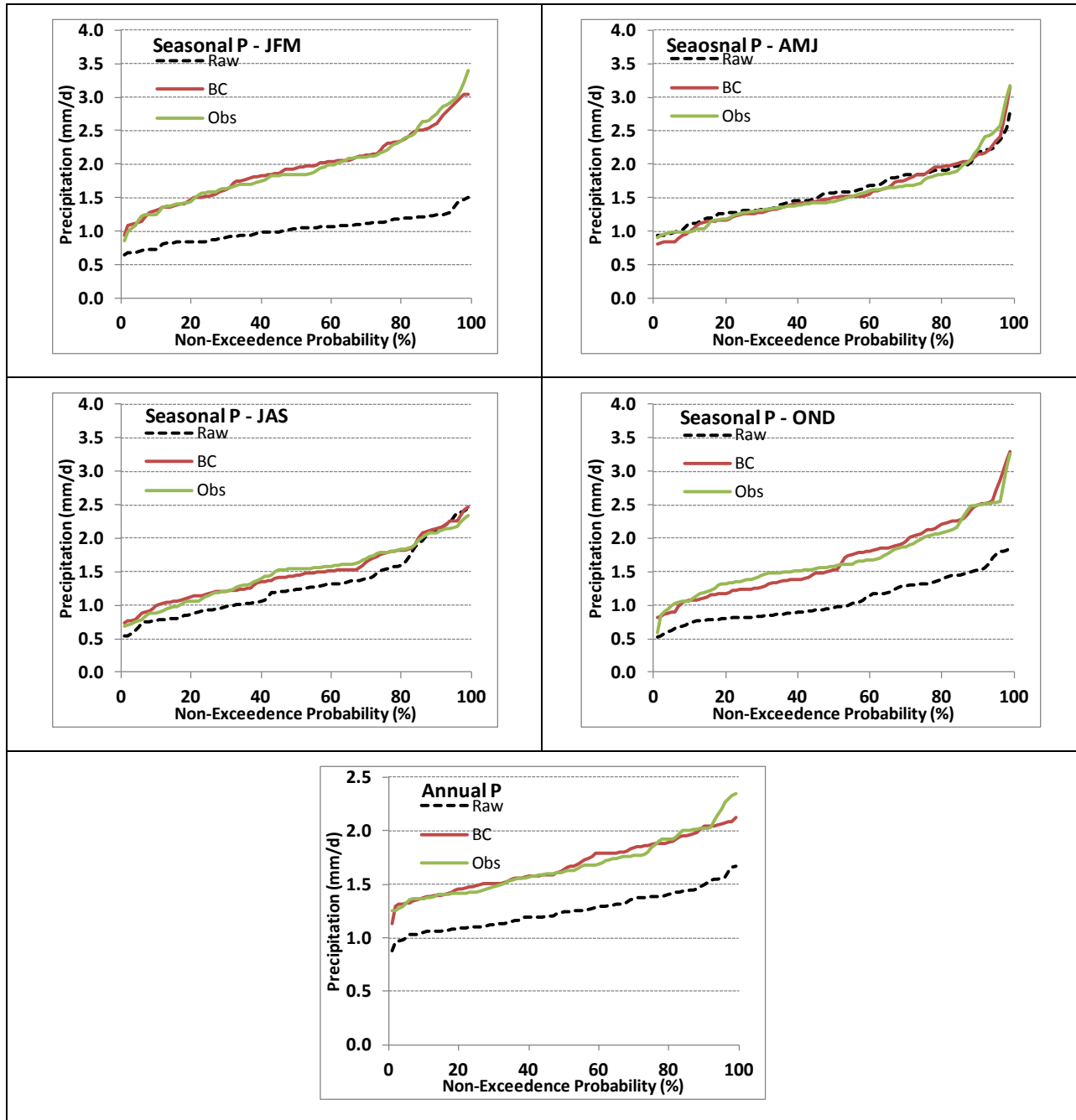
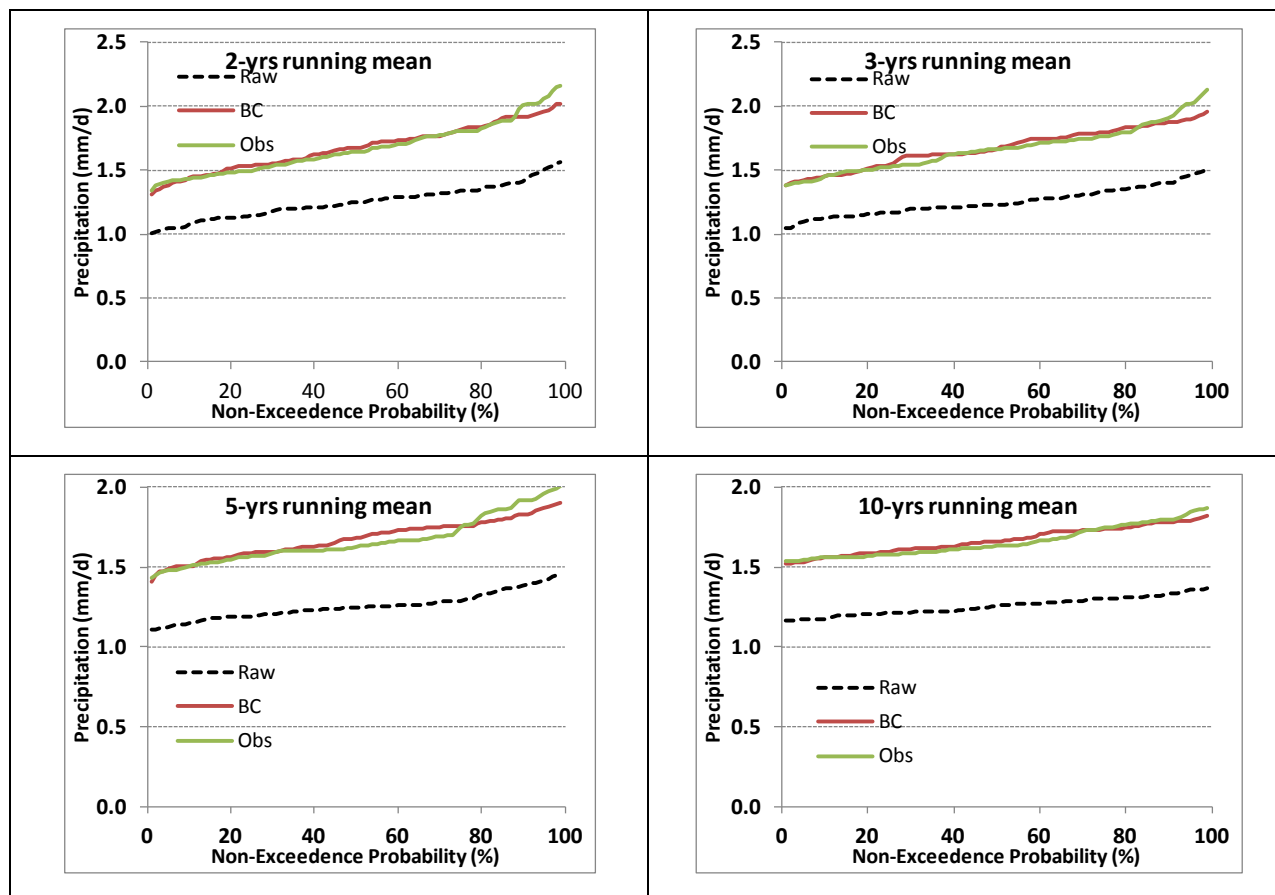


FIGURE B3-3

Comparison of non-exceedance probability for precipitation averaged over 2-year, 3-year, 5-year, and 10-year periods, using 2-degree raw GCM (raw), 2-degree bias corrected GCM using Trace 44 - sresa2.ccm3\_1.4 (BC) with 2-degree spatially aggregated precipitation from observation taken from Maurer et al. (2002) (Obs), for a GCM gridcell at the Colorado River at Glenwood Springs, Colorado, location.



## 2.0 Bias Due to 1/8<sup>th</sup>-degree Spatial Downscaling

The BCSD method adjusts for monthly biases in climate projections at 2-degree spatial scale. By construction, the method preserves monthly precipitation and temperature statistics to the observed for the overlapping 1950–1999 period at the 2-degree spatial scale. However, to be useful for most watershed assessments the climate information is needed at finer spatial scales. The spatial downscaling transforms the climate information to the 1/8<sup>th</sup>-degree scale. The 1/8<sup>th</sup>-degree spatial scale climate data are used as input into the VIC hydrologic model. Analyses were performed to investigate bias after downscaling to this finer spatial scale.

As shown in figures B3-4A and B3-4B, while there is generally good agreement between the observed and simulated historical climate statistics at the 1/8<sup>th</sup>-degree scale, bias exists even at the monthly scale. As with the 2-degree climate information, the biases are largest in winter; particularly December and January. Biases continue to exist at the seasonal, annual, and multi-year scales (figure B3-5 and B3-6). These longer time-scale biases are larger at the 1/8<sup>th</sup>-degree than at the 2-degree spatial scales.

FIGURE B3-4A

Comparison of non-exceedance probability for monthly precipitation using BCS D 1/8<sup>th</sup>-degree precipitation downscaled from Trace 44 - sresa2.cccma\_cgcm3\_1.4 with Maurer Observed precipitation at 1/8<sup>th</sup>-degree (Obs), for a GCM grid cell at the Colorado River at Glenwood Springs, Colorado location. January–June shown.

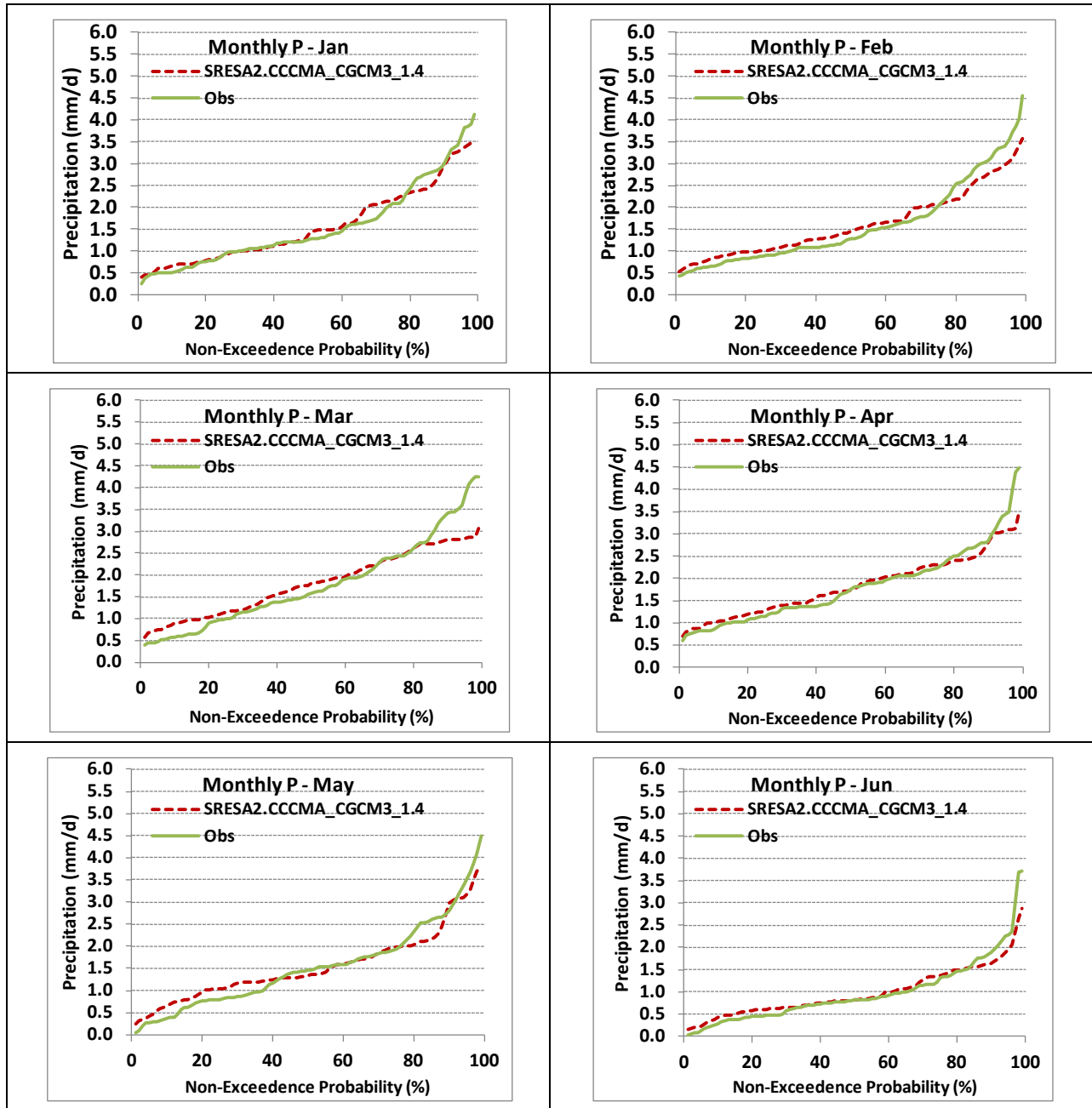


FIGURE B3-4B

Comparison of non-exceedance probability for monthly precipitation using BCS D 1/8<sup>th</sup>-degree precipitation downscaled from Trace 44 - sresa2.cccma\_cgcm3\_1.4 with Maurer Observed precipitation at 1/8<sup>th</sup>-degree (Obs), for a GCM gridcell at the Colorado River at Glenwood Springs, Colorado location. July–December shown.

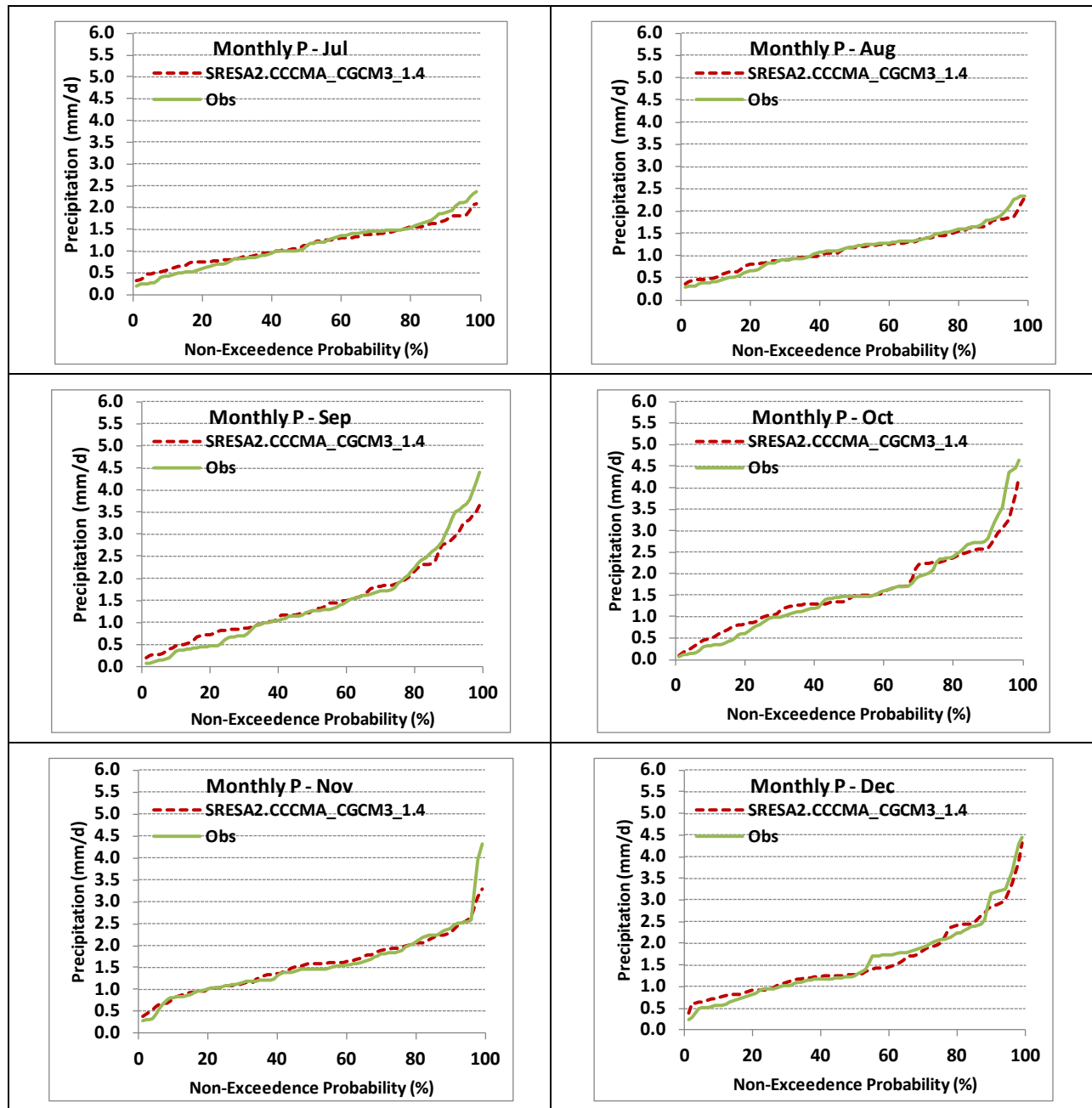


FIGURE B3-5

Comparison of non-exceedance probability for seasonal precipitation using BCSD 1/8<sup>th</sup>-degree precipitation downscaled from Trace 44 - sresa2.cccma\_cgcm3\_1.4 with Maurer Observed precipitation at 1/8<sup>th</sup>-degree (Obs), for a GCM grid cell at the Colorado River at Glenwood Springs, Colorado location.

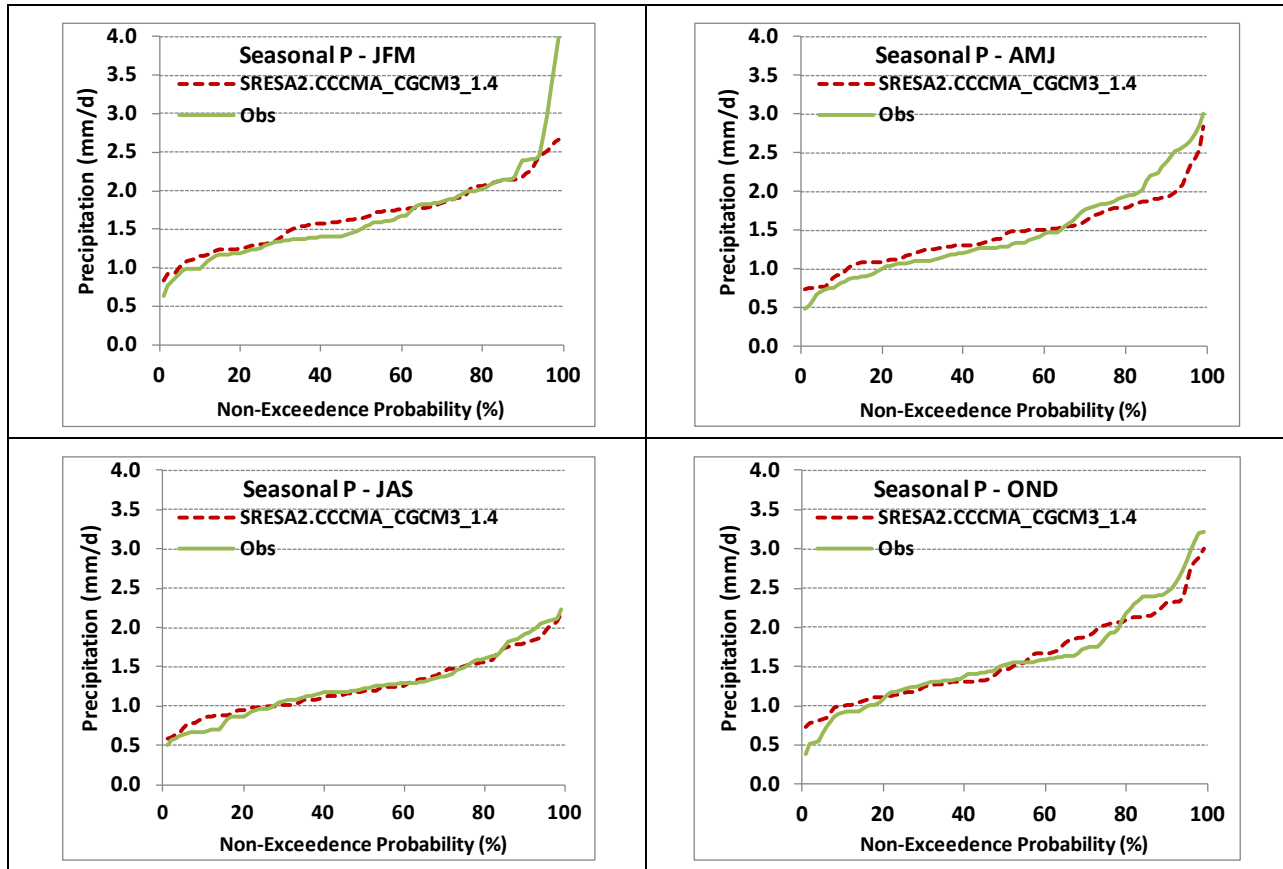


FIGURE B3-6

Comparison of non-exceedance probability for seasonal precipitation averaged over 2-year, 3-year, 5-year, and 10-year periods, using BCSD 1/8<sup>th</sup>-degree precipitation downscaled from Trace 44 - sresa2.cccma\_cgcm3\_1.4 with Maurer Observed precipitation at 1/8<sup>th</sup>-degree (Obs), for a GCM grid cell at the Colorado River at Glenwood Springs, Colorado location.

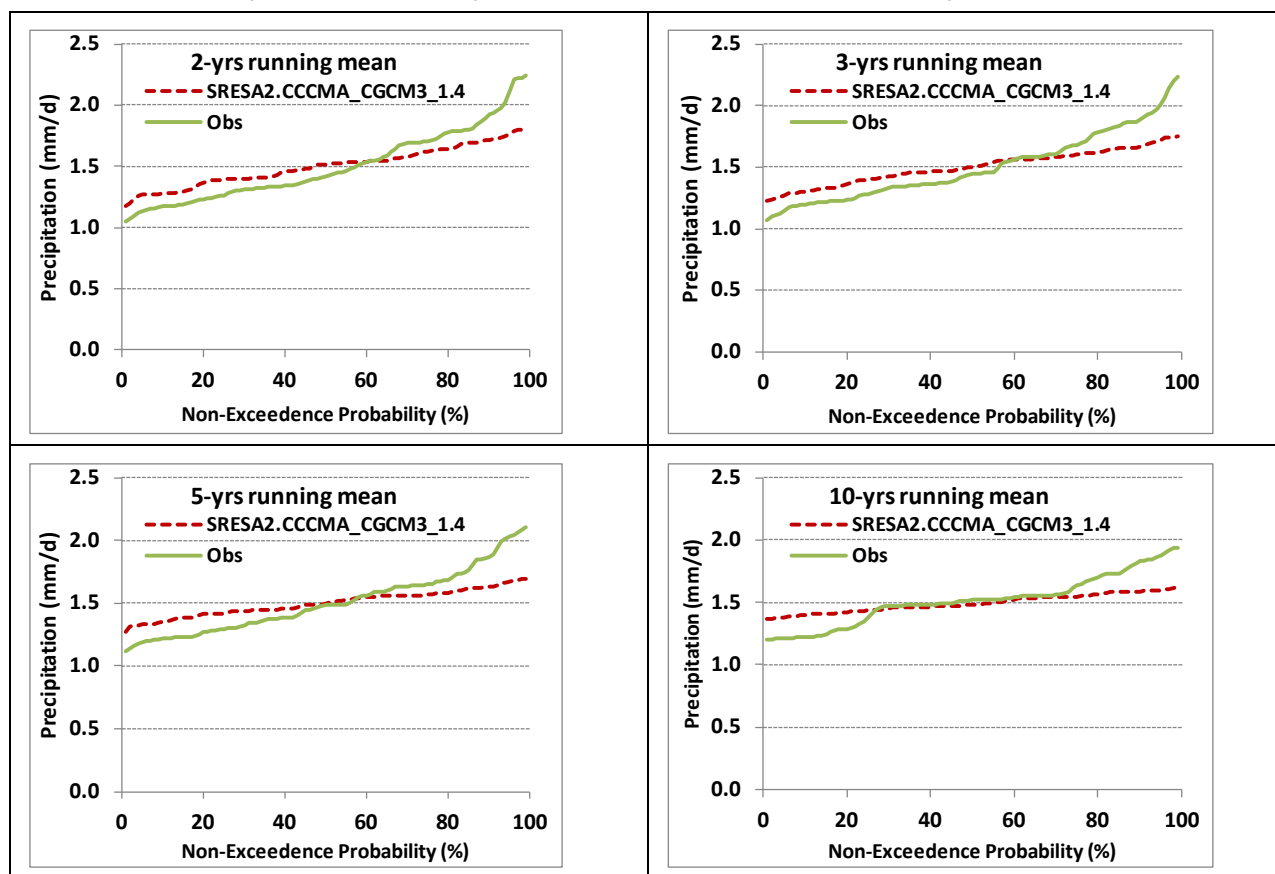
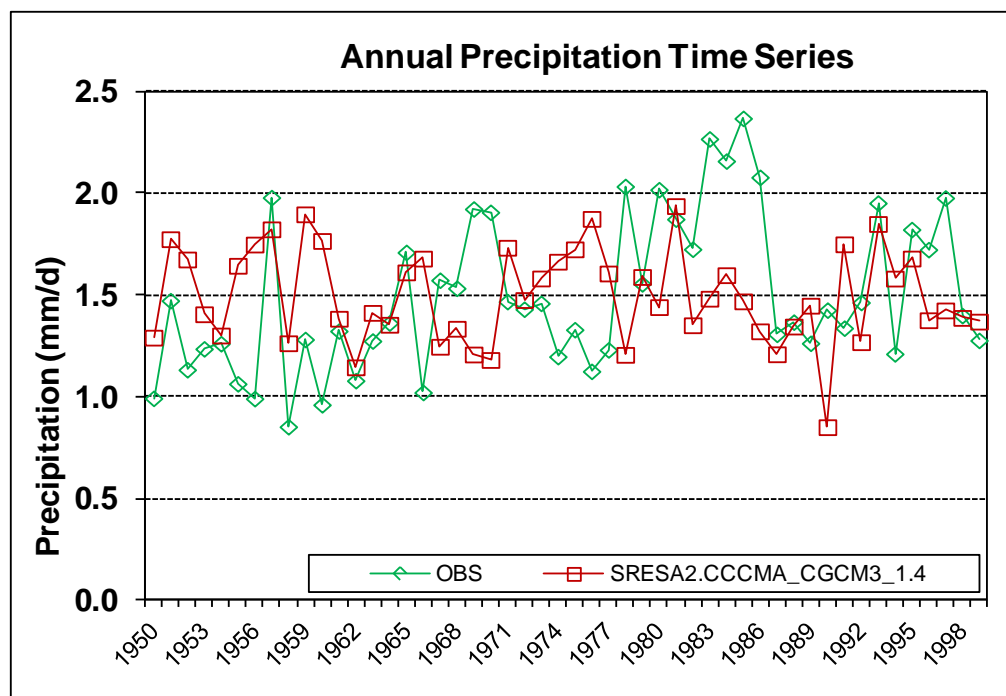


Figure B3-7 shows the annual time history of the observed precipitation and the simulated historical period precipitation for one particular GCM projection for 1950–1999. The GCMs are not expected to reproduce the identical sequences of observed precipitation due to differences between actual and simulated initial ocean and climate states, differences between actual and simulated emissions and other radiative forcings, and other model limitations. As shown in the figure, multi-year wet periods such as that observed in 1983–1986 are not expected to occur at the same time in the historical simulations, but would be expected to be reproduced over some historical period. However, the magnitude of this wet persistence is not reproduced in the simulated climate (see figure B3-7). This under-representation of wet persistence appears to be common across all 112 projections.

FIGURE B3-7

Comparison of annual precipitation for the period 1950–1999, using BCSD 1/8<sup>th</sup>-degree precipitation downscaled from Trace 44 sresa2.cccma\_cgcm3\_1.4 with Maurer Observed precipitation at 1/8<sup>th</sup>-degree (Obs), for a GCM gridcell at the Colorado River at Glenwood Springs, Colorado location.



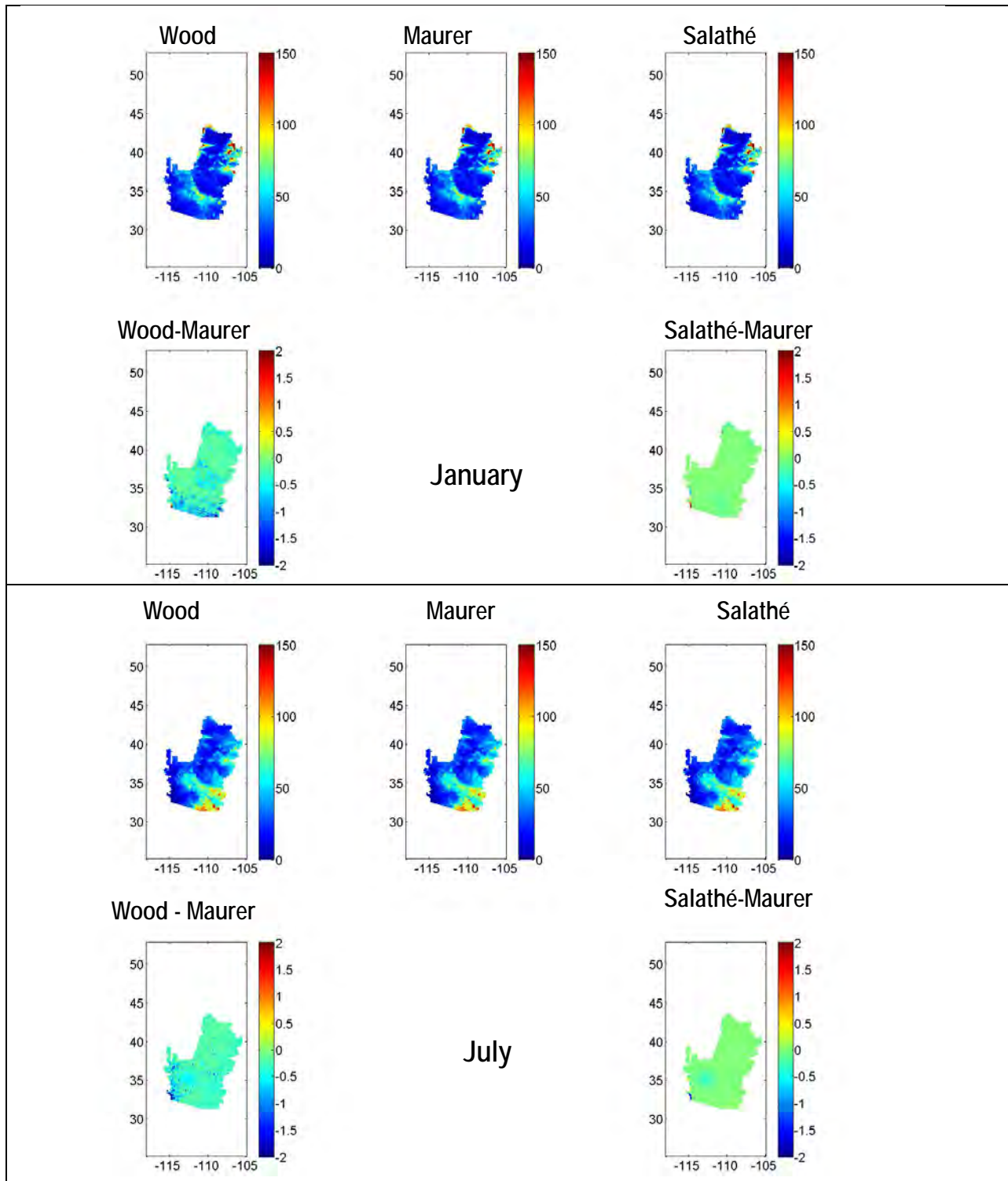
### 3.0 Comparison of Daily Weather Generation (Temporal Disaggregation) Methods

As part of the assessment of future climate data and their impact on streamflow, two different daily weather datasets were available for this study. The two methods used to develop these datasets are: (1) a method developed by the Climate Impacts Group at the University of Washington (Salathé 2005) and that used in the Bureau of Reclamation's (Reclamation's) Westwide Climate Risk Assessment; and (2) the method developed by Wood et al. (2002) and used in previous Colorado River VIC assessments (Christianson and Lettenmaier 2007). Both daily weather generation methods preserve monthly total precipitation from the downscaled climate projections and use the historical database to develop realistic daily storm patterns through a temporal disaggregation method. The differences between the two approaches are relatively subtle, but it was found that VIC hydrologic model results were sensitive to the choice of method.

Analysis of the precipitation statistics between the two methods indicates no significant differences at the *monthly* scale. The observational data set is that derived from Maurer et al. (2002). Comparisons have been prepared for one downscaled climate projection: Trace 44 sresa2.cccma\_cgcm3\_1.4 under the two different daily weather generation methods. Figure B3-8 illustrates a graphical comparison of the monthly precipitation for January and July between the two methods and the observed. The differences between simulated and observed are generally zero as can be seen from the bottom plots. However, some small differences occur in the extreme southwest of the Basin under the Wood methodology.

**FIGURE B3-8**

Comparison of monthly precipitation between Maurer et al. (Maurer) and downscaled precipitation (only January and July monthly averaged values in millimeters/day [mm/d] are shown). Downscaled climate data for Wood et al. (Wood) and Salathé are from Trace 44 - sresa2.ccma\_cgcm3\_1.4. Maps are shown with decimal latitude and longitude coordinates.



To better understand the differences in storm patterns generated under each weather generation method, analyses of precipitation events greater than certain thresholds were conducted. Figure B3-9 shows the comparison for 2 mm/d (0.08 inches/day [in/d]) and 20 mm/d (0.8 in/d) precipitation events. Figure B3-10 shows the comparison for 50 mm/d (2 in/d) and 100 mm/d (4 in/d) precipitation events. In general, the method applied in the Westwide Climate Risk Assessment (WWRCA) (Salathé 2005) produces precipitation events more similar to those in the observed record, although differences exist at all precipitation thresholds.

**FIGURE B3-9**

Comparison of number of days (percent) with precipitation greater than 2 mm/d (top) and 20 mm/d (bottom) between Maurer et al. (Maurer) and downscaled precipitation for Wood et al. and Salathé (downscaled precipitation from Trace 44 - sresa2.cccma\_cgcm3\_1.4). Maps are shown with decimal latitude and longitude coordinates.

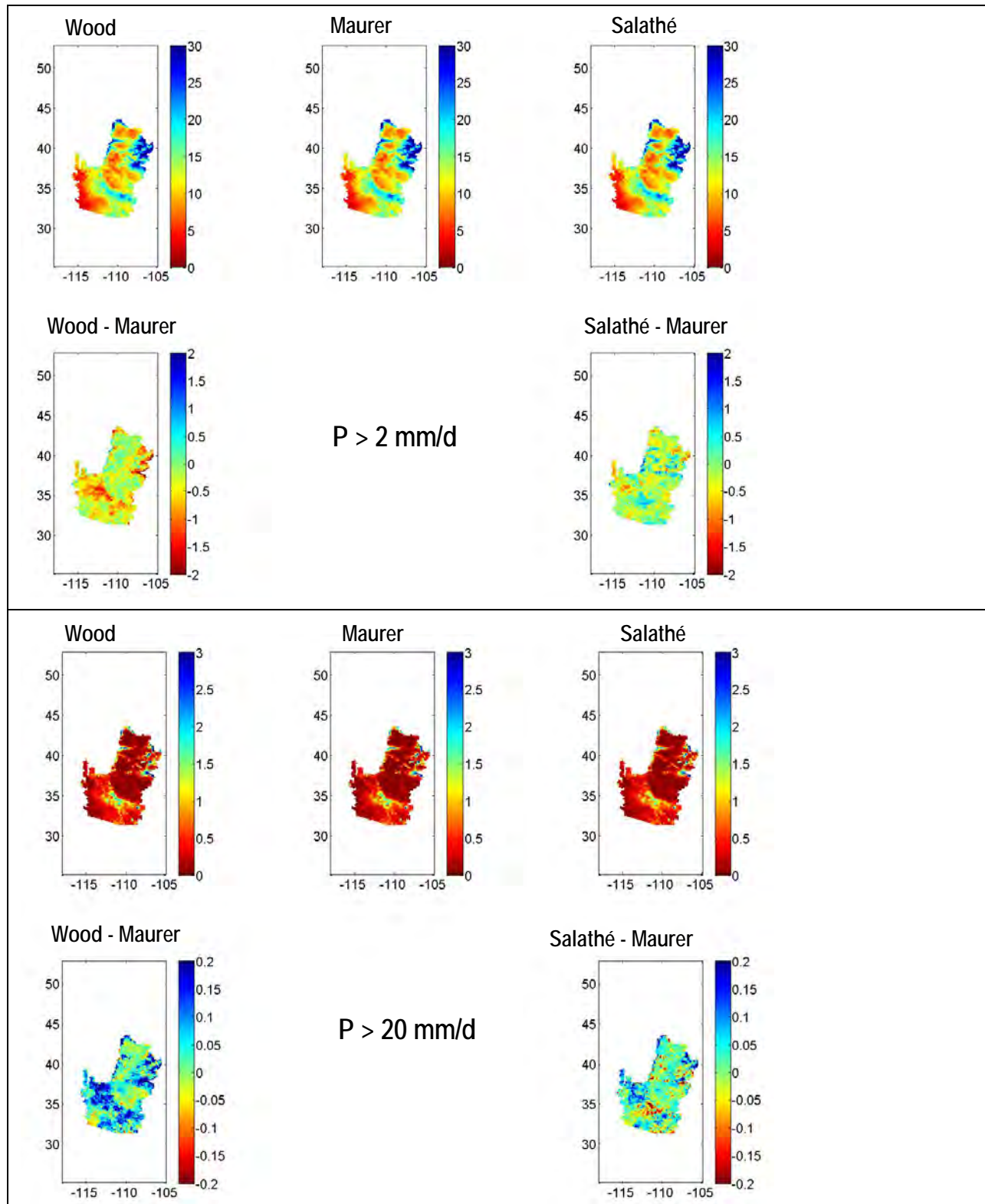
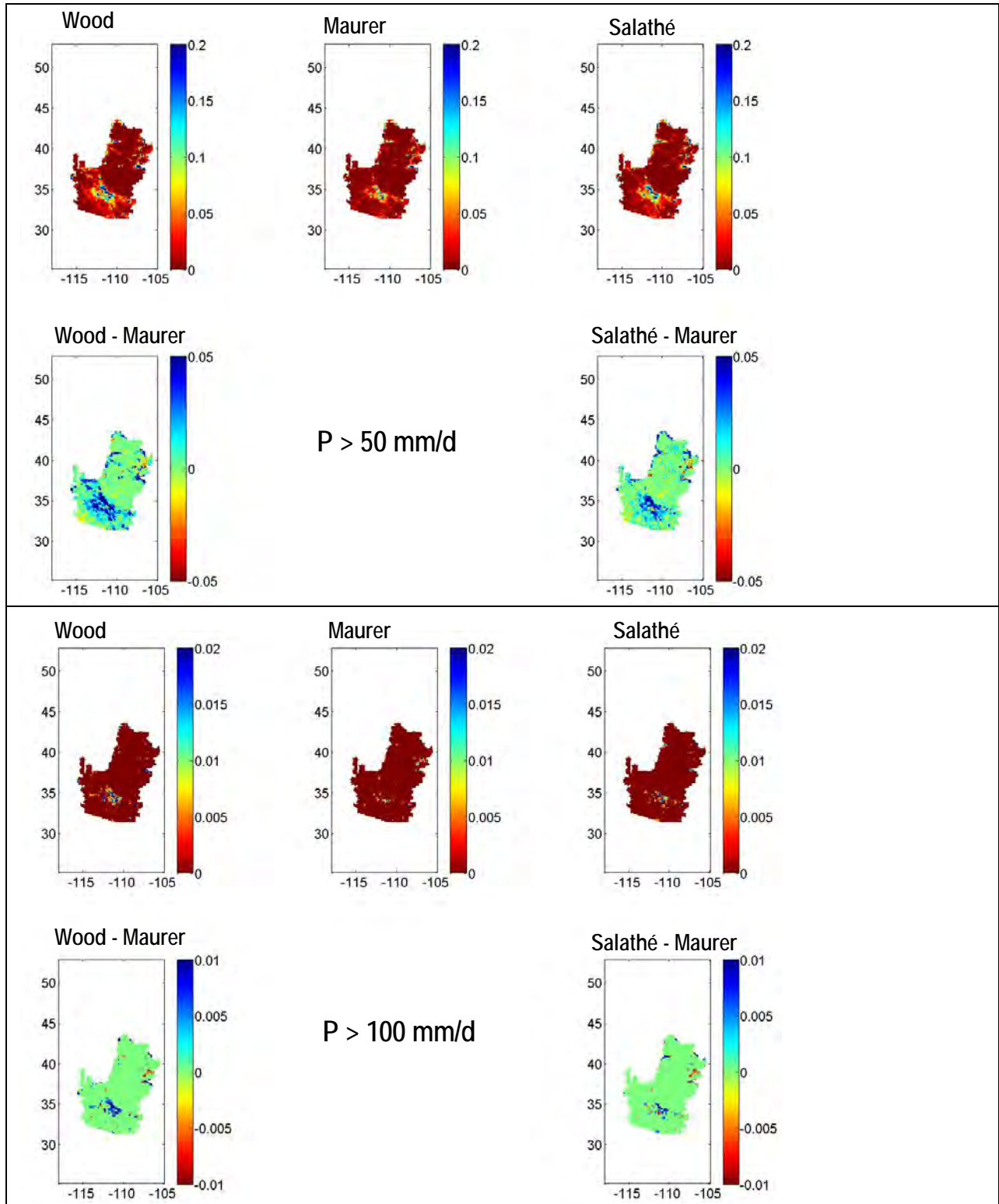


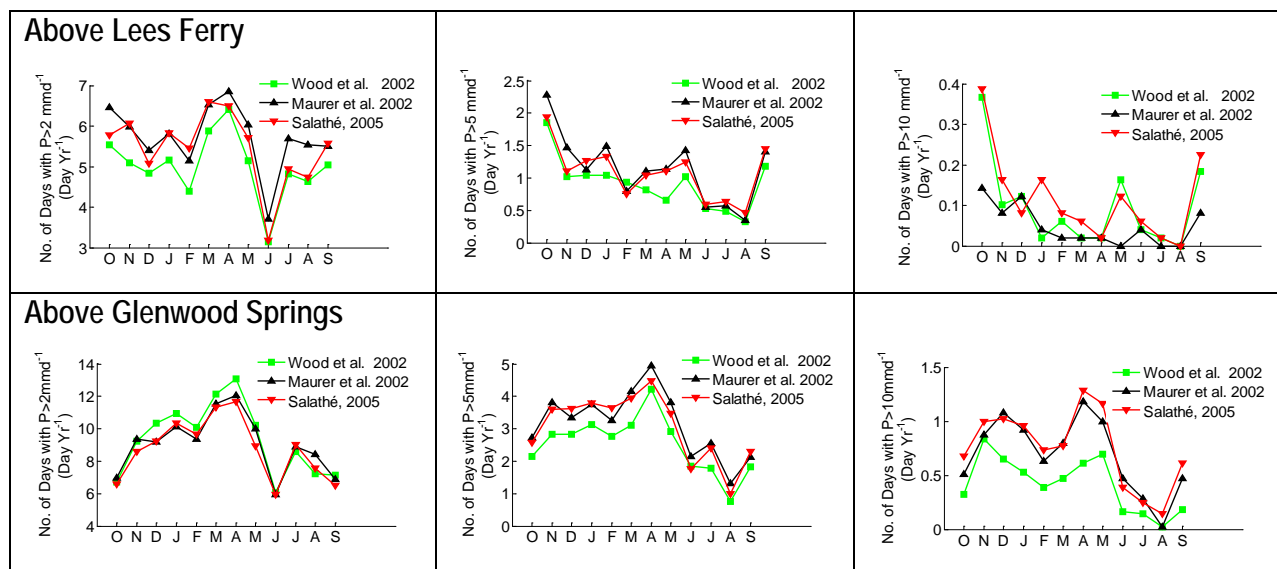
FIGURE B3-10

Comparison of number of days (percent) with precipitation greater than 50 mm/d (top) and 100 mm/d (bottom) between Maurer et al. (Maurer) and downscaled precipitation for Wood et al. and Salathé (downscaled precipitation from Trace 44 - sresa2.cccma\_cgcm3\_1.4). Maps are shown with decimal latitude and longitude coordinates.



The analysis shown in the spatial figures is performed for each grid cell independently and does not reflect spatial correlation during storm events. In figure B3-11, the spatially averaged precipitation for all grid cells above Lees Ferry has been analyzed for thresholds likely to produce runoff (2 mm/d, 5 mm/d, and 10 mm/d). The method employed by Salathé (2005) and incorporated in the WWCRA appears to more faithfully reflect observed precipitation frequencies for this spatial area. This method produces significantly more representative precipitation frequencies to the observed than that used in the previous VIC simulations, particularly at the 2mm/d and 5 mm/d thresholds. At the 10 mm/d threshold, both methods overestimate the frequency of occurrence; however, the observed frequency is already low. For the area above Glenwood Springs (figure B3-12), the method applied by Salathé is significantly better at all precipitation frequencies considered.

**FIGURE B3-11**  
 Number of days per year (averaged over the 1950–1999 period) having precipitation larger than selected thresholds (2 mm/d, 5 mm/d, and 10 mm/d), computed from the daily precipitation over the period 1950–1999 using spatially averaged precipitation for all grid cells above Colorado River at Lees Ferry contributing area (top) and above Colorado River at Glenwood Springs (bottom). Wood et al. and Salathé are from downscaled data from Trace 44 - sresa2.cccma\_cgcm3\_1.4. Values are also shown from Maurer et al. observed daily forcing for comparison purpose.



Finally, VIC simulations were prepared using the two methods of daily weather generation for the historical period 1950–1999 using identical GCM-simulated monthly climate. These simulations were compared to the VIC simulation using historical observed climate; and the natural flow estimates for the Colorado River at Lees Ferry, Arizona. The VIC historical validation (VIC simulation using the historical observed methodology) suggests an overestimation of mean annual flows by about 4 percent. Of the two daily weather generation methods, the VIC simulation using the Salathé method is closest to this historical validation simulation (table B3-2); 2.8 percent compared to 5.8 percent using the Wood et al. method. While the differences between methods appear to be relatively small in percentage terms, the difference in mean annual flows is nearly 500,000 acre-feet between methods.

TABLE B3-2

Annual average streamflows at Colorado at Lees Ferry computed from the period 1950–1999.

<b>Colorado River at Lees Ferry Estimate (1950–1999)</b>	<b>Mean Annual Flow (maf)</b>	<b>% Difference from Natural Flow Estimate (% Difference from Validation)</b>
Reclamation Natural Flow Estimate	14.673	--
VIC Historical Validation	15.248	3.9%
VIC Historical Simulation (Trace 44, Wood et al.)	14.362	-2.1% (-5.8%)
VIC Historical Simulation (Trace 44, Salathé)	14.839	1.1% (-2.8%)

## 4.0 Conclusions

Based on the analysis of climate data, biases, and weather generation methods, several conclusions can be drawn. First, while the bias correction of GCM-simulated climate occurs to preserve monthly statistics, biases for seasonal, annual, and multi-year exist even at the 2-degree spatial resolution. Second, spatial downscaling of climate data to the 1/8<sup>th</sup>-degree resolution, required for hydrologic analysis, introduces small biases at the monthly scale that do not exist in the 2-degree data. Finally, even under identical monthly climate forcings, the method for developing daily patterns of precipitation is important and can contribute to substantially different streamflow results. The analysis included in this study addresses these findings by adopting the Salathé approach of daily weather generation because it produced smaller overall biases as compared to the historical validation simulations. In addition, the analysis indicates that biases in climate data and hydrologic simulation will continue to be present, and that a final adjustment to VIC-simulated streamflows is necessary to use these flows in comparable fashion in systems modeling. For these reasons, a method for bias correction of resulting VIC-simulated flows is incorporated and discussed in the appendix B4, *Variable Infiltration Capacity (VIC) Hydrologic Modeling Methods and Simulations*.

## 5.0 References

- Christensen, N.S., Lettenmaier, D.P. 2007. A Multimodel Ensemble Approach to Assessment of Climate Change Impacts on the Hydrology and Water Resources of the Colorado River Basin. *Hydrology and Earth System Sciences*, 11, 1417–1434.
- Maurer, E.P., Wood, A.W., Adam, J.C., Lettenmaier, D.P., Nijssen, B. 2002. A Long-Term Hydrologically-Based Data Set of Land Surface Fluxes and States for the Conterminous United States, *Journal of Climate*, 15(22), 3237-3251.
- Salathé E.P. 2005. Downscaling simulations of future global climate with application to hydrologic modeling. *Int J Climatol* 25:419–436
- Wood, A.W., E.P. Maurer, A. Kumar, and D.P. Lettenmaier. 2002. Long-range experimental hydrologic forecasting for the Eastern United States, *J. Geophysical Research-Atmospheres*, 107(D20), 4429, DOI:10.1029/ 2001JD000659.



**Appendix B4**  
**Variable Infiltration Capacity (VIC) Hydrologic**  
**Modeling Methods and Simulations**

---



# Appendix B4—Variable Infiltration Capacity (VIC) Hydrologic Modeling Methods and Simulations

The Variable Infiltration Capacity (VIC) model (Liang et al., 1994; Liang et al., 1996) is the hydrology model used in this study to simulate the hydrologic response of the Colorado River Basin (Basin) to historical and future climate. The results from VIC simulations are used to describe the range of streamflows under the Downscaled General Circulation Model (GCM) Projected scenario. Each of the 112 downscaled climate projections is used as input into the VIC hydrology model. The VIC hydrology model uses the climate projections along with land cover, soils, elevation, and other watershed information to simulate hydrologic fluxes. The hydrologic fluxes are then routed to each of the 29 natural flow locations using a routing network derived from the topography. The result of this approach is 112 unique sequences of natural flow under future climate projections. However, the simulated natural flows can contain significant monthly and annual biases when compared to the natural flows of the historical period. These biases are generally small for mainstem Colorado River locations, but can be large for smaller watersheds and in areas where the VIC model was not specifically calibrated. To account and compensate for these biases, the VIC-simulated streamflows for both the historical and future periods are first adjusted for biases before incorporating into systems modeling. This appendix describes the VIC hydrology model, methods, and simulations included in the Colorado River Basin Water Supply and Demand Study (Study).

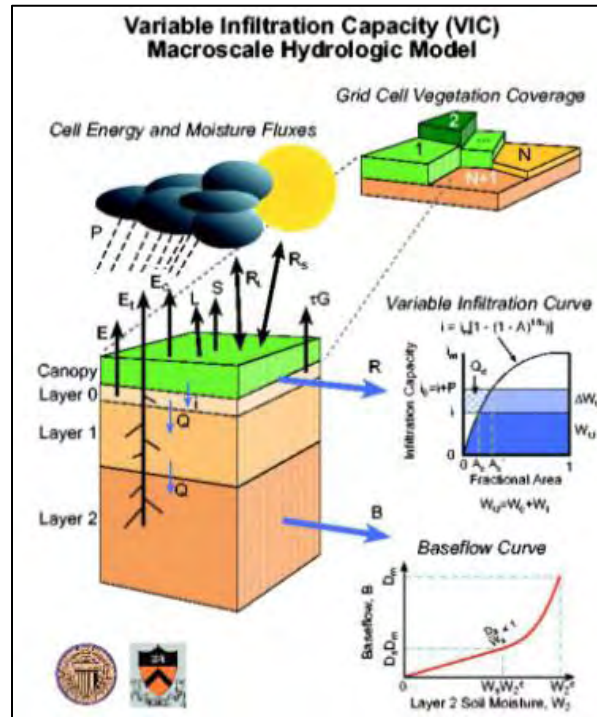
## 1.0 General Description of VIC

The VIC model (Liang et al., 1994; Liang et al., 1996) is a spatially distributed hydrologic model that solves the water balance at each model grid cell. It incorporates spatially distributed parameters describing topography, soils, land use, and vegetation classes. VIC is considered a macro-scale hydrologic model in that it is designed for larger basins with fairly coarse grids. In this manner, it accepts input meteorological data directly from global or national gridded databases or from GCM projections. To compensate for the coarseness of the discretization, VIC is unique in its incorporation of sub-grid variability to describe variations in the land parameters as well as precipitation distribution. Parameterization within VIC is performed primarily through adjustments to parameters describing the rates of infiltration and baseflow as a function of soil properties, as well as the soil layers' depths. When simulating in water balance mode, VIC is driven by daily inputs of precipitation, maximum and minimum temperature, and wind speed. The model internally calculates additional meteorological forcings such as short- and long-wave radiation, relative humidity, vapor pressure, and vapor pressure deficits. Rainfall, snow, infiltration, evapotranspiration (ET), runoff, soil moisture, and baseflow are computed over each grid cell on a daily basis for the entire period of simulation. An offline routing tool then processes the individual cell runoff and baseflow terms and routes the flow to develop streamflow at various locations in the watershed. Figure B4-1 shows the hydrologic processes included in the VIC model.

FIGURE B4-1

Hydrologic Processes Included in the VIC Model

Source: <http://www.hydro.washington.edu/Lettenmaier/Models/VIC/Overview/ModelOverview.shtml>.



The VIC model has been applied to many major basins in the United States, including large-scale applications to California’s Central Valley (Maurer et al., 2002; Brekke et al., 2008; Cayan et al., 2010), Colorado River Basin (Christensen and Lettenmaier, 2007), Columbia River Basin (Hamlet et al., 2010), and for several basins in Texas (Maurer et al., 2002; CH2M HILL, 2008). The VIC model has a number of favorable attributes for the Study, but VIC’s three most significant advantages are that it has a reliable, physically based model of ET, it has a physically based model of snow dynamics, and it has been used for two studies of climate change in the Basin for which calibrated parameters are available.

## 2.0 VIC Modeling Methods Specific to the Colorado River Basin

### 2.1 Model Inputs

The VIC model was driven by meteorological forcing data. Although the model has some flexibility in what variables are required, forcing files typically include daily values for precipitation, maximum temperature, minimum temperature, and wind speed. The VIC model required that the forcing files be in either American Standard Code for Information Interchange or binary format, with one file for each grid cell of the simulation domain. The model grid for the Basin consists of approximately 4,500 grid cells at a 1/8<sup>th</sup>-degree latitude by longitude spatial resolution.

Daily gridded observed meteorology data were obtained from Santa Clara University (Maurer et al., 2002) for the period 1950–1999. Projections of monthly future climate data

were obtained from the Lawrence Livermore National Laboratory under the World Climate Research Program's (WCRP's) Coupled Model Intercomparison Project Phase 3 (CMIP3) and using the weather general (temporal disaggregation) methods described in appendix B3. Wind speed in the future projections was not adjusted in these analyses because downscaling of this parameter was not available, nor well translated from global climate models to local scales.

## 2.2 VIC Model Processes and Output

The VIC model was simulated in water balance mode. In this mode, a complete land surface water balance is computed for each grid cell on a daily basis for the entire model domain. Unique to the VIC model is its characterization of sub-grid variability. Sub-grid elevation bands enable more-detailed characterization of snow-related processes. Five elevation bands are included for each grid cell. In addition, VIC also includes a sub-daily (1-hour) computation to resolve transients in the snow model. The soil column is represented by three soil zones extending downward from the land surface to capture the vertical distribution of soil moisture. The VIC model represents multiple vegetation types using the National Atmospheric and Space Administration's (NASA's) Land Data Assimilation System databases as the primary input data set.

For the simulations performed for the Basin, the following water balance parameters were produced as output on a daily and monthly time step: precipitation, runoff, baseflow, ET, soil moisture, and snow water equivalent. The runoff simulated from each grid cell is routed to various river flow locations using VIC's offline routing tool. The routing tool processes individual cell runoff and baseflow terms and routes the flow based on flow direction and flow accumulation inputs derived from digital elevation models. For the simulations performed for the Basin, intervening streamflow was routed to 29 locations that align with the 29 natural flow locations in the Colorado River Simulation System, the Bureau of Reclamation's (Reclamation's) long-term planning model and the primary modeling tool that will be used in the Study. Flows are output in both daily and monthly time steps. Only the monthly flows were used in subsequent analyses. It is important to note that VIC routed flows are considered "naturalized" in that they do not include effects of diversions, imports, storage, or other human management of the water resource.

## 3.0 Colorado River Basin VIC Model Validation

A VIC model of the Basin was previously developed by the University of Washington (Christensen and Lettenmaier, 2007), and was provided to Reclamation for this study. The VIC model has not been further calibrated or refined as part of this Study, but the model performance over the 1950–1999 validation period is described in this section.

The VIC historical validation run is simulated on a daily time step over the 1950–1999 period. Historical observed climate inputs are from Maurer et al. (2002). Streamflow is routed to each of the 29 natural flow locations used by Reclamation in Basin planning. Figure B4-2 shows the validation results for the Colorado River at Lees Ferry, Arizona location. The VIC simulation results in an overestimation of mean annual flows of about 3.9 percent when compared to the Reclamation natural flow estimate. The validation run captures the low and moderate annual flows, but has a slight overestimation of the high annual flows. Simulated flows in April and May flows are higher than Reclamation

calculated historical natural flows, while July and August flows are slightly lower. Simulated flows for Colorado River at Cisco, Green River at Green River, Utah, and the San Juan River near Bluff, Utah, are shown in figures B4-3 through B4-5. The simulated flows show a slight overestimation for the Colorado River at Cisco and Green River at Green River stations when compared to the Reclamation natural flow estimates, while an underestimation is apparent for the San Juan River near Bluff station. Pearson's linear correlation coefficient, bias, and root mean square error (RMSE) are computed using the observed naturalized and VIC simulated streamflows as driven by Maurer et al. (2002) over the 1950–1999 validation period for all 20 locations in the Upper Basin. These results are summarized in table B4-1. In general, the VIC model appears to have relatively small biases for the larger watersheds as compared to the Reclamation natural flow estimates, but can be larger for smaller watersheds and in areas where the VIC-model was not specifically calibrated. The VIC model appears to have higher biases in the upper watersheds and lower biases farther downstream as more watershed contributes to the flow.

FIGURE B4-2  
VIC Validation Summary for Colorado River at Lees Ferry, Arizona

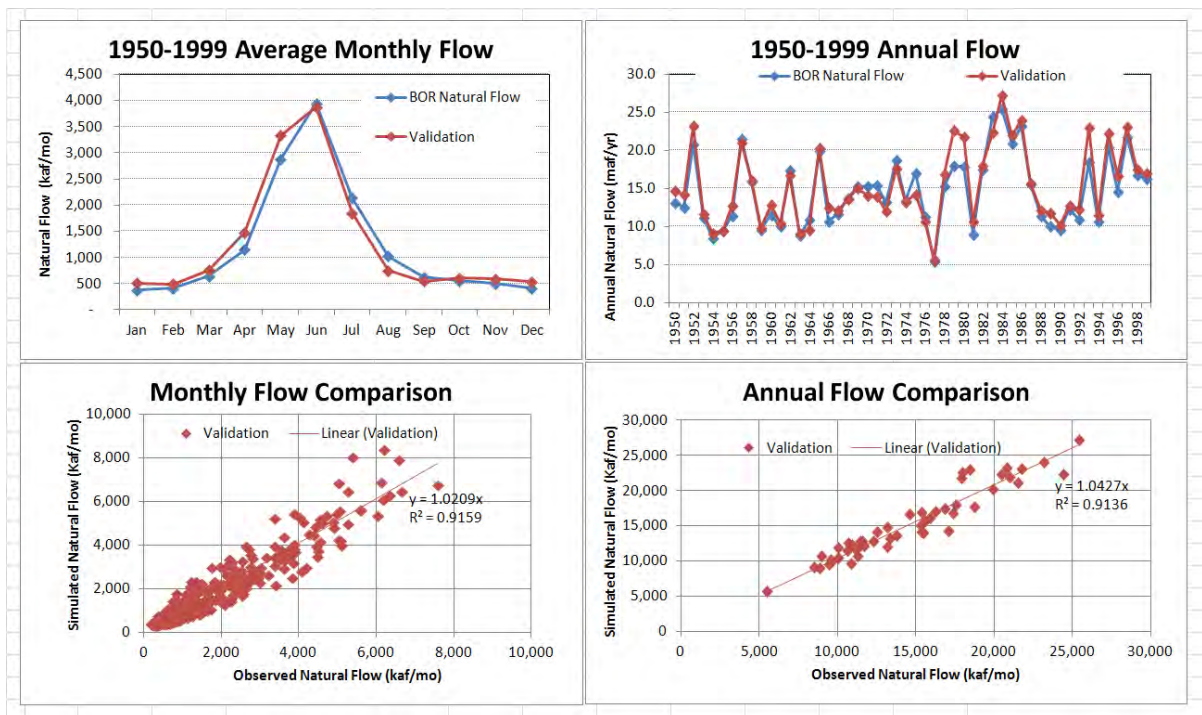


FIGURE B4-3  
VIC Validation Summary for Colorado River at Cisco, Utah

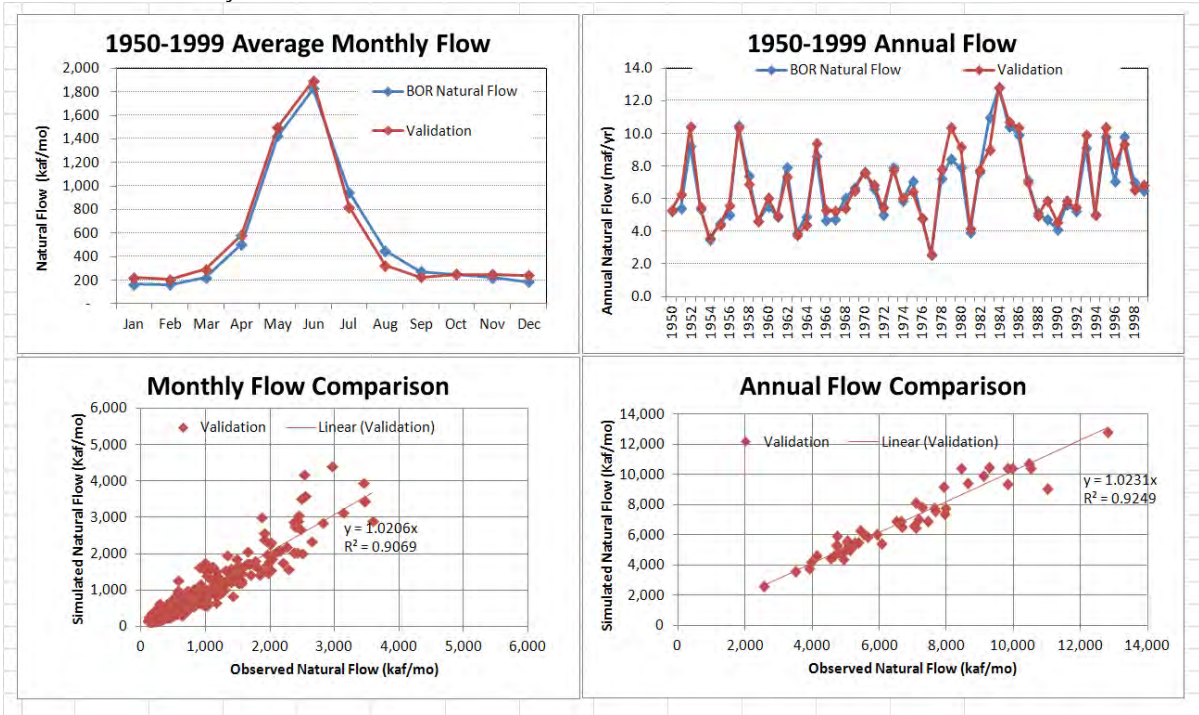


FIGURE B4-4  
VIC Validation Summary for Green River at Green River, Utah

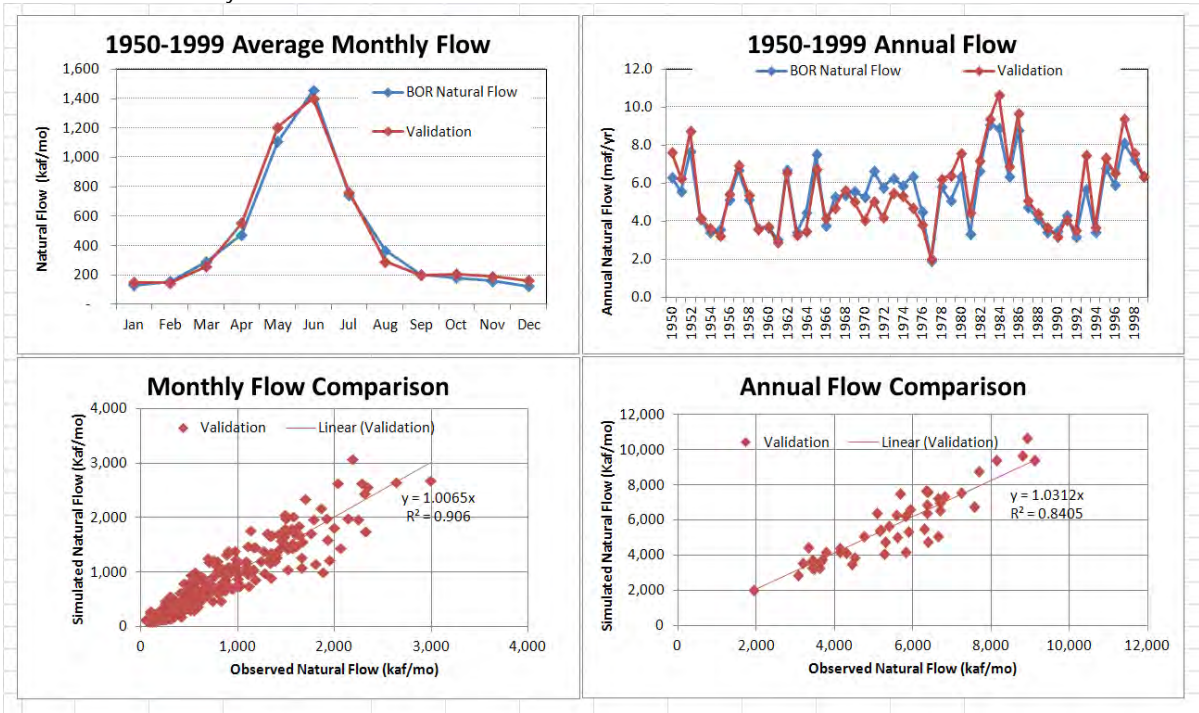


FIGURE B4-5  
VIC Validation Summary for San Juan River near Bluff, Utah

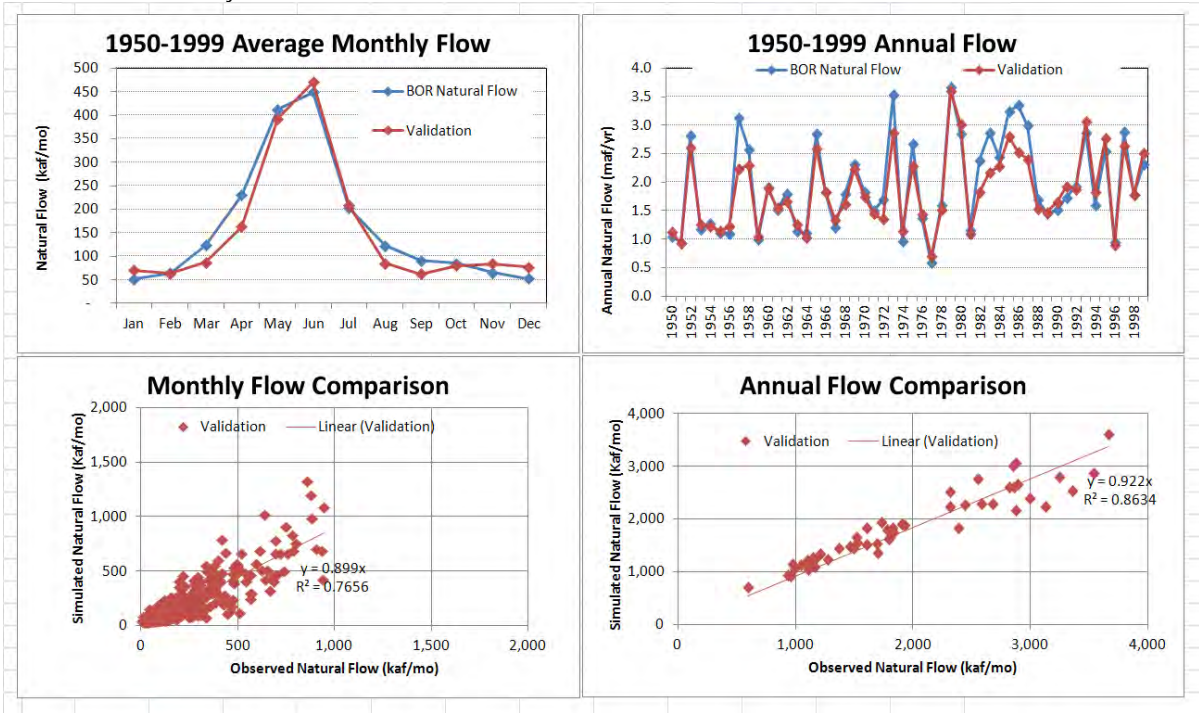


TABLE B4-1

Observed annual naturalized streamflow and VIC simulated streamflow (with Maurer et. al (2002) historical meteorology) comparison statistics (1950–1999)

ID	Location	Obs Nat Flow (KAF)	VIC Nat Flow (KAF)	Bias (%)	Pearson's linear correl coef	RMSE (KAF)	RMSE (% of mean flow)
1	Colorado River At Glenwood Springs, CO	2,071	2,192	5.8%	0.9	360.0	17.4%
2	Colorado River Near Cameo, CO	3,489	3,741	7.2%	0.9	546.4	15.7%
3	Taylor River Below Taylor Park Reservoir, CO	148	172	15.9%	0.8	48.2	32.5%
4	Gunnison River Above Blue Mesa Reservoir, CO	1,045	1,316	26.0%	0.9	332.3	31.8%
5	Gunnison River At Crystal Reservoir, CO	1,273	1,494	17.4%	0.9	325.5	25.6%
6	Gunnison River Near Grand Junction, CO	2,304	2,336	1.4%	0.9	295.2	12.8%
7	Dolores River Near Cisco, UT	789	554	-29.7%	0.9	307.0	38.9%
8	Colorado River Near Cisco, UT	6,647	6,829	2.7%	1.0	640.4	9.6%
9	Green R Bel Fontenelle Res, WY	1,364	1,079	-20.9%	0.8	396.8	29.1%
10	Green R. Nr Green River, WY	1,469	1,226	-16.5%	0.8	359.1	24.5%
11	Green River Near Greendale, UT	2,009	1,971	-1.9%	0.8	392.3	19.5%
12	Yampa River Near Maybell, CO	1,210	1,086	-10.2%	0.9	196.4	16.2%
13	Little Snake River Near Lily, CO	466	580	24.3%	0.8	173.1	37.1%
14	Duchesne River Near Randlett, UT	778	920	18.2%	0.9	291.1	37.4%
15	White River Near Watson, UT	557	525	-5.7%	0.8	167.1	30.0%
16	Green River At Green River, UT	5,397	5,440	0.8%	0.9	785.7	14.6%
17	San Rafael River Near Green River, UT	161	273	69.1%	0.7	152.8	94.8%
18	San Juan River Near Archuleta, NM	1,028	869	-15.5%	0.9	268.2	26.1%
19	San Juan River Bluff, UT	1,953	1,856	-5.0%	0.9	292.6	15.0%
20	Colorado R At Lees Ferry, AZ	14,673	15,248	3.9%	1.0	1550.9	10.6%

## 4.0 Application of Streamflow Bias Correction

The analysis presented in appendix B3 shows that there are some biases in the VIC streamflows as driven by GCM simulated historic meteorological forcings in comparison with the naturalized streamflows for the Basin for the overlapping period 1950–1999. These

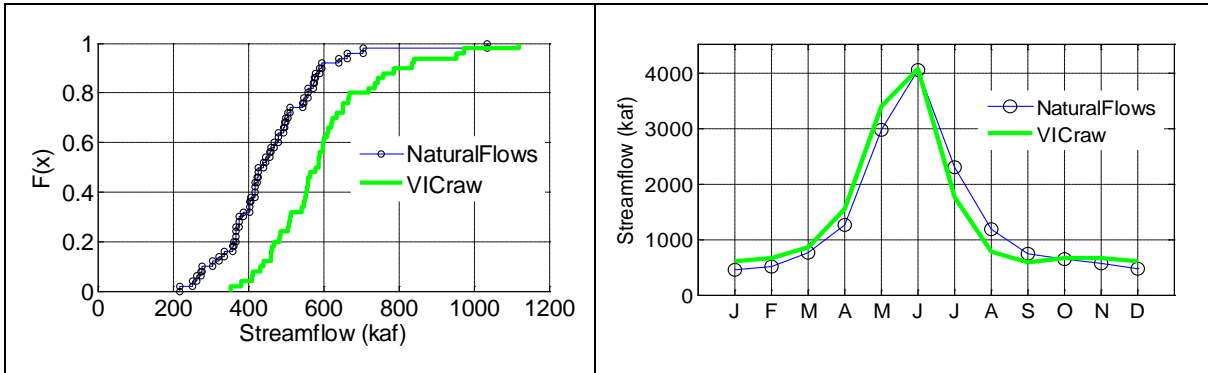
biases result from several factors, including spatial and temporal errors in downscaled climate model forcings, complex groundwater interactions, and other complexities normally inherent to VIC hydrologic model parameter calibration. The analysis showed there are some uncertainties in the daily disaggregation method that was used to produce daily meteorological forcings from the monthly downscaled meteorology (see appendix B3). Daily meteorological data are required to drive the VIC. Moreover, there are uncertainties related to VIC model processes and parameter calibration demonstrated through comparisons of VIC simulated historical streamflows with the naturalized streamflows for the Basin. Bias-corrections of the downscaled climate model simulated VIC streamflows are performed to better reflect the statistics of the observed streamflows for the historical simulation period. This document describes the method developed to bias-correct the streamflows for the Basin. The method has been implemented for all 29 river locations for the period 1950–1999 for VIC simulation for each of the 112 projections. Results are presented for one particular projection (Trace 44, sresa2.cccma\_cgcm3\_1.4) to demonstrate the process. VIC streamflows generated under future climate projections incorporate the same bias correction process before determining the flow projections for use in systems modeling.

The streamflow bias correction accounts for monthly and annual statistical bias at each of the 29 flow locations. Following the station-specific adjustments, the total Basin mass balance is again checked and adjustments are made such that flow continuity is maintained throughout the Basin. The streamflow bias correction involves the following steps:

1. Evaluate the monthly and annual bias in VIC simulated streamflows as compared to the observed natural flows for each of the 29 locations.

FIGURE B4-6

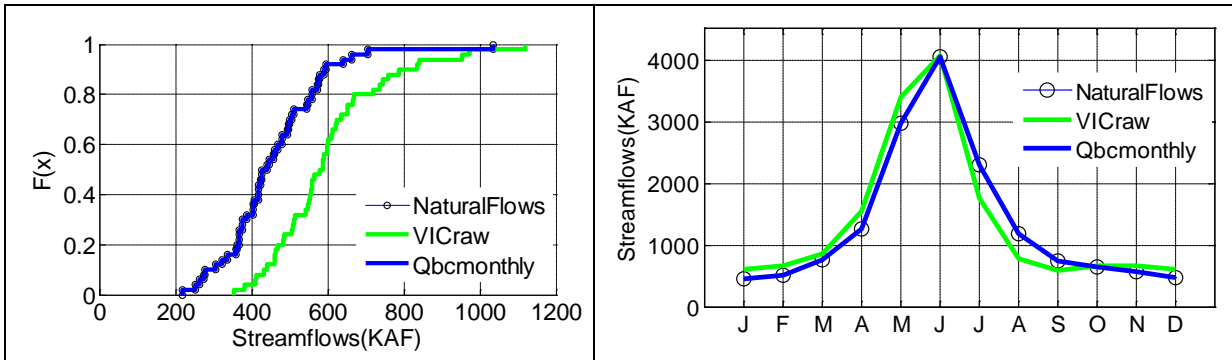
Left, comparisons of the common data formats (CDFs) developed from the VIC simulated streamflows as driven by downscaled climate model forcings from Trace44 and the naturalized streamflows for the month of January for the Colorado River at Parker Dam, Arizona. Right, comparisons of mean monthly streamflows from the VIC simulated and naturalized streamflows.



2. Develop a quantile map that aligns the observed CDF with the simulated CDF for each simulated month for the period 1950–1999 at each location. For each simulated value, determine the simulated percentile and adjust to be equal to the observed flow at the same percentile. This method preserves the mean and variance of the observed flows.

FIGURE B4-7

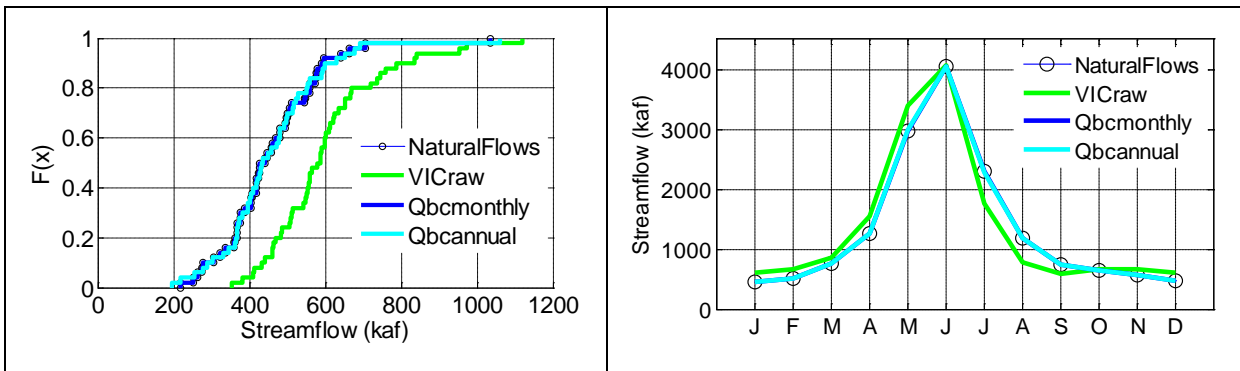
Left, comparisons of the CDFs developed from the VIC simulated streamflows as driven by downscaled climate model forcings from Trace44, the naturalized streamflows and bias corrected streamflows for the month of January. Right, comparisons of mean monthly streamflows from the VIC simulated, naturalized and bias corrected streamflows.



3. Re-scale the monthly values (if needed) to ensure that the annual simulated CDF aligns with the observed CDF. For each simulated annual flow value from step 2, determine the percentile and adjust to be equal to the observed flow at the same percentile. This step ensures that the adjusted streamflows are consistent at the annual scale.

FIGURE B4-8

Same as figure B4-7, but with adjustment in the streamflows based on the annual flows.



Since the bias correction is performed for each station independently, this can create discrepancies in spatial mass balance. Additional steps described below are performed to remove any spatial mass balance inconsistencies. The procedure begins from the most downstream location and moving upstream, as described below:

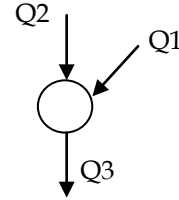
4. Anchor the calculations at the most downstream location (i.e., bias corrected streamflows at the Imperial Dam are unaltered).

- Compare bias corrected flows at upstream locations (including incremental flows) with the downstream location. Compute the difference ( $\Delta_{mon}$ ) as the downstream-computed monthly flow ( $Q_{ds}$ ) minus the upstream-computed monthly flow ( $Q_{us}$ ), then adjust all upstream flows based on their relative flow contribution.

$$\Delta_{mon} = Q_{ds} - Q_{us} \text{ or (e.g. } Q_3 - (Q_1+Q_2) \text{)}$$

$$Adj_{i, mon} = \Delta_{mon} * |Q_i| / \sum(|Q_{i..n}|) \text{ or}$$

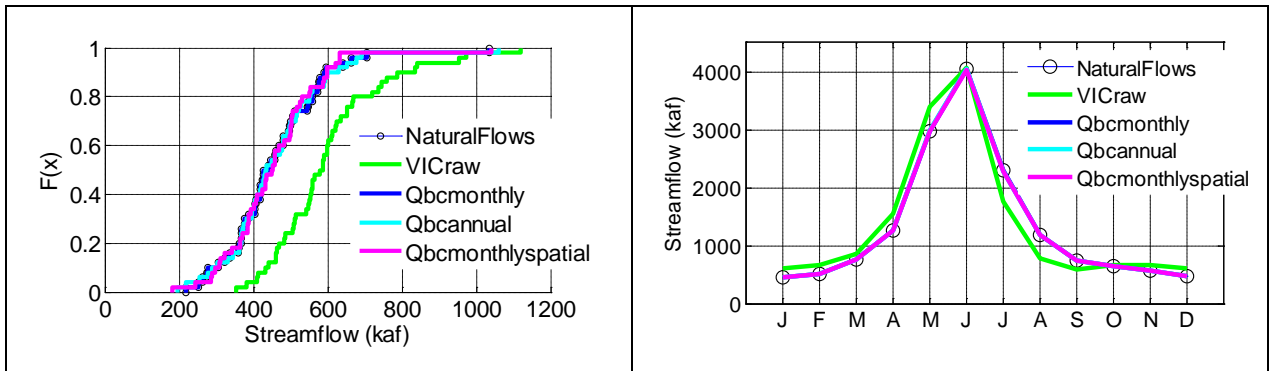
$$[\text{e.g. } Adj_{1, mon} = \Delta_{mon} * |Q_1| / (|Q_1| + |Q_2|)]$$



This process results in consistent mass balance on monthly scales (i.e.,  $Q_3=Q_1+Q_2$ ).

FIGURE B4-9

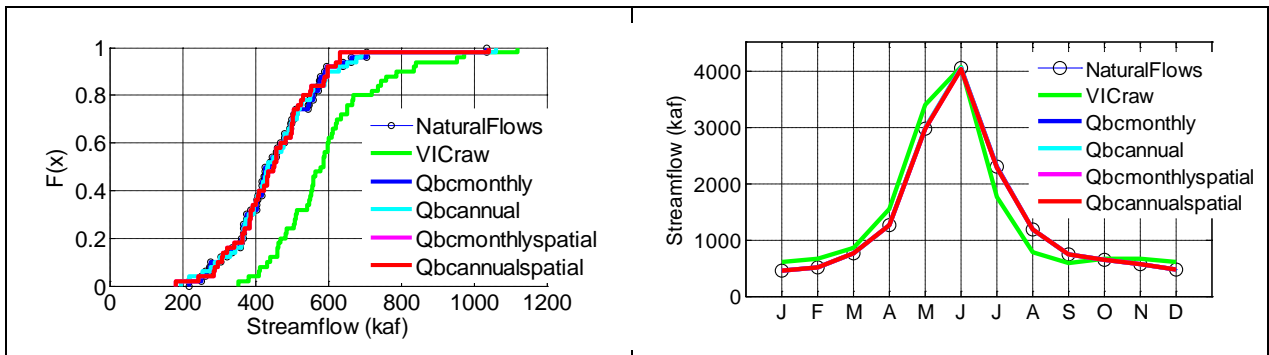
Same as figure B-8, but with spatial mass balance adjustment in the streamflows based on the monthly flows.



- Finally, a verification check is performed based on the annual flows to ensure that all mass balance and corrections have been implemented correctly.

FIGURE B4-10

Same as figure B4-9, but with adjustment in the streamflows based on the annual flows.



A summary of the biases for each step in the bias correction process is shown for one climate projection simulation (table B4-2). The process is automated such that each Downscaled GCM Projection streamflow is bias corrected independently. The results from the VIC simulation presented in table B4-2 will be different than those presented in table B4-1 because the VIC simulation is driven by two different meteorological datasets. Table B4-2

shows the results when simulated over the historical period with one GCM simulated historical climate. The bias thus represents both hydrologic and meteorologic bias. The “station” bias correction column shows the resulting biases after conducting steps 1 through 3 in the streamflow bias correction above. The “spatial balance” bias correction column shows the resulting biases after conducting steps 1 through 6, and represents the final residual bias in the model results.

TABLE B4-2

Summary of biases at the 20 Upper Basin natural flow stations at each step in the bias correction process.

ID	Location	Obs Nat Flow	VIC Nat Flow	% Bias	% Differences of Streamflows	
					Station Bias-correction	Spatial Balance Bias-correction
Stn01	Colorado River At Glenwood Springs, CO	2,071	2,181	5.3%	0.0%	1.3%
Stn02	Colorado River Near Cameo, CO	3,489	3,701	6.1%	0.0%	0.9%
Stn03	Taylor River Below Taylor Park Reservoir, CO	148	174	17.0%	0.0%	2.4%
Stn04	Gunnison River Above Blue Mesa Reservoir, CO	1,045	1,314	25.8%	0.0%	1.3%
Stn05	Gunnison River At Crystal Reservoir, CO	1,273	1,486	16.7%	0.0%	0.6%
Stn06	Gunnison River Near Grand Junction, CO	2,304	2,293	-0.5%	0.0%	-0.3%
Stn07	Dolores River Near Cisco, UT	789	537	-32.0%	0.0%	-2.5%
Stn08	Colorado River Near Cisco UT	6,647	6,699	0.8%	0.0%	0.2%
Stn09	Green R Bel Fontenelle Res WY	1,364	1,062	-22.1%	0.0%	2.1%
Stn10	Green R. Nr Green River, WY	1,469	1,198	-18.5%	0.0%	1.7%
Stn11	Green River Near Greendale, UT	2,009	1,881	-6.4%	0.0%	1.6%
Stn12	Yampa River Near Maybell, CO	1,210	1,078	-10.9%	0.0%	0.9%
Stn13	Little Snake River Near Lily, CO	466	558	19.6%	0.0%	0.2%
Stn14	Duchesne River Near Randlett, UT	778	872	12.1%	0.0%	1.3%
Stn15	White River Near Watson, UT	557	516	-7.2%	0.0%	1.0%
Stn16	Green River At Green River, UT	5,397	5,234	-3.0%	0.0%	1.0%
Stn17	San Rafael River Near Green River, UT	161	262	62.2%	0.0%	-1.3%
Stn18	San Juan River Near Archuleta, NM	1,028	867	-15.7%	0.0%	-0.8%
Stn19	San Juan River Near Bluff, UT	1,953	1,835	-6.0%	0.0%	-0.7%
Stn20	Colorado R At Lees Ferry, AZ	14,673	14,839	1.1%	0.0%	0.3%

## 5.0 VIC Simulated Hydrologic Fluxes

While the primary result of the VIC modeling is streamflow for use in Colorado River system modeling, the model also produces hydrologic fluxes that are important in describing the causes of changes in streamflows. This section provides details on the methods and use of such hydrologic fluxes.

### 5.1 Climate and Gridded Hydrologic Process Analysis Methods

Gridded climate and hydrologic process data were generated by the VIC model for the historical and the 112 climate projection scenarios. These data were converted to a specialized format, allowing for statistical analysis and visualization via spatial mapping. This analysis was performed to better understand the primary factors, both climatological and hydrological, that drive projected changes in streamflows relative to historical conditions.

### 5.2 Production of Gridded Data Sets

In addition to streamflows, the VIC model exports climate and hydrologic data for each simulation. The climate data include average air temperature (°C) generated during the model simulations and precipitation (mm), which is consistent with the data provided in the model input files. Hydrologic parameters include evapotranspiration (ET), runoff (surface runoff), baseflow (subsurface runoff), soil moisture (in each of three soil layers), and snow water equivalent (SWE). Both the climate and hydrologic data are stored in American Standard Code for Information Interchange (ASCII)-formatted text files known as “flux files.” One

flux file is produced for every grid cell of the study area, and each file contains values for the specified parameters at every time step of the simulation.

The flux file output generated by the VIC model was converted to netCDF to more readily evaluate and visualize the data. Developed by the staff at the Unidata Program Center in Boulder, Colorado, netCDF is a machine-independent data format for array-oriented (i.e., multi-dimensional) scientific data. In particular, netCDF is well suited to spatially gridded time series data, such as gridded climate data. Unidata has developed a variety of software libraries and tools that support the creation, manipulation, and analysis of multi-dimensional data. Unidata's netCDF-Java library was used to develop an application-specific Java program to convert the VIC flux files from ASCII format to netCDF format.

The resulting netCDF files are each three-dimensional, defined by latitude, longitude, and time. The spatial extent of the hydrologic basin spans from 31.3125 °N to 43.4375 °N and from 115.6875 °W to 105.6875 °W. Given a grid cell size of 1/8th-degree, the latitude dimension spans 98 grid cells and the longitude dimension spans 81 grid cells, for a total 7,938 grid cells. The temporal extent of the data is from 1950 to 2099. Given a monthly time step, the time dimension consists of 1,800 values.

The complete list of parameters included in the netCDF files is as follows:

- Average air temperature (°C)
- Precipitation (mm)
- ET (mm)
- Potential ET (mm)
- ET Efficiency (percent)
- Runoff (surface) (mm)
- Baseflow (subsurface) (mm)
- Total Runoff (mm)
- Total Runoff Efficiency (percent)
- Soil Moisture Sum (mm)
- Maximum Soil Moisture (mm)
- Soil Moisture Fraction (percent)
- SWE (mm)

One netCDF file was produced for each climate projection and for the historic scenario, for a total of 113 netCDF files.

### **5.3 Statistical Analysis**

To quantify potential changes between historical and future time periods, the VIC output data were statistically evaluated. For each historical and future time period of interest, statistics were developed for the consolidated dataset consisting of all 112 projections, such that the resulting statistics are representative of the 112-member ensemble. Statistics were generated for a subset of the VIC output parameters and derived parameters described previously. The eight parameters evaluated are as follows:

- Average air temperature (°C)
- Precipitation (mm)

- ET (mm)
- ET Efficiency (percent)
- Total Runoff (mm)
- Total Runoff Efficiency (percent)
- Soil Moisture Fraction (percent)
- SWE (mm)

A Java program was developed to process the VIC model output data stored in the netCDF files described previously. The Java program relies heavily on the netCDF-Java library, and on the Descriptive Statistics package of the Apache Commons math library. The statistics generated for each parameter include the mean, standard deviation, variance, skew, minimum, and maximum. In addition, the cumulative distribution function (CDF) for each time period was produced. A CDF describes the probability that a data point will be found at a value less than or equal to some value, “*x*.” For this analysis, “*x*” values corresponding to all integer percentiles from 1 to 100 (inclusive) were generated for each CDF.

### **5.3.1 Analysis Time Periods**

Three future periods were selected for comparison to the historical period. Each period, including the historical, consists of 30 years and is identified by the representative middle value that defines that period. For example, the historical period consists of the years 1971–2000, and is represented by the year 1985. The historical period of 1971–2000 is selected as the reference climate because it was the established climate normal used by the National Oceanic and Atmospheric Administration at the onset of this study. The three future periods selected for analysis were 2011–2040 (represented by the year 2025), 2041–2070 (represented by the year 2055), and 2066–2095 (represented by the year 2080). The last year of the climate projections is 2099, which is 1 year short of a 30-year period starting in 2071. Therefore, the end year for the 2080 period was selected to be 2095. Thus, the 2080 period includes 5 years of overlap (2066–2070) with the 2055 period. For each of the four time periods specified, the representative statistics described previously were generated on a monthly, seasonal, and annual basis. In this analysis, the seasons are defined as follows:

- Fall: October, November, and December
- Winter: January, February, and March
- Spring: April, May, and June
- Summer: July, August, and September

### **5.3.2 Analysis Spatial Scale**

The statistical analysis described previously was conducted on both a grid cell and watershed basis. The results of the grid cell analysis produce the most informative map graphics and clearly show spatial variation at the greatest resolution possible. At this spatial scale, the statistics for each grid cell are developed independently.

In contrast, watershed statistics are developed concurrently for all grid cells that are members of a watershed unit. In this case, a time series of watershed data is generated for each parameter prior to conducting the statistical analysis. For a given watershed, this is done by averaging the values of all member grid cells for each time step of the simulation period. The statistical analysis is then applied to the watershed time series, such that the resulting values

are representative of the watershed as a whole. The watershed analysis results in a more manageable set of outputs and is useful for evaluating trends in different regions of the basin.

### **5.3.3 Statistical Analysis Output**

The resulting statistics are stored in four-dimensional netCDF files, which are defined by latitude, longitude, time, and statistic. The spatial extent of the study area spans from 31.3125 °N to 43.4375 °N and from 115.6875 °W to 105.6875 °W. Given a grid cell size of 1/8<sup>th</sup>-degree, the latitude dimension spans 98 grid cells and the longitude dimension spans 81 grid cells, for a total 7,938 grid cells. The temporal extent of the data consists of 17 values, each of which represents a monthly (1 to 12), annual (13), or seasonal (14 to 17) analysis time. The “statistic” dimension contains 111 values. The first 100 values are integer percentiles corresponding to the CDF distribution. The last 11 values represent the general statistics—mean, standard deviation, variance, skewness, minimum, P10, P25, P50, P75, P90, and maximum. Two netCDF files are produced for each of the four time periods—one for the grid cell-based statistics and one for the watershed-based statistics. Each netCDF file contains statistics representative of the 112-member projection ensemble for each of the eight climatological and hydrologic parameters identified previously. For watershed statistics, text files containing the general statistics and CDF values are also produced for each variable and time period. This output allows for ready production of spreadsheet charts, such as those presented in the results section.

### **5.3.4 Change Metrics**

Finally, change metrics are generated for each parameter, in which the difference between future period statistics and historical period statistics are calculated on both absolute and percent change bases. These results are again stored in netCDF files, with two files generated for each future period—one for grid cell data and one for watershed data. The format of these files is identical to those containing the results of the statistical analysis.

## **6.0 VIC Model Limitations**

The VIC model and simulations described in this appendix include several limitations that should be considered:

- Although the VIC model contains several sub-grid mechanisms, the coarse-grid scale should be noted when considering results and analysis of local-scale phenomenon. The VIC model is currently best applied for the regional scale hydrologic analyses.
- The VIC model has been applied without re-calibration. As the results suggest, the model is reasonable for capturing flow changes at the larger watersheds in the Basin, but has significant bias at smaller scales. The streamflow bias correction method corrects for much of the bias, but improved VIC calibration would limit the extent of these adjustments.
- The VIC model has been evaluated for monthly and annual time-scales, but daily results have not been assessed. Caution should be used in the use of any daily results due to issues related to daily weather generation of inputs, lack of hydrology model evaluation, and inherent limitations with climate bias correction for extreme events.

- The VIC model is only as good as its inputs. There are several limitations to long-term gridded meteorology related to data, spatial-temporal interpolation, and bias correction that should be considered. In addition, the inputs to the model do not include any transient trends in the vegetation or water management that may affect streamflows; they should only be analyzed from a naturalized flow change standpoint.
- Finally, the VIC model includes three soil zones to capture the vertical movement of soil moisture, but does not include groundwater. In areas where groundwater connectivity with surface process or streamflow is important, the VIC model may not have sufficient subsurface characterization to capture hydrologic responses.

## 7.0 References

- Brekke, L.D., M.D. Dettinger, E.P. Maurer, and M. Anderson. 2008. Significance of Model Credibility in Estimating Climate Projection Distributions for Regional Hydroclimatological Risk Assessments, *Climatic Change* Vol. 89 No. 3-4, 371-394, DOI: 10.1007/s10584-007-9388-3.
- Cayan D.R., Das T., Pierce D.W., Barnett T.P., Tyree M. and Gershunov A. 2010. Future dryness in the southwest US and the hydrology of the early 21st century drought. *Proceedings of the National Academy of Sciences*, 107(50), 21271-21276, DOI: 10.1073/pnas.0912391107.
- CH2M HILL. 2008. Climate Change Study, Report on Evaluation Methods and Climate Scenarios. Lower Colorado River Authority – San Antonio Water System.
- Christensen, N.S., Lettenmaier, D.P. 2007. A Multimodel Ensemble Approach to Assessment of Climate Change Impacts on the Hydrology and Water Resources of the Colorado River Basin. *Hydrology and Earth System Sciences*, 11, 1417–1434.
- Hamlet, A.F., P. Carrasco, J. Deems, M.M. Elsner, T. Kamstra, C. Lee, S-Y Lee, G. Mauger, E. P. Salathé, I. Tohver, L. Whitely Binder. 2010. Final Project Report for the Columbia Basin Climate Change Scenarios Project, <http://www.hydro.washington.edu/2860/report/>.
- Liang, X., Lettenmaier, D.P., Wood E.F., Burges S.J. 1994. A Simple Hydrologically Based Model of Land Surface Water and Energy Fluxes for General Circulation Models. *Journal of Geophysical Research*, vol. 99, pp 14415-14428.
- Liang, X., Lettenmaier, D.P., Wood E.F. 1996. Surface Soil Moisture Parameterization of the VIC-2L Model: Evaluation and Modification.
- Maurer, E.P., Wood, A.W., Adam, J.C., Lettenmaier, D.P., Nijssen, B. 2002. A Long-Term Hydrologically-Based Data Set of Land Surface Fluxes and States for the Conterminous United States, *Journal of Climate*, 15(22), 3237-3251.
- Maurer, E. P., Brekke, L., Pruitt, T., Duffy, P. B. 2007. Fine-resolution climate projections enhance regional climate change impact studies, *Eos Trans. AGU*, 88(47), 504.



**Appendix B5**  
**Supplemental Streamflow Analysis**

---



# Appendix B5— Supplemental Streamflow Analysis

The streamflow analyses presented in this appendix provide additional supporting information consistent with that provided in the Technical Report. The streamflow analysis, as described here, was based on reconstructed natural flows in the Colorado River Basin (Basin). The data consist of two historical datasets. The first dataset (referred to as the observed record) consists of monthly observed natural flows for the period October 1905 to September 2007. The second dataset (referred as the paleo record) consists of monthly flows reconstructed from tree ring analysis for the period October 761 to September 2005.

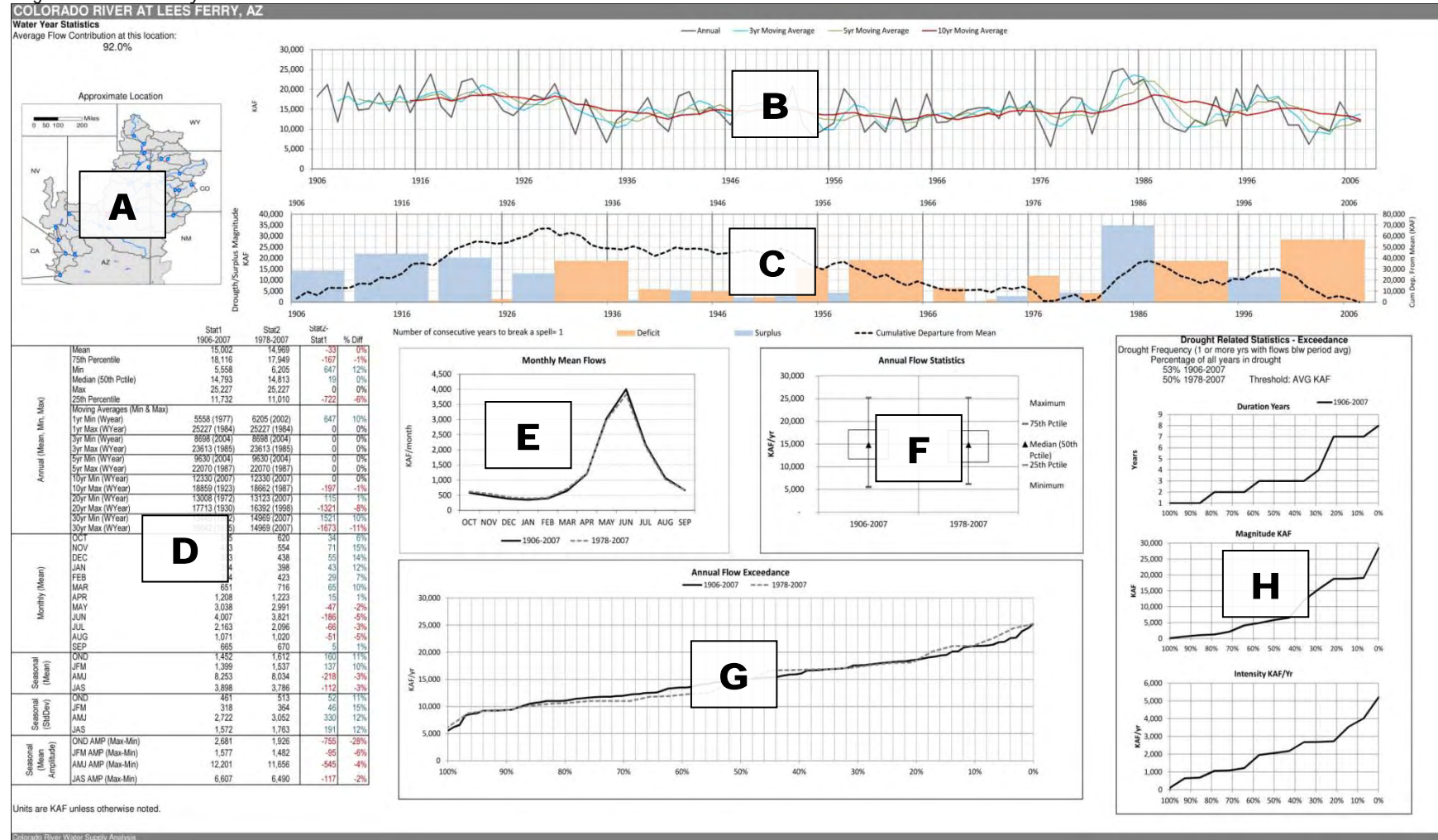
The observed record was provided in the total flows format (flows accumulating from upstream to downstream locations) and intervening format (single watershed flows). The paleo record was provided in an intervening format and had to be accumulated from upstream to downstream basins to obtain a total flows format.

## 1.0 Streamflow Data Summary

Streamflow was analyzed for the 29 natural flow stations that serve as the primary inflow locations for the Colorado River Simulation System (CRSS) model. A spreadsheet tool was constructed to provide an interactive environment to explore the temporal and spatial characteristics of streamflow in the Basin, as shown in figure B5-1. The features of this visual summary are described as follows:

FIGURE B5-1

Summary Graphic for Colorado River at Lees Ferry, Arizona Displaying Streamflow, Annual Exceedance Probabilities, Streamflow Deficits and Surpluses, and Drought Duration, Magnitude and Intensity.



- A. **Streamflow Location:** The approximate location of the flow station being summarized in the spreadsheet within the Basin.
- B. **Observed Annual Streamflow Graphic:** A time series plot of volume in thousands of acre-feet (kaf) for the selected location. This chart also shows the 3-, 5-, and 10-year moving averages for annual streamflow.
- C. **Deficit/Surplus Evaluation Graphic:** This dual-axis plot displays deficits and surpluses (colored vertical bars) based on the long-term average of 15 million acre-feet (maf) and accumulated streamflows (dashed black line) based on the long-term average. The left axis provides the scale for the colored vertical bars and the right axis provides the scale for the dashed line. The vertical bars represent periods of uninterrupted deficit or surplus. The width of the bar indicates the number of years of uninterrupted deficit or surplus, and the bar height indicates the magnitude of the accumulated deficit or surplus. The values were computed by evaluating how long annual flows would be below (deficit) or above (surplus) the long-term average. The dashed line provides a streamflow rate of change indicator; the greater the slope, the greater the rate of change in accumulated flows from the long-term average.
- D. **Table of Statistics:** The table includes statistics (Stat1 and Stat2) for two periods in columns that represent the absolute and percentage difference between the two time periods. The Stat1 and Stat2 columns present the long-term water year streamflow average for the two periods. The “Annual” statistic block shows the minimum and the maximum observed for the 1-year totals and 3-, 5-, 10-, 20-, and 30-year moving averages, followed by the year that the value was observed (e.g., the line “3yr Min (WYear) 7370 (1847)” represents a minimum value of 7,370 kaf per year for a 3-year moving average time series ending in the year of 1847). The “Averages per month” section shows the monthly streamflow averages for each month, followed by the seasonal statistics (average, standard deviation, and amplitude [maximum-minimum]). The amplitude accounts for all seasons, for example, for amplitude October-November-December (OND), the value on the table is computed as the maximum flow observed in a OND season minus the minimum flow observed in a OND season. The minimum and the maximum do not necessarily occur in the same water year.
- E. **Average Monthly Streamflow Graphic:** Average monthly streamflow (kaf) is shown for the water year over the time periods. The data used for this plot are also presented in the Table of Statistics as Stat1 (solid line) and Stat2 (dashed line). This graphic can be used to assess monthly and seasonal shifts in streamflow from the comparison periods.
- F. **Annual Streamflow Box and Whiskers Graphic:** This plot illustrates annual streamflow variability for the two time periods. The box represents the range of half of annual observed flows (inter-quartile range between 25th and 75th percentile). The triangle represents the median; and the horizontal lines at the top of the vertical line represent the period of record maximum and minimum annual values. This graphic can be used to assess trends in period streamflow variability and volumes.
- G. **Annual Streamflow Exceedance Graphic:** This plot presents the full range of probabilities of exceeding a given streamflow for two selected periods. The plot is equivalent to the Box and Whiskers plot but provides probabilities ranging from zero to 100 percent. This graphic can be used to assess trends in period streamflow variability and volumes. For example, at the

Lees Ferry, Arizona location, 90 percent of the years had streamflows exceeding 10,000 kaf for both periods.

- H. Deficit Related Statistics – Exceedance Plots: The deficit statistics are illustrated in three charts: duration, magnitude, and intensity. The statistics presented in these charts refer only to deficit periods defined as only the years when streamflows were below the specified threshold. The “percentage of all years in a deficit” takes into account all years in the time period and determines how many were within a “deficit.” Below is a more detailed description of the deficit related statistics.

The average streamflow for each time period is the default threshold to define deficit or surplus periods (e.g., a sequence of years with streamflows below the average will be considered a deficit period).

**Duration:** The duration chart presents the exceedance probability of deficit duration in years. For example, the chart illustrates that at Lees Ferry, 30 percent of the years defined as deficit years (only deficit years) had a deficit that lasted or exceeded 3 years in duration.

**Magnitude:** The magnitude of a deficit (in kaf) corresponds to the cumulative difference between observed streamflows and long-term average streamflows for an uninterrupted drought period. The exceedance plot will show the probability of a deficit to exceed a certain magnitude based on observed flows.

**Intensity:** Deficit intensity is presented as magnitude divided by duration. The chart presents the exceedance probabilities for two selected periods.

## 2.0 Streamflow Data Summaries

Sample streamflow data summaries are provided in the following pages for the following natural flow stations:

Figure B5-2. Colorado River at Lees Ferry, Arizona (Station 20)

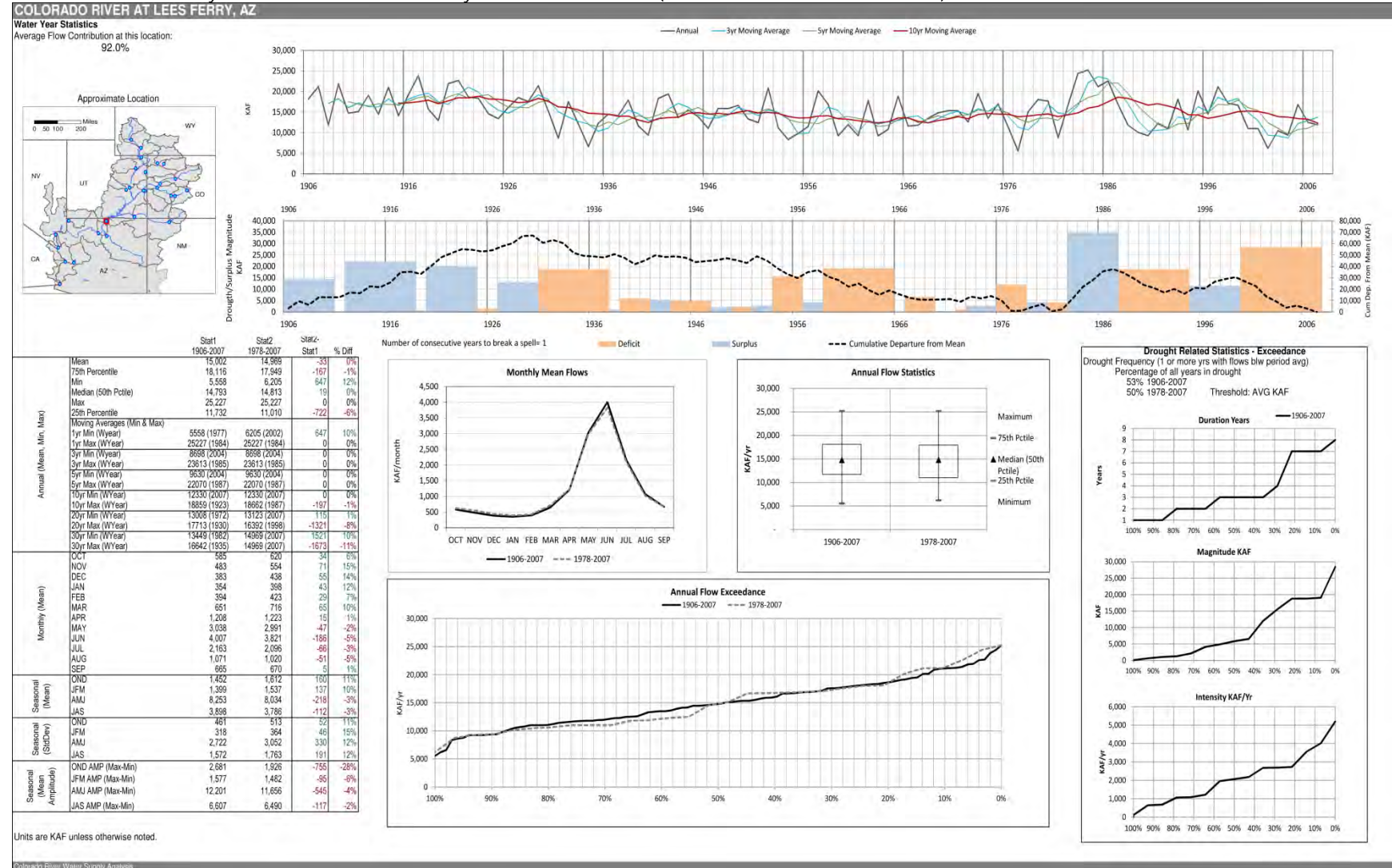
Figure B5-3. Green River at Green River, Utah (Station 16)

Figure B5-4. Colorado River near Cisco, Utah (Station 8)

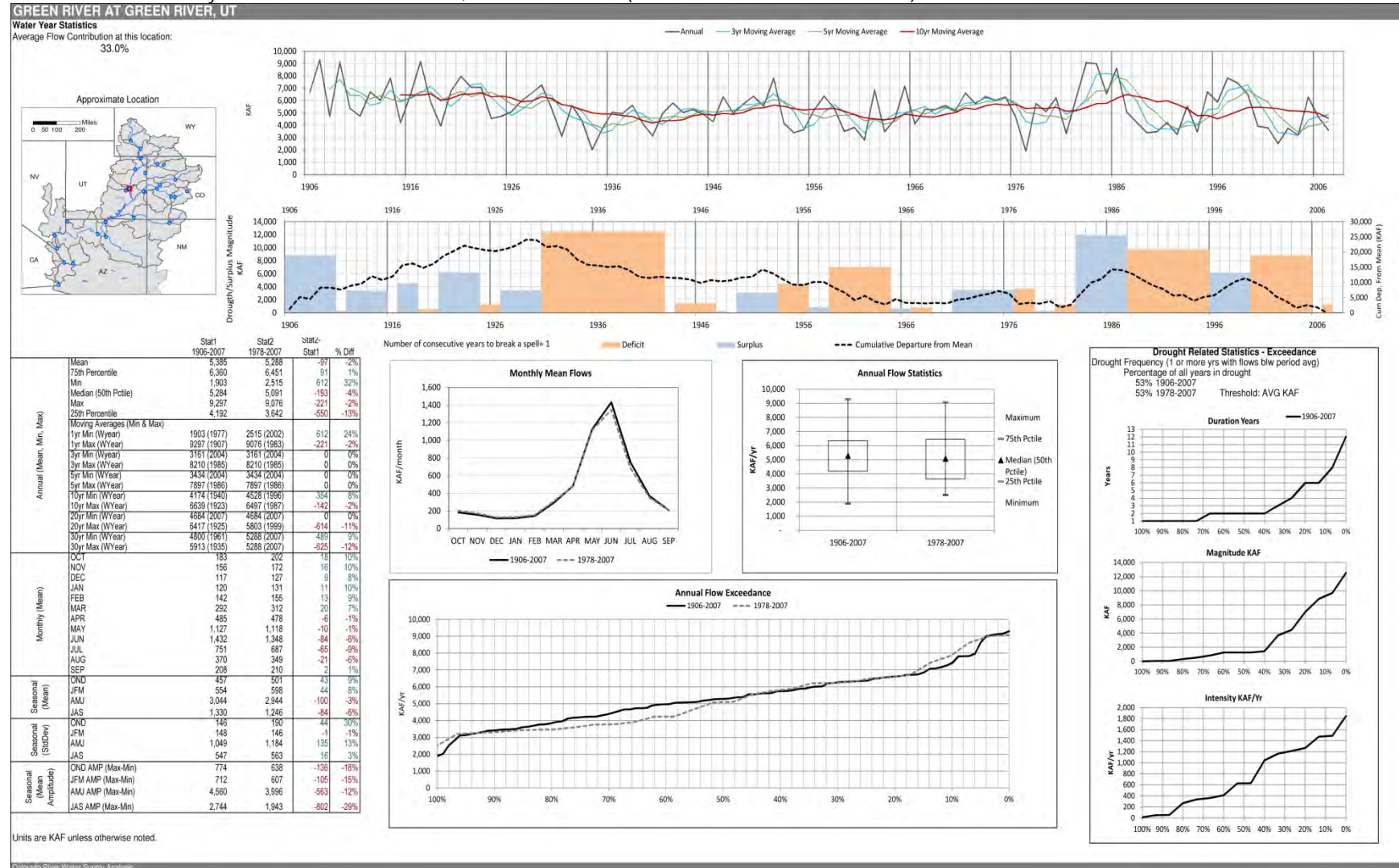
Figure B5-5. San Juan River near Bluff, Utah (Station 19)

Figure B5-6. Colorado River above Imperial Dam, Arizona (Station 29)

**FIGURE B5-2**  
Streamflow Data Summary for Colorado River at Lees Ferry, Arizona Natural Flows (based on historical 1906–2007 data).



**FIGURE B5-3**  
Streamflow Data Summary for Green River at Green River, Utah Natural Flows (based on historical 1906–2007 data).



**FIGURE B5-4**  
Streamflow Data Summary for Colorado River near Cisco, Utah Natural Flows (based on historical 1906–2007 data).

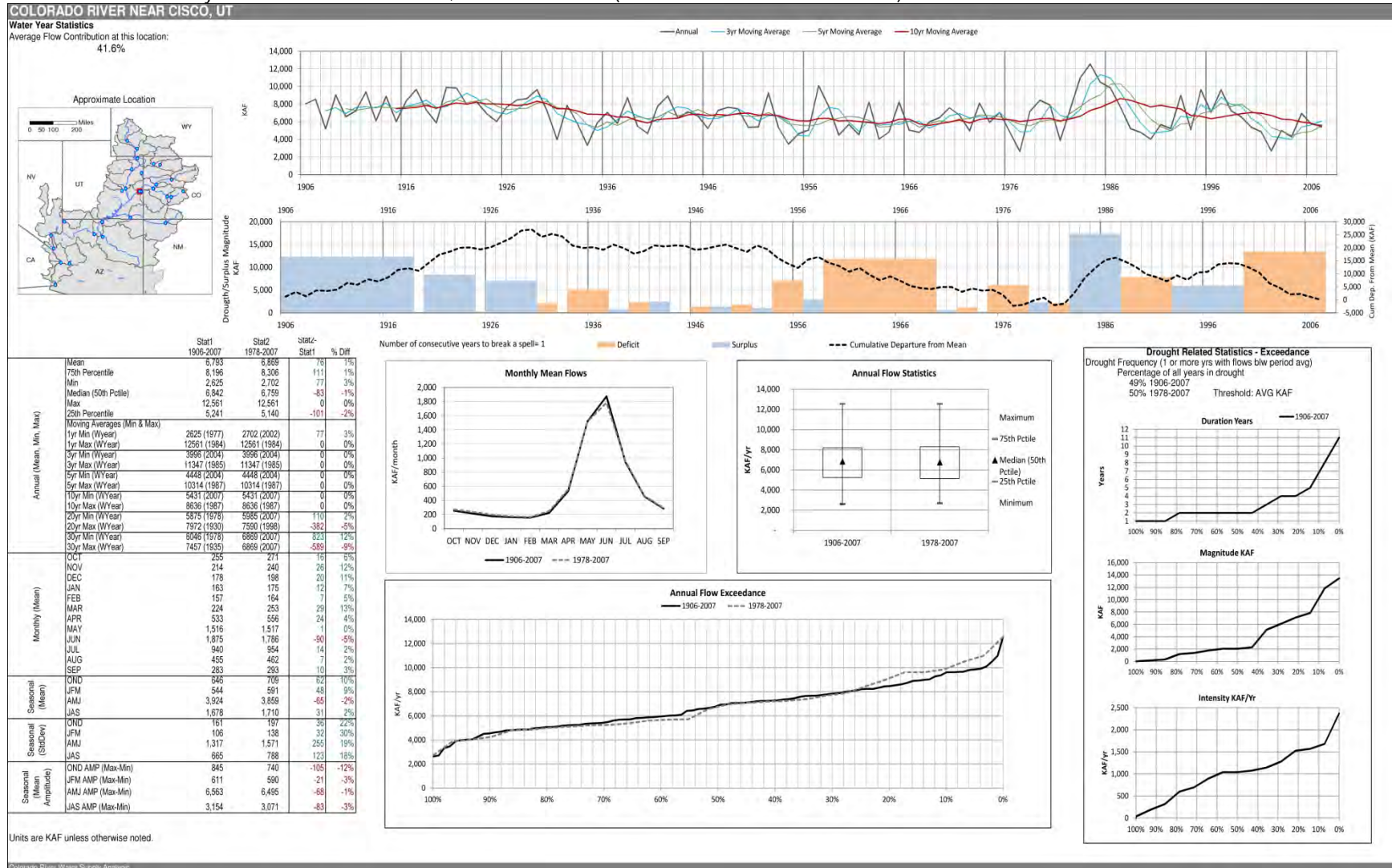


**FIGURE B5-5**  
Streamflow Data Summary for San Juan River near Bluff, Utah Natural Flows (based on historical 1906–2007 data).

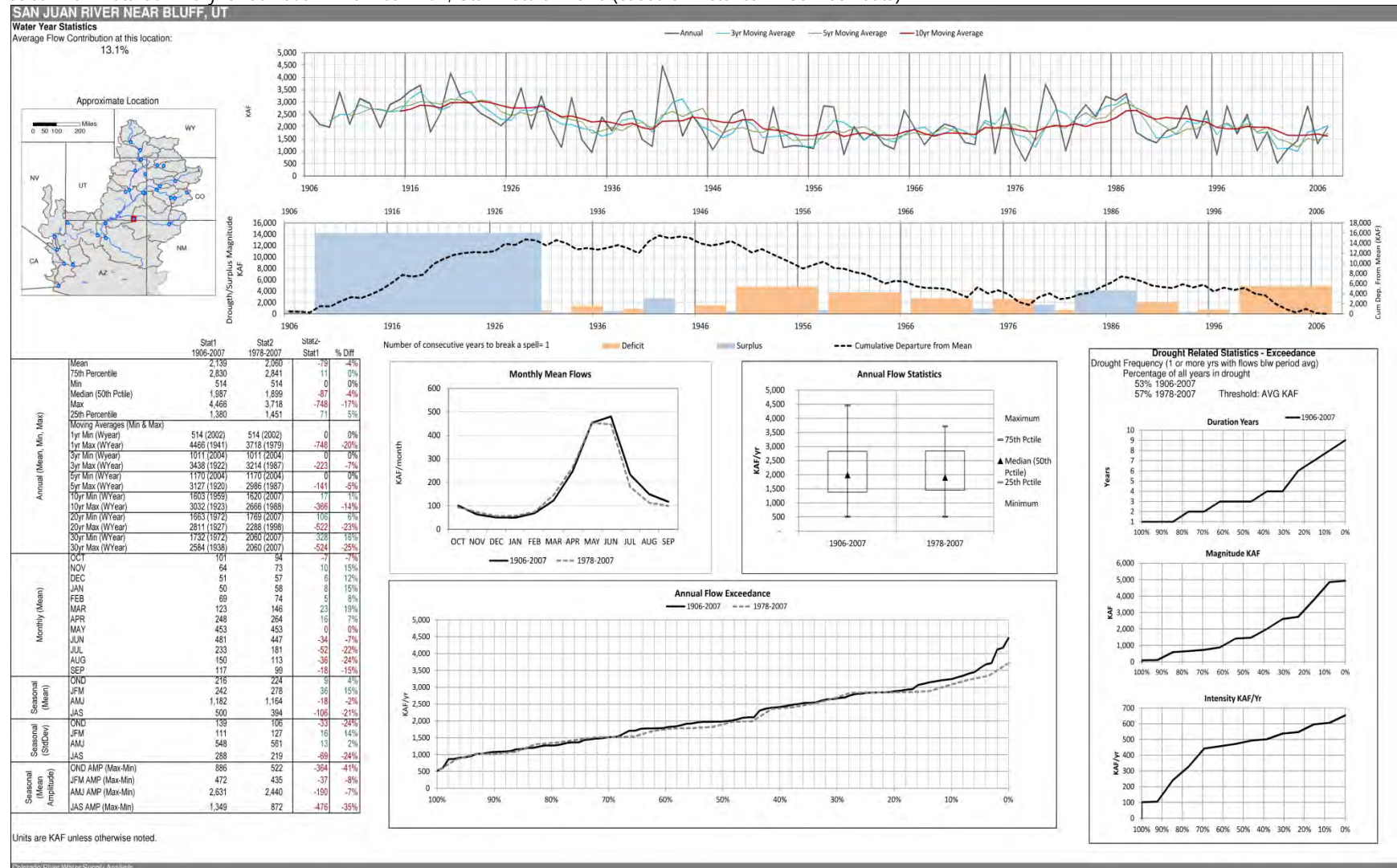
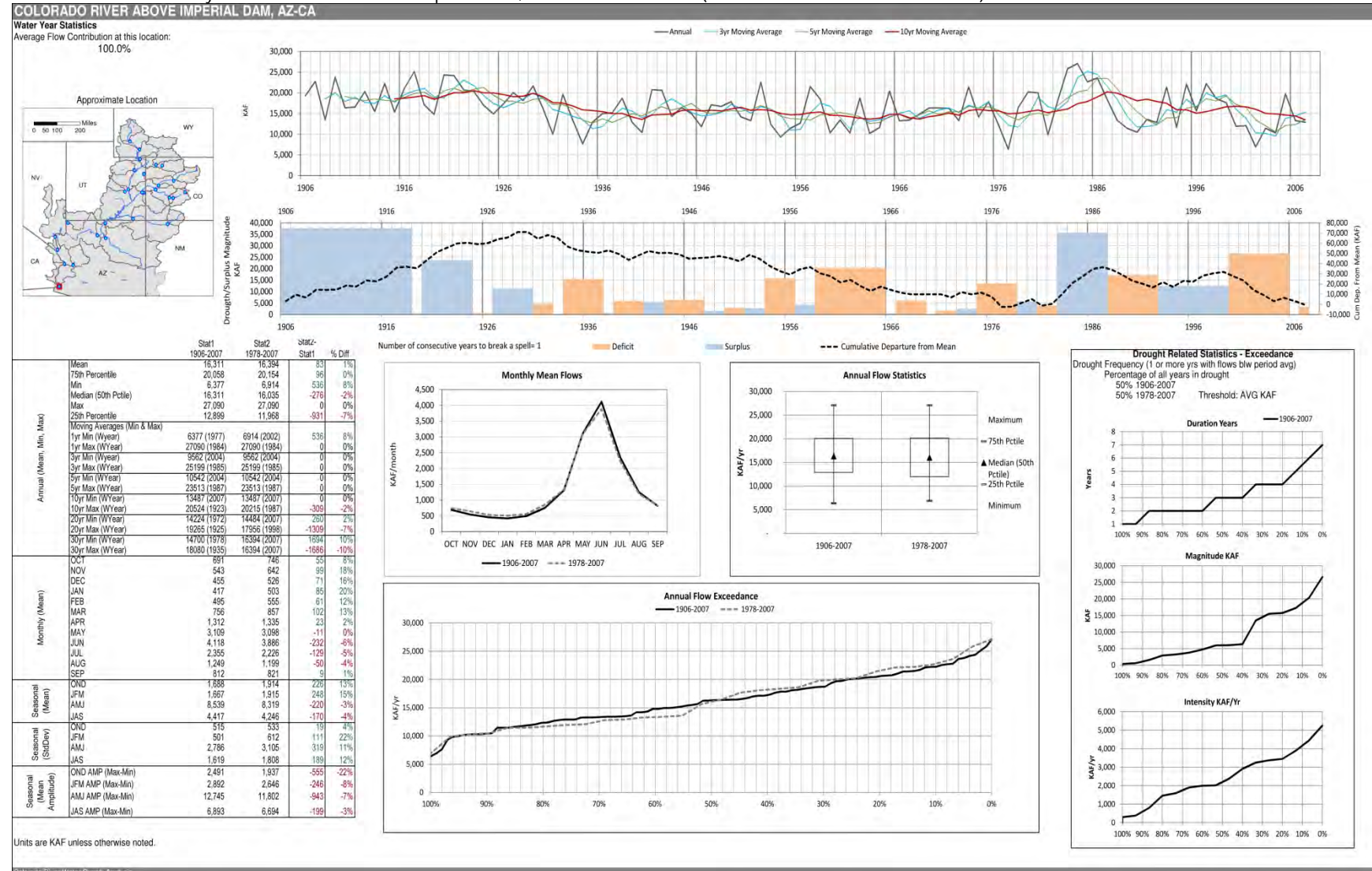


**FIGURE B5-6**  
**Streamflow Data Summary for Colorado River above Imperial Dam, Arizona Natural Flows (based on historical 1906–2007 data).**





**Appendix B6**  
**Watershed-based Climate and**  
**Hydrologic Process Changes**

---



# Appendix B6—Watershed-based Climate and Hydrologic Process Changes

The results of the watershed-based statistical analysis of the Variable Infiltration Capacity (VIC) model output (climatological and hydrologic parameters) are presented for a subset of the Colorado River Basin (Basin) watersheds. The selected watersheds span the geographic range of the Basin. One group of watersheds was selected from the Upper Basin, and each of these watersheds contains the headwaters of a significant river. A second group of watersheds was selected from the Lower Basin, and each contains a streamflow station of significance. The selected watersheds are as follows:

## Upper Basin

- 01 – Colorado River at Glenwood Springs, Colorado
- 04 – Gunnison River at Blue Mesa Reservoir, Colorado
- 09 – Green River below Fontenelle Reservoir, Wyoming
- 12 – Yampa River near Maybell, Colorado
- 13 – Little Snake River near Lily, Colorado
- 18 – San Juan River near Archuleta, New Mexico
- 20 – Colorado River at Lees Ferry, Arizona

## Lower Basin

- 25 – Colorado River below Hoover Dam, Arizona-Nevada
- 29 – Colorado River Above Imperial Dam, Arizona

Figures B6-1 through B6-9 depict the relative changes in monthly precipitation, temperature, evapotranspiration, runoff, snow water equivalent, and soil moisture for these selected watersheds. Separate lines depict the changes for the periods 2011–2040 (2025), 2041–2070 (2055), and 2066–2094 (2080) as compared to the base period 1971–2000 (1985). Hydrologic variables were produced using VIC as driven by downscaled climate model forcings. The selection of time periods is explained in appendix B-5, section 3.3.1.

Figures B6-10 through B6-20 are spatial plots of the changes in these parameters for four seasons. The seasons are defined as: Fall (October, November, and December [OND]); Winter (January, February, and March [JFM]); Spring (April, May, and June [AMJ]); and Summer (July, August, and September [JAS]). Separate figures have been provided for the three future periods.

**FIGURE B6-1**  
 Projected Change in Mean Monthly Climatological and Hydrologic Parameters  
 01 – Colorado River at Glenwood Springs, Colorado

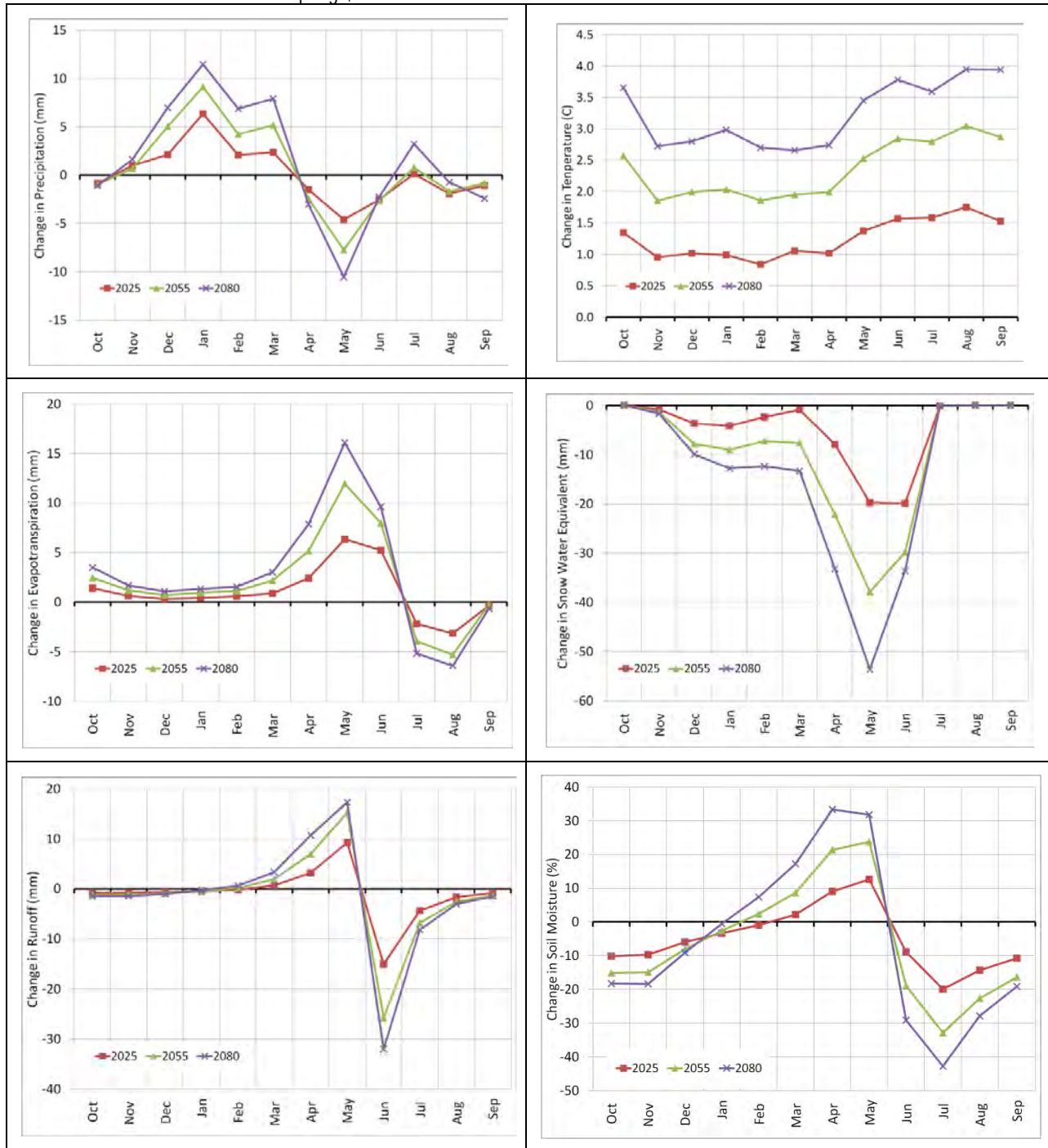


**FIGURE B6-2**  
 Projected Change in Mean Monthly Climatological and Hydrologic Parameters  
 04 – Gunnison River at Blue Mesa Reservoir, Colorado

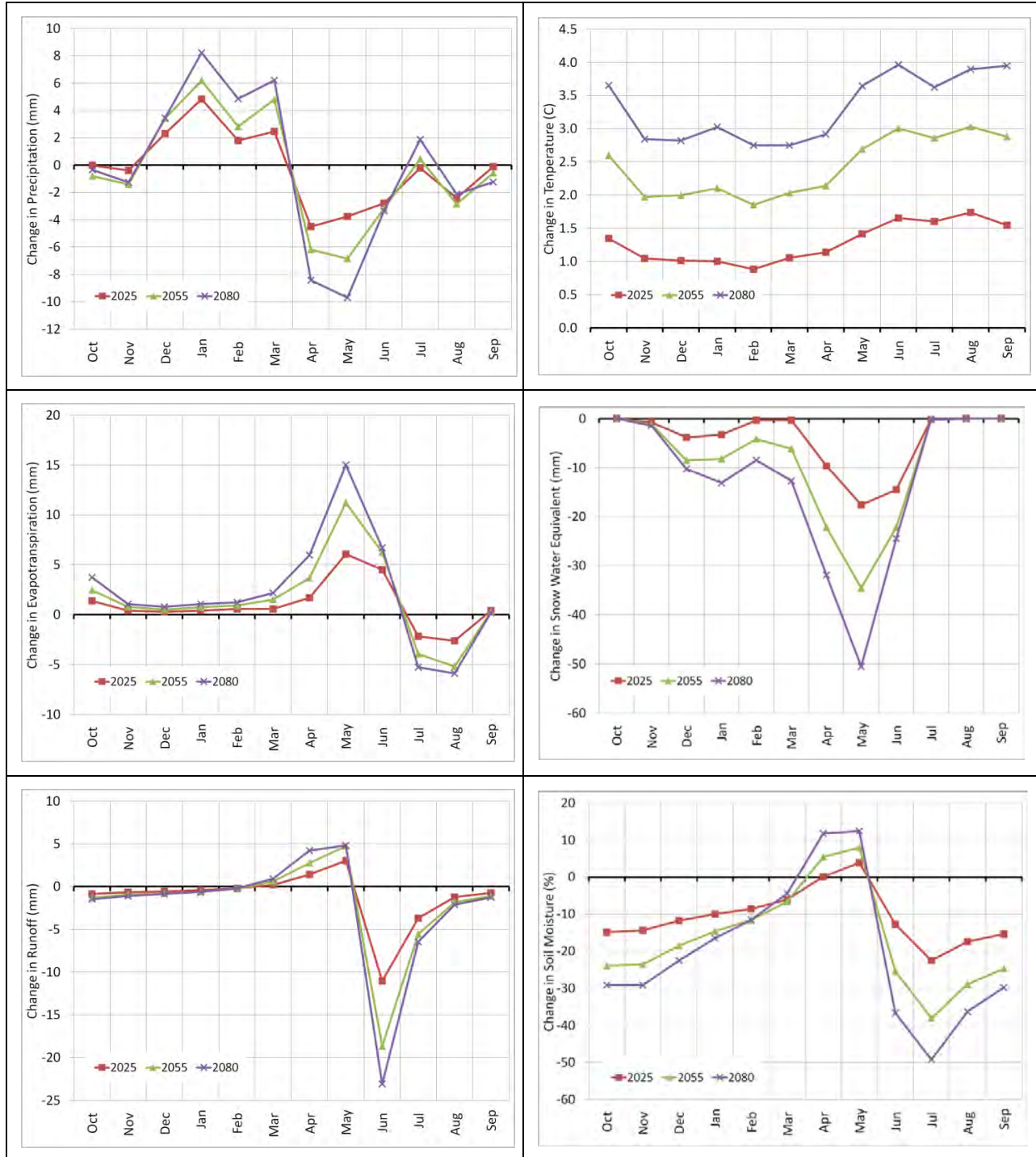


**FIGURE B6-3**  
 Projected Change in Mean Monthly Climatological and Hydrologic Parameters  
 09 – Green River below Fontenelle Reservoir, Wyoming

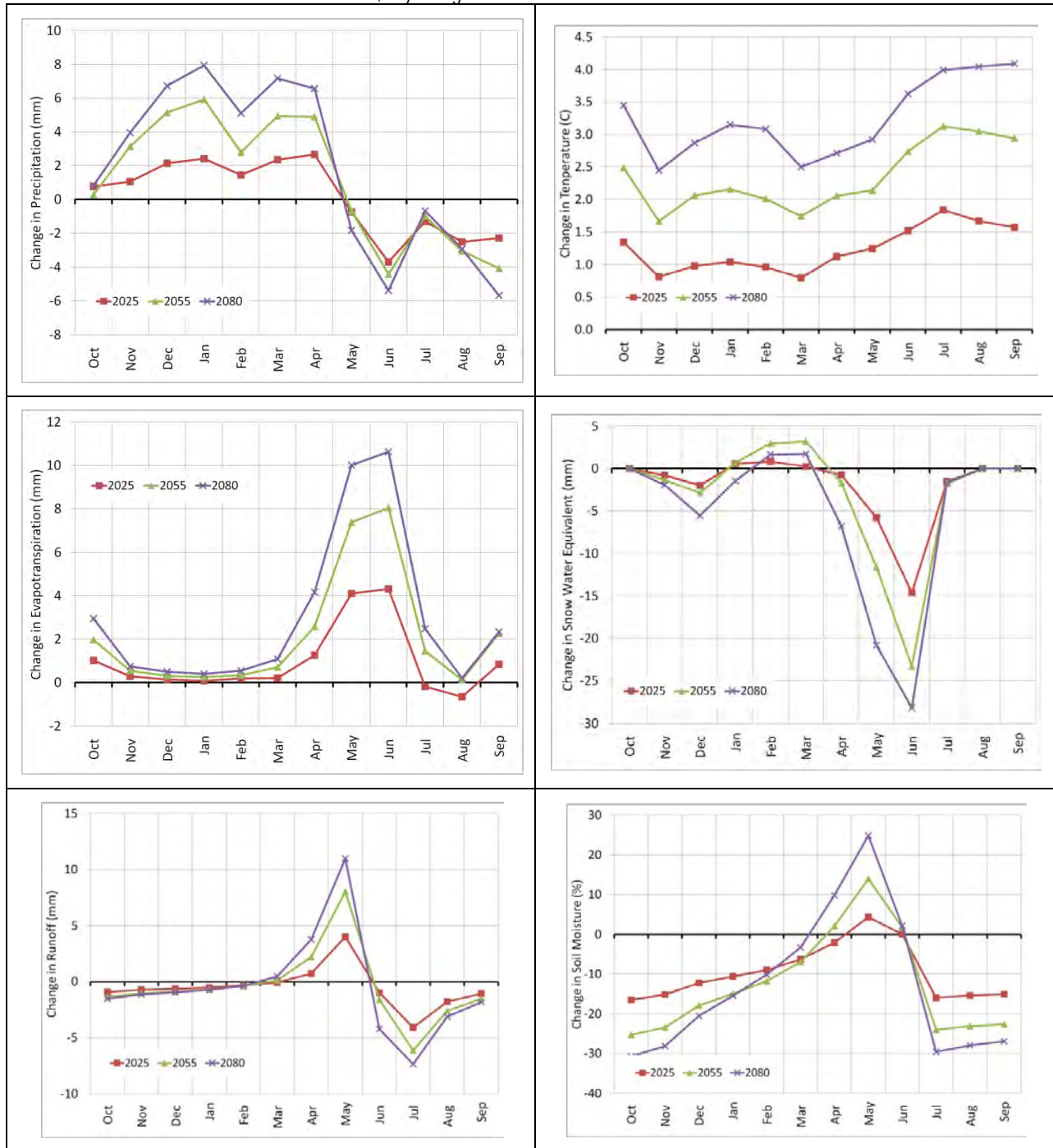


**FIGURE B6-4**  
 Projected Change in Mean Monthly Climatological and Hydrologic Parameters  
 12 – Yampa River near Maybell, Colorado

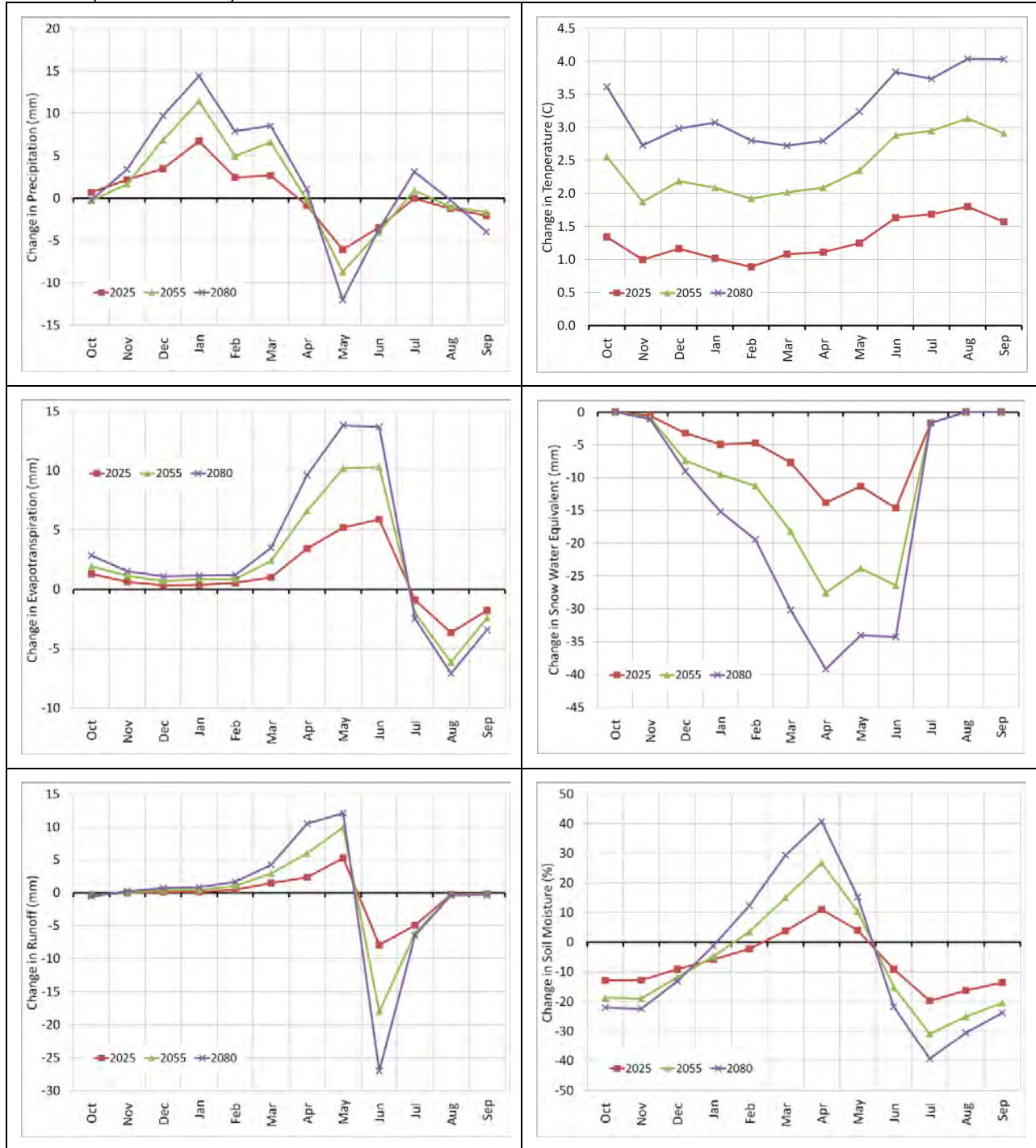


**FIGURE B6-5**  
 Projected Change in Mean Monthly Climatological and Hydrologic Parameters  
 13 – Little Snake River near Lily, Colorado

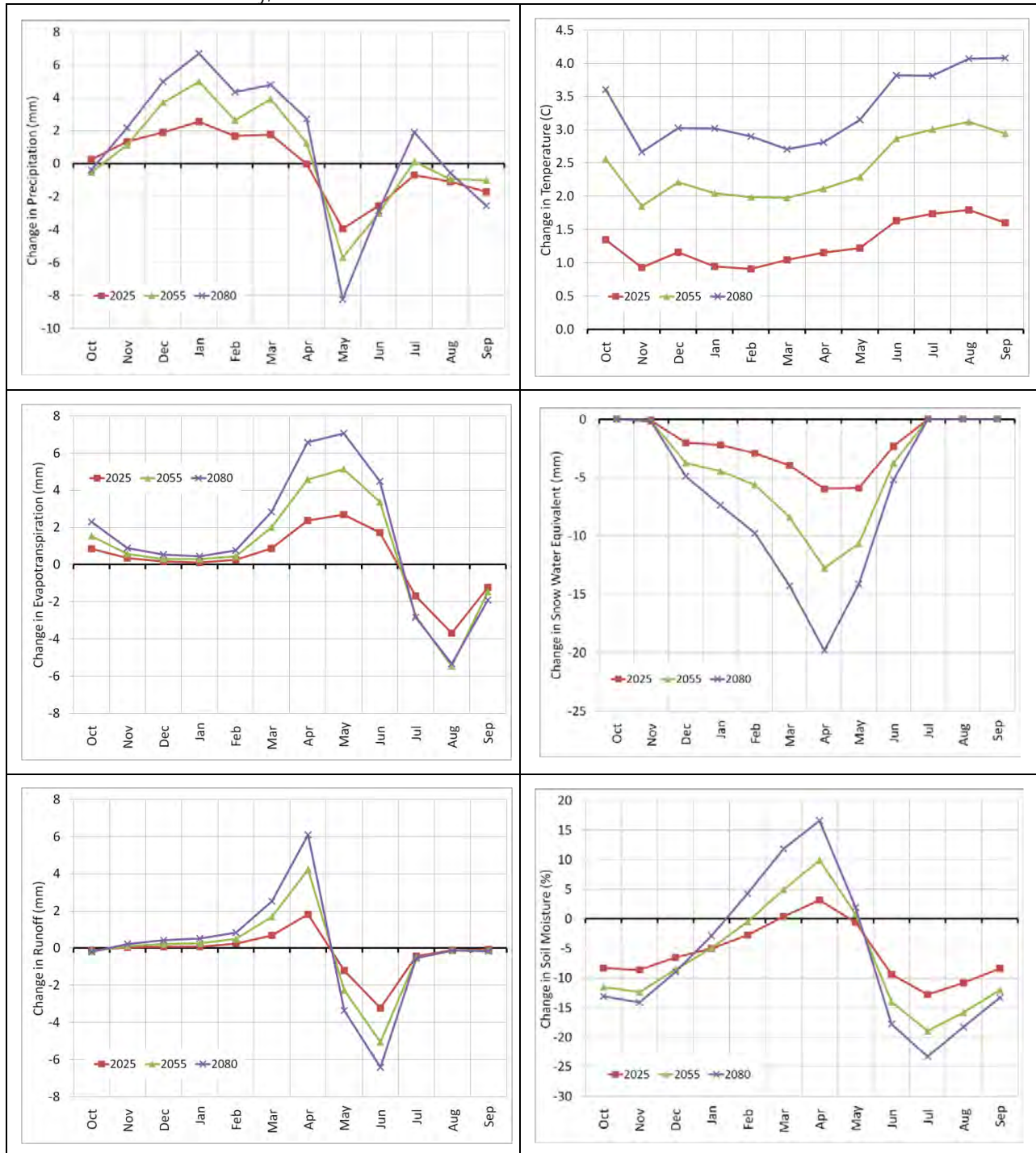


**FIGURE B6-6**  
 Projected Change in Mean Monthly Climatological and Hydrologic Parameters  
 18 – San Juan River near Archuleta, New Mexico

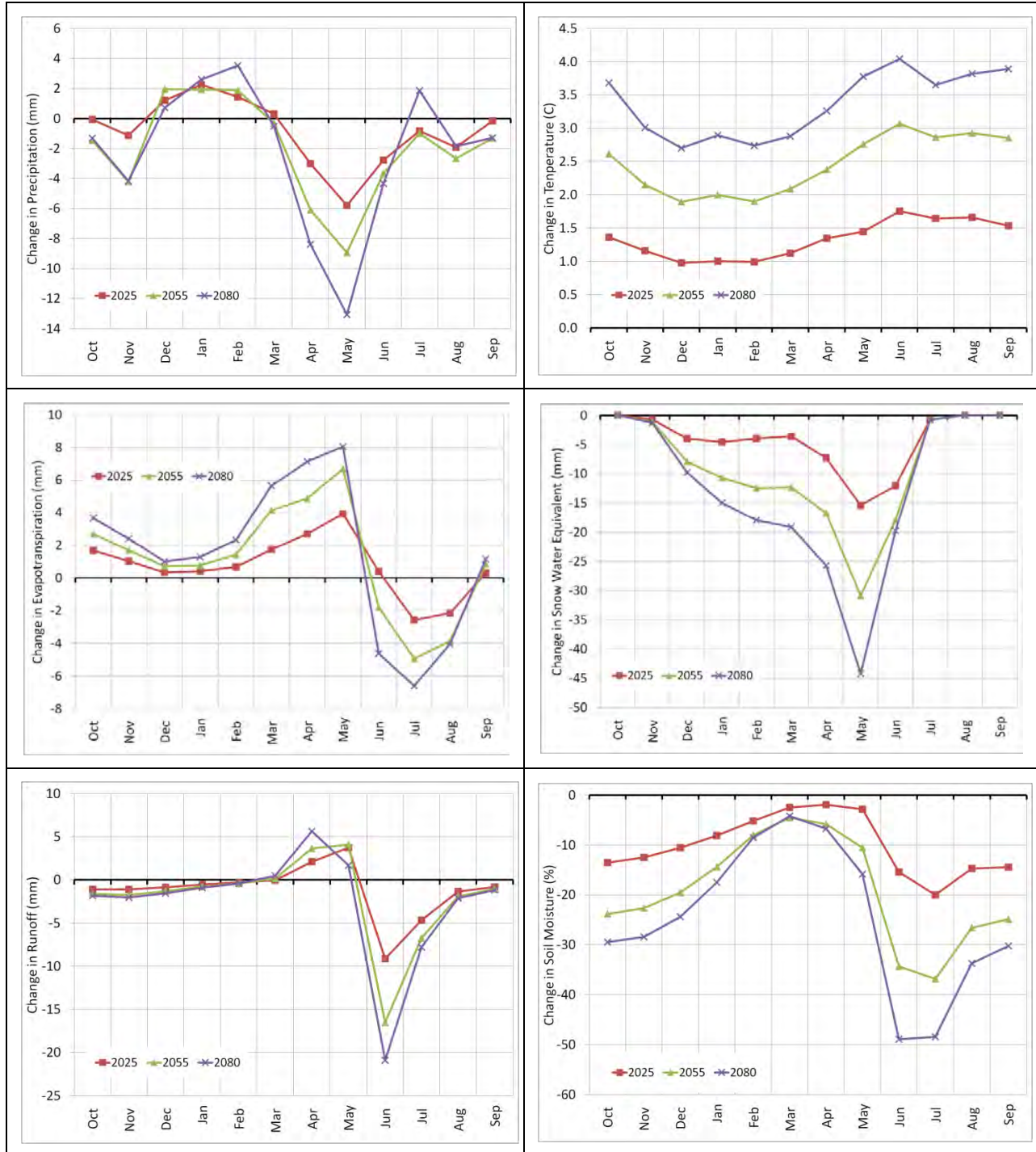


**FIGURE B6-7**  
 Projected Change in Mean Monthly Climatological and Hydrologic Parameters  
 20 – Colorado River at Lees Ferry, Arizona

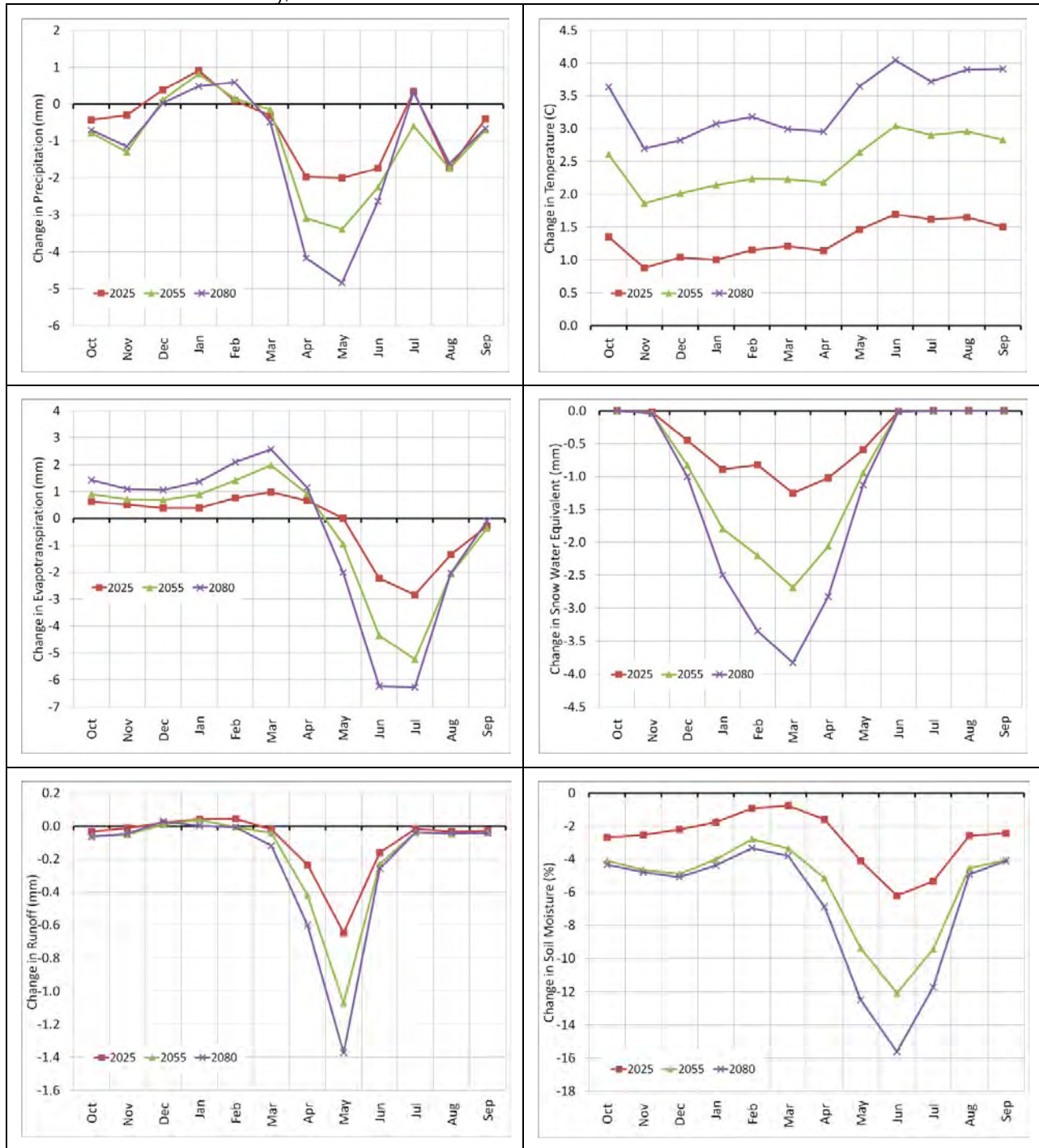


**FIGURE B6-8**  
 Projected Change in Mean Monthly Climatological and Hydrologic Parameters  
 25 – Colorado River below Hoover Dam, Arizona-Nevada

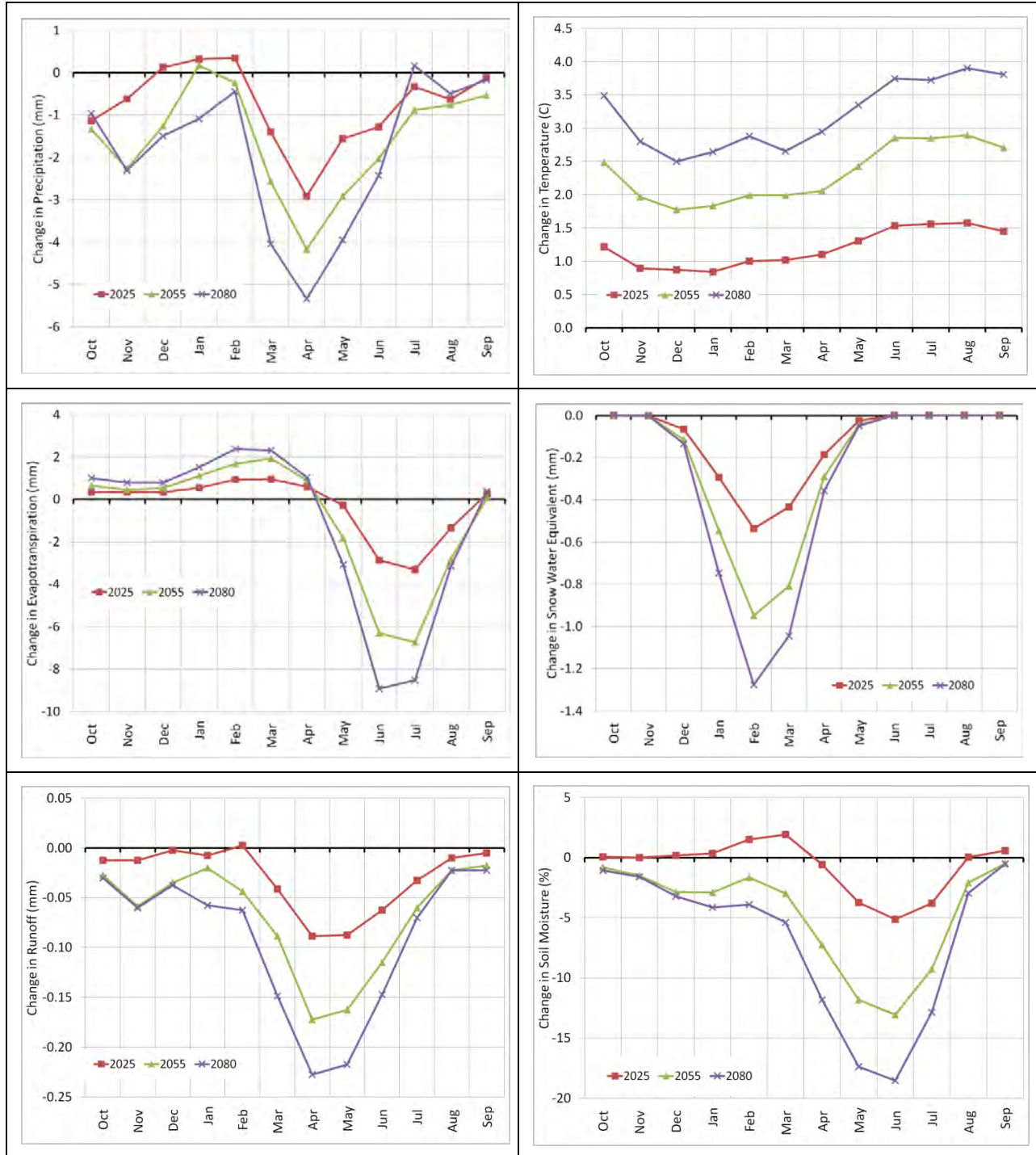


**FIGURE B6-9**  
 Projected Change in Mean Monthly Climatological and Hydrologic Parameters  
 29 – Colorado River Above Imperial Dam, Arizona

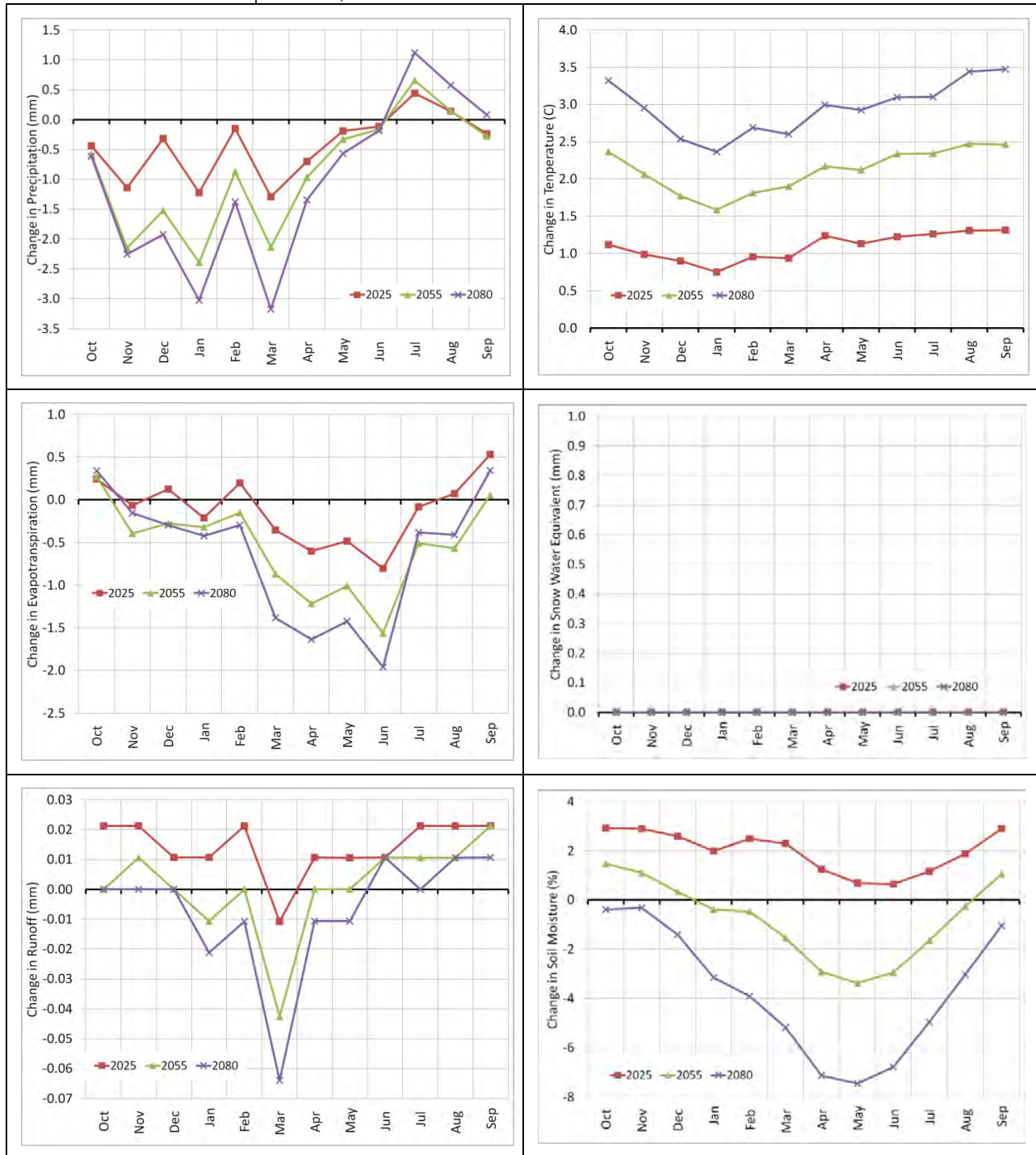


**FIGURE B6-10**

Projected Percent Change in Mean Seasonal Precipitation (OND is October, November, and December; JFM is January, February, and March; AMJ is April, May, and June; and JAS is July, August, and September) 2025 (2011–2040) versus 1985 (1971–2000).

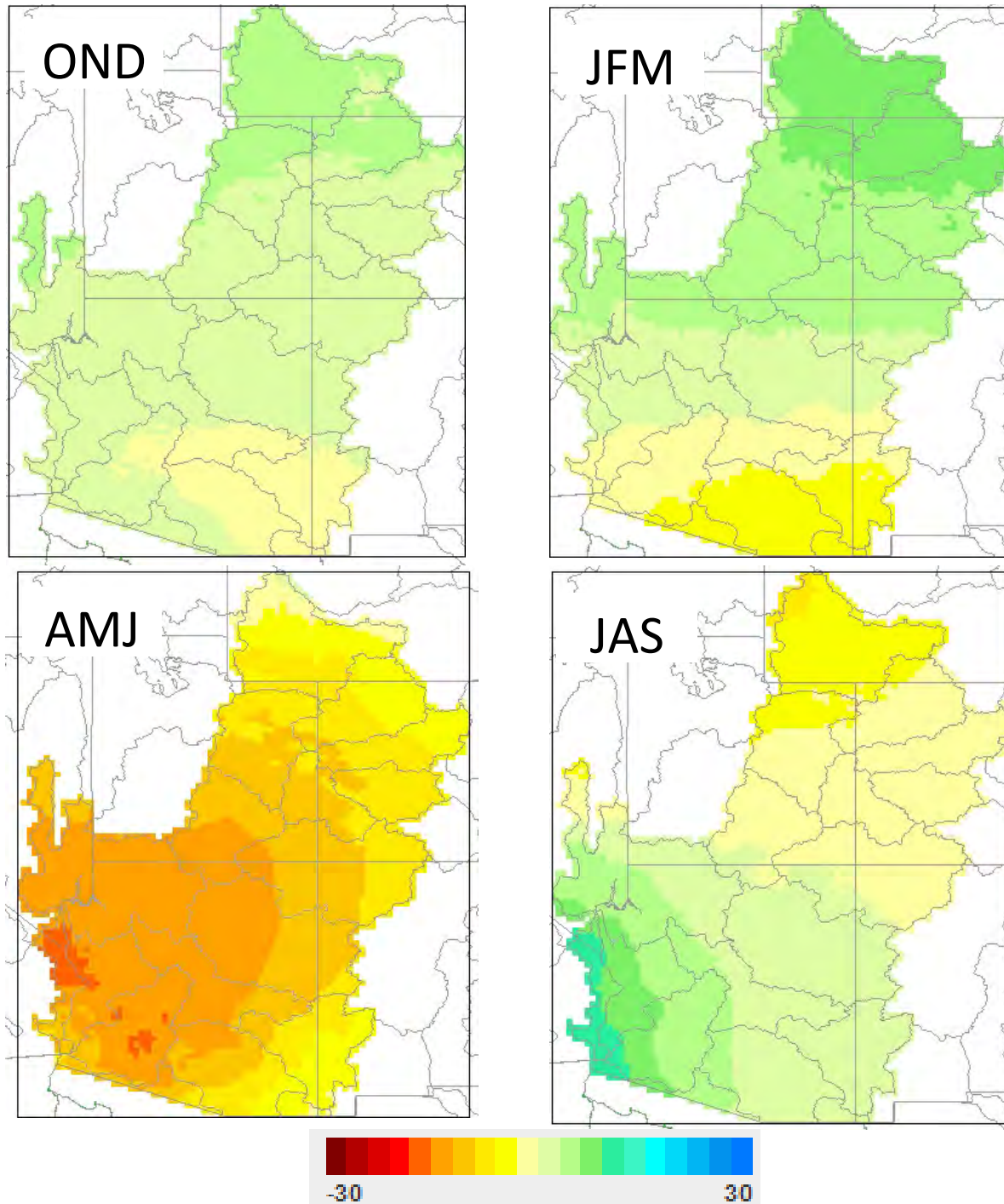


**FIGURE B6-11**  
Projected Change (°C) in Mean Seasonal Air Temperature  
2025 (2011–2040) versus 1985 (1971–2000).

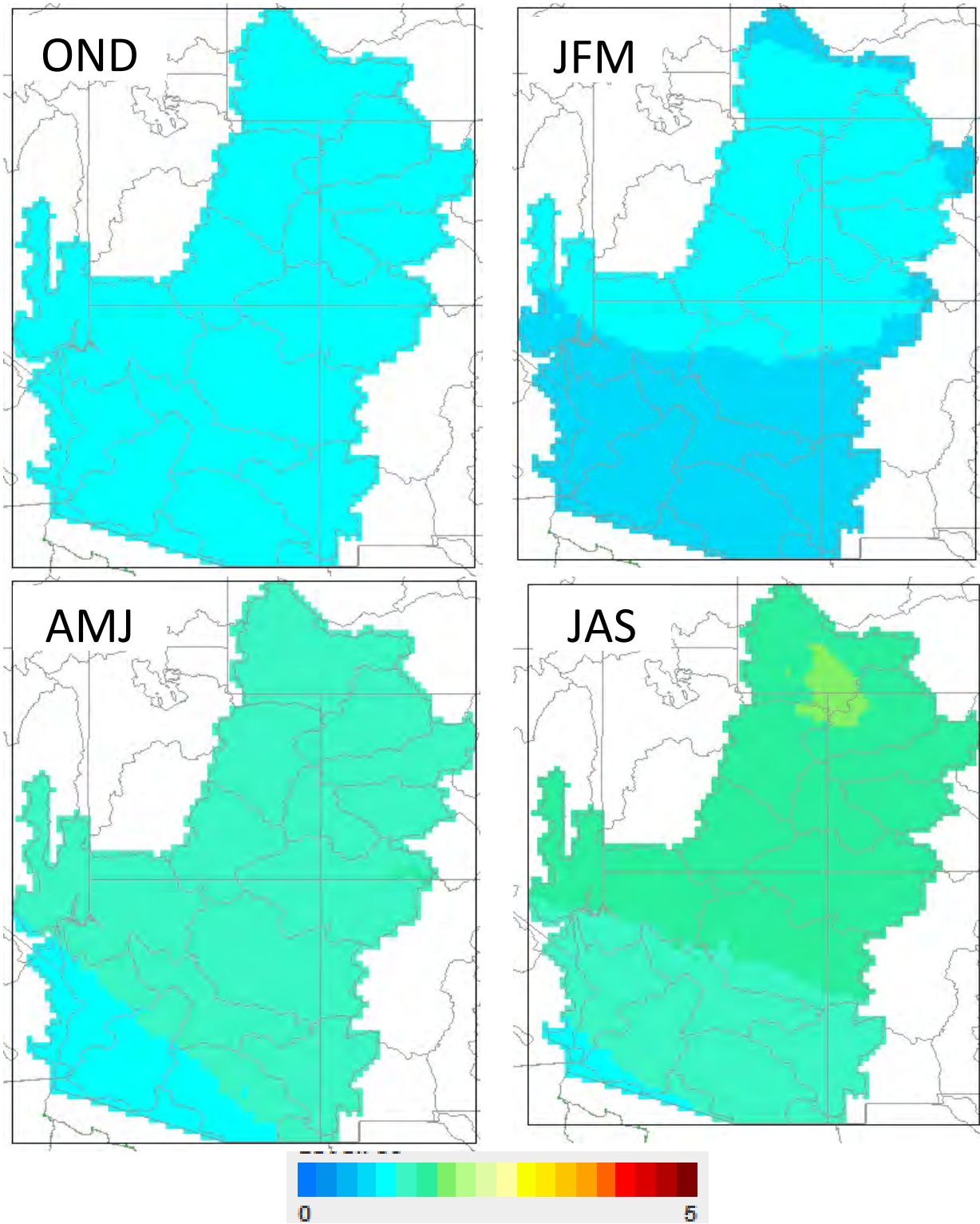


**FIGURE B6-12**  
 Projected Percent Change in Mean Seasonal Evapotranspiration  
 2025 (2011–2040) versus 1985 (1971–2000).

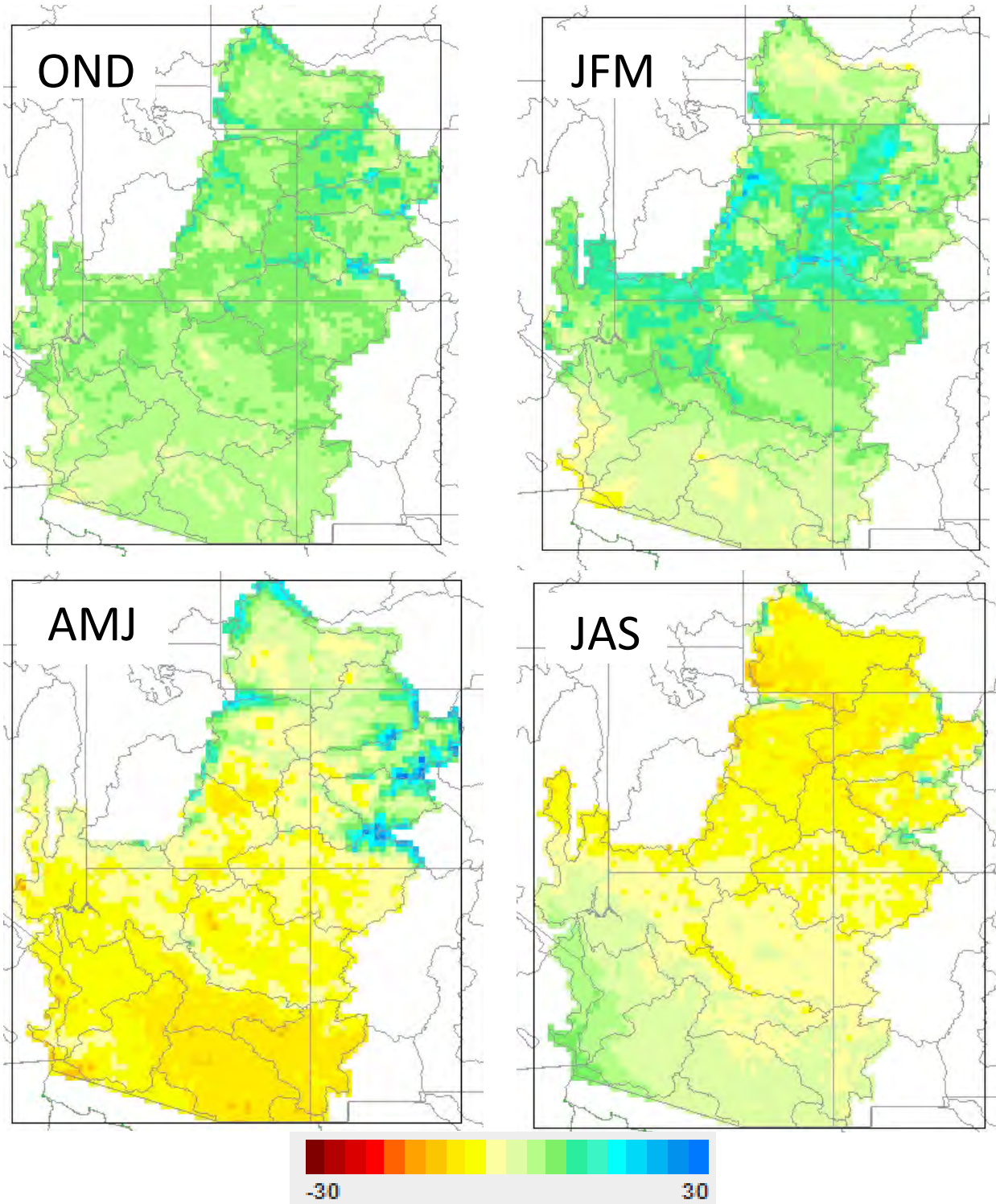


**FIGURE B6-13**  
Projected Percent Change in Mean Seasonal Runoff  
2025 (2011–2040) versus 1985 (1971–2000).

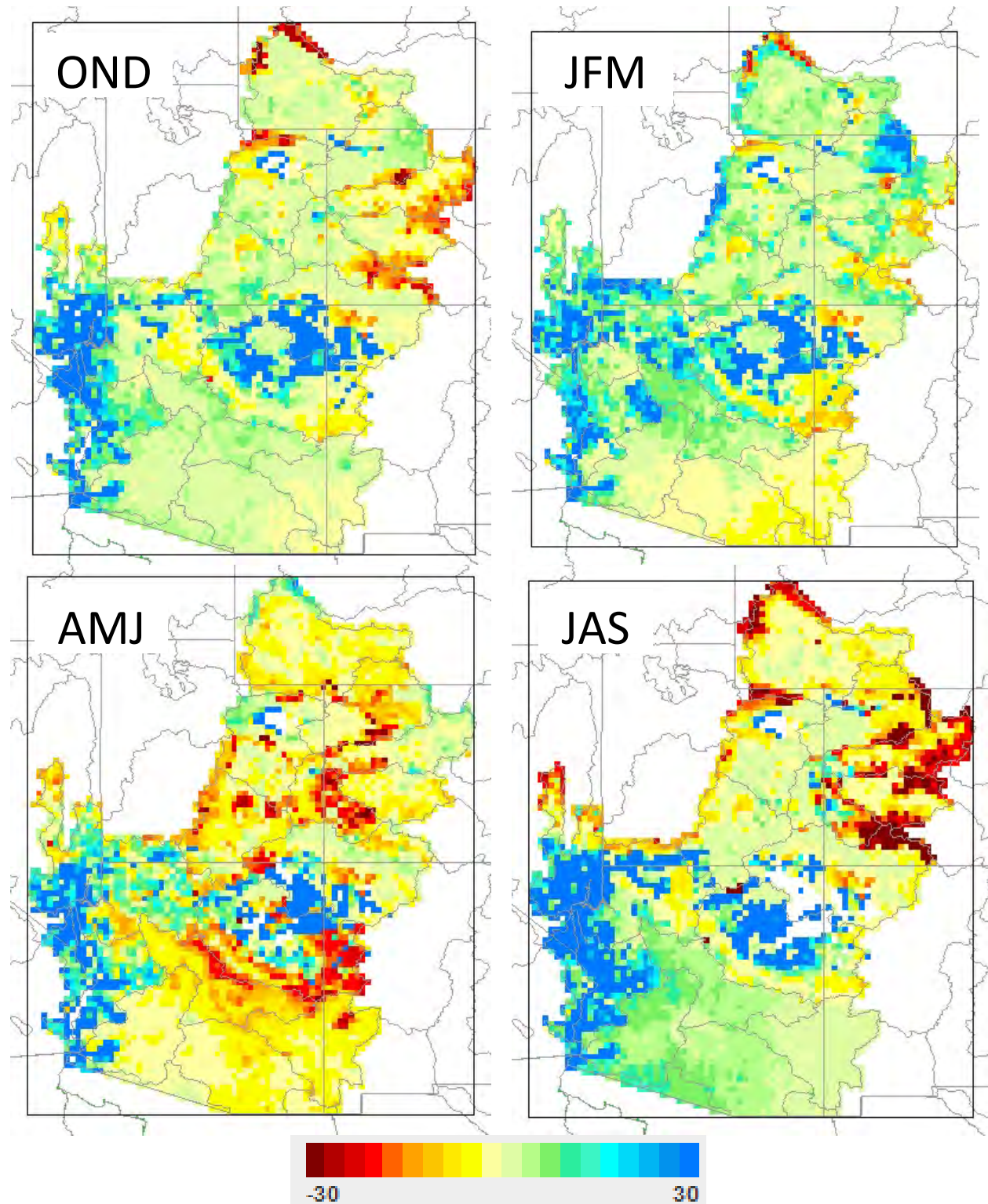


**FIGURE B6-14**  
 Projected Percent Change in Mean Seasonal Precipitation  
 2055 (2041–2070) versus 1985 (1971–2000).

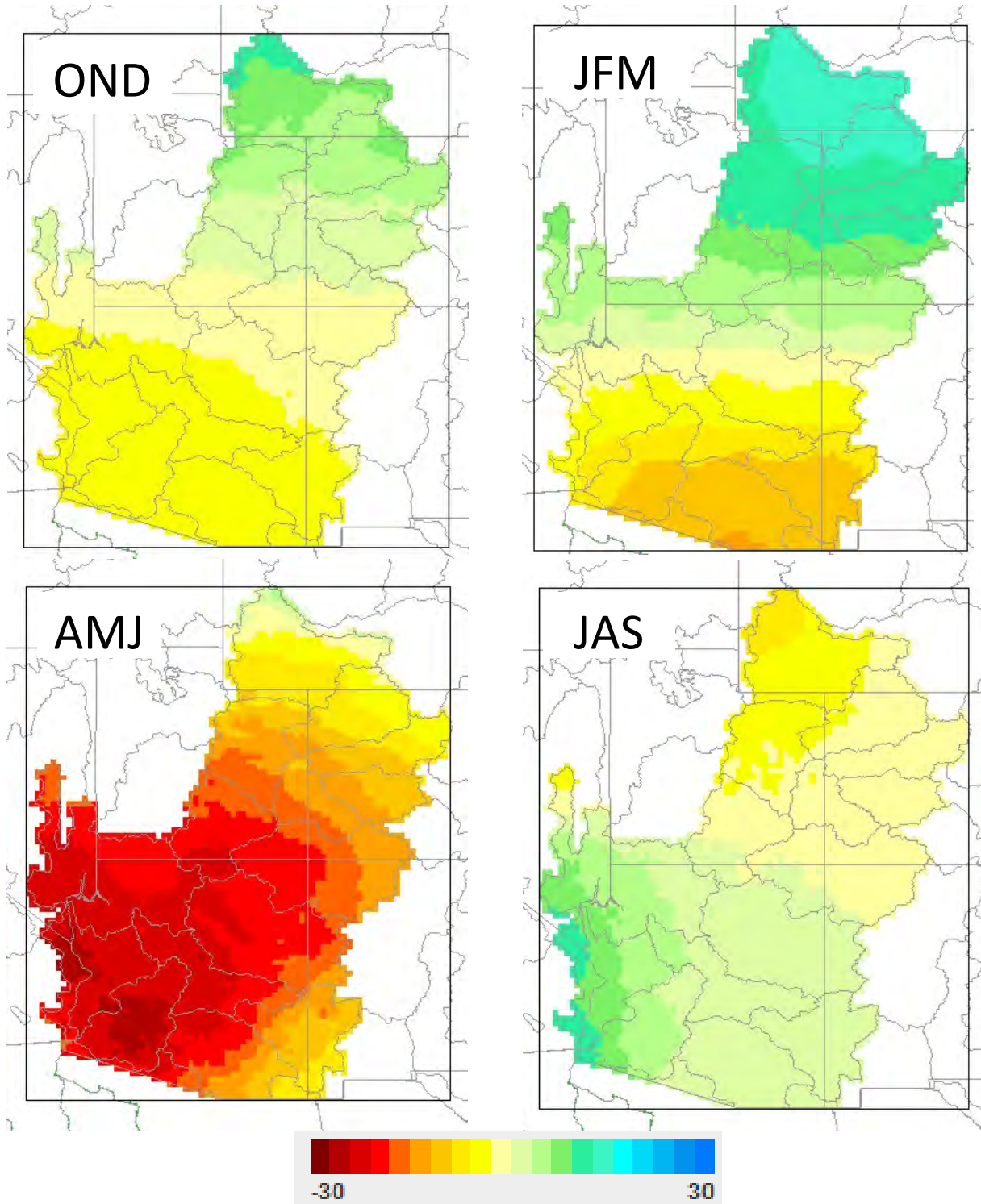


**FIGURE B6-15**  
Projected Change (°C) in Mean Seasonal Air Temperature  
2055 (2041–2070) versus 1985 (1971–2000).

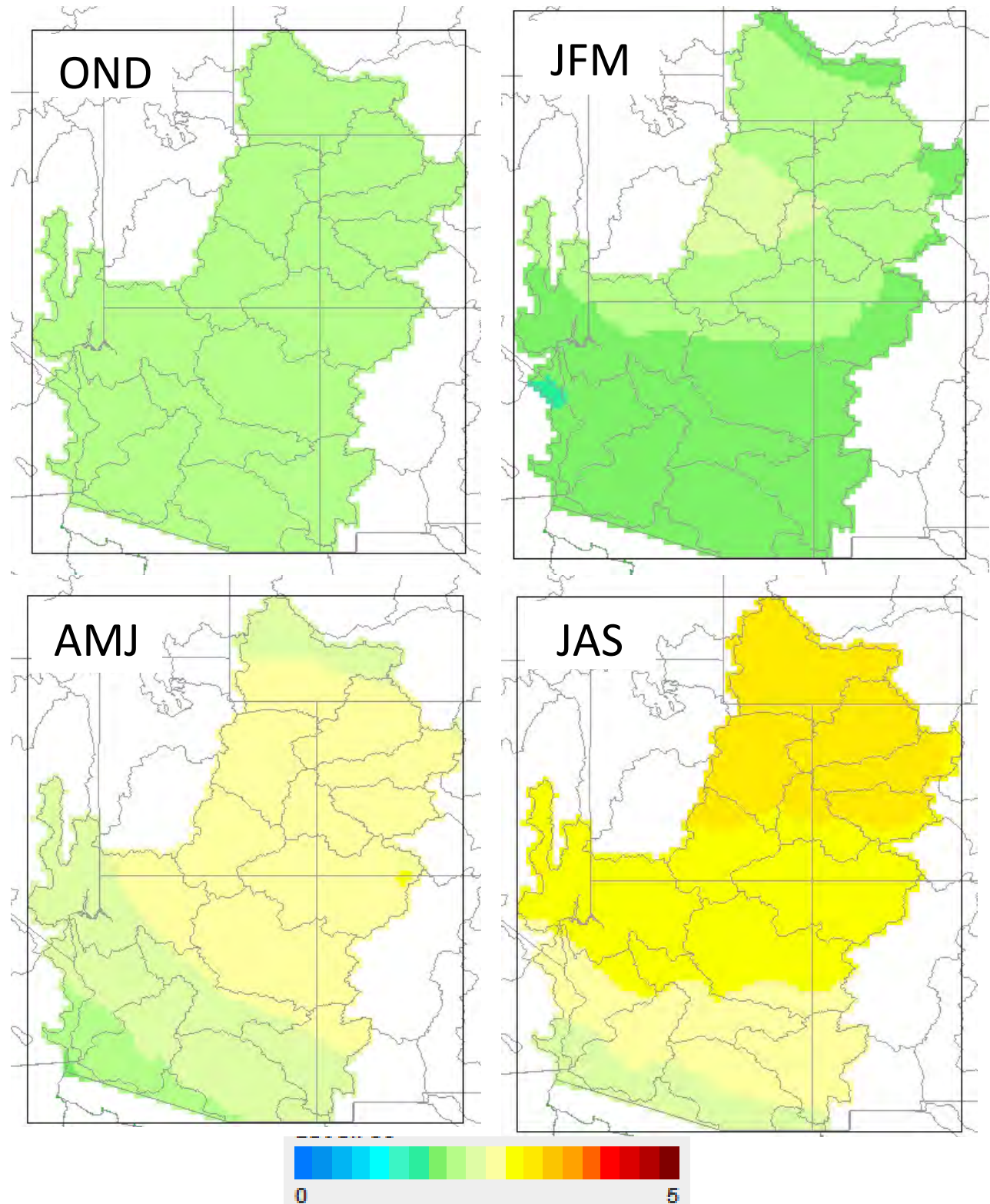


**FIGURE B6-16**  
 Projected Percent Change in Mean Seasonal Evapotranspiration  
 2055 (2041–2070) versus 1985 (1971–2000).

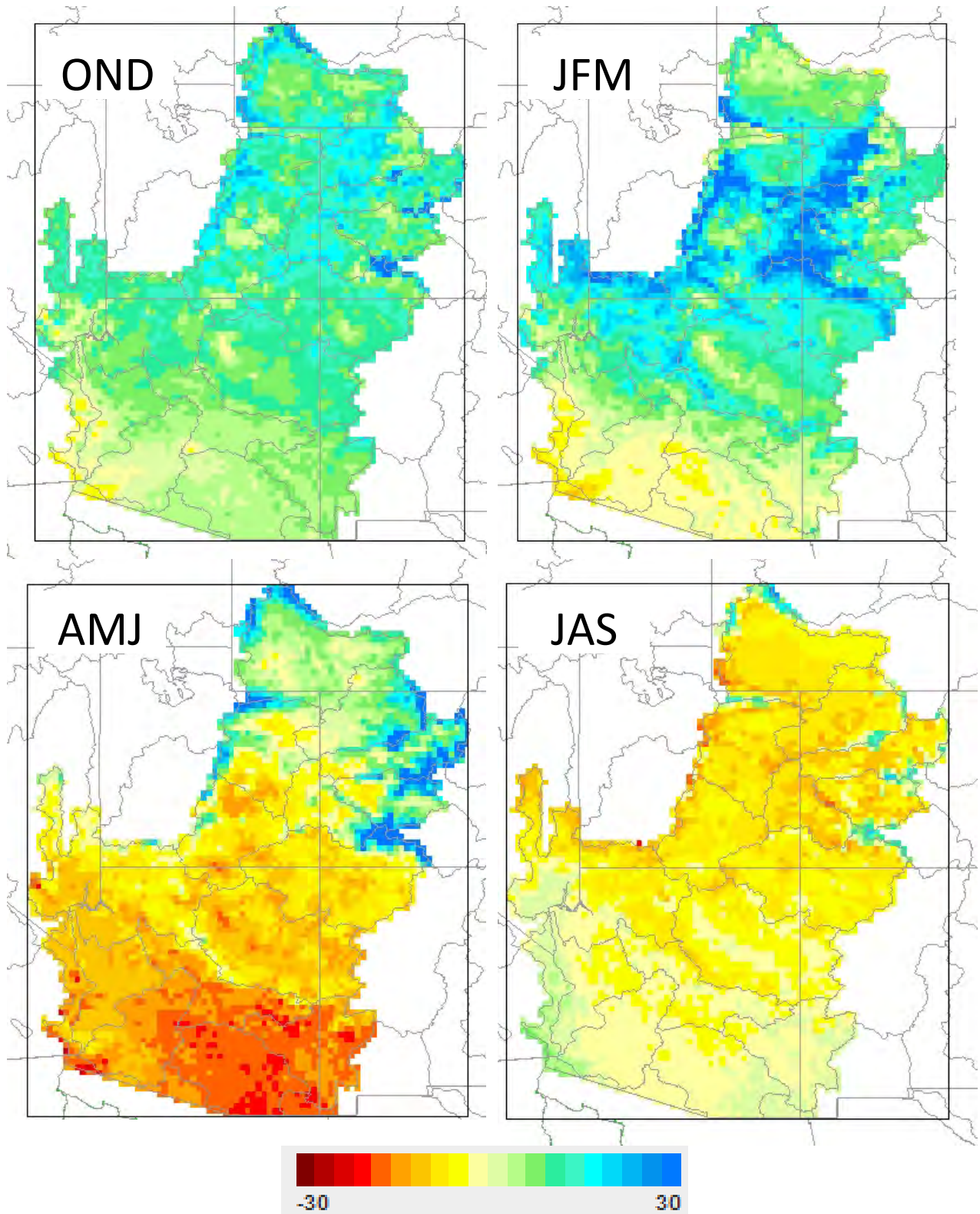


**FIGURE B6-17**  
Projected Percent Change in Mean Seasonal Runoff  
2055 (2041–2070) versus 1985 (1971–2000).

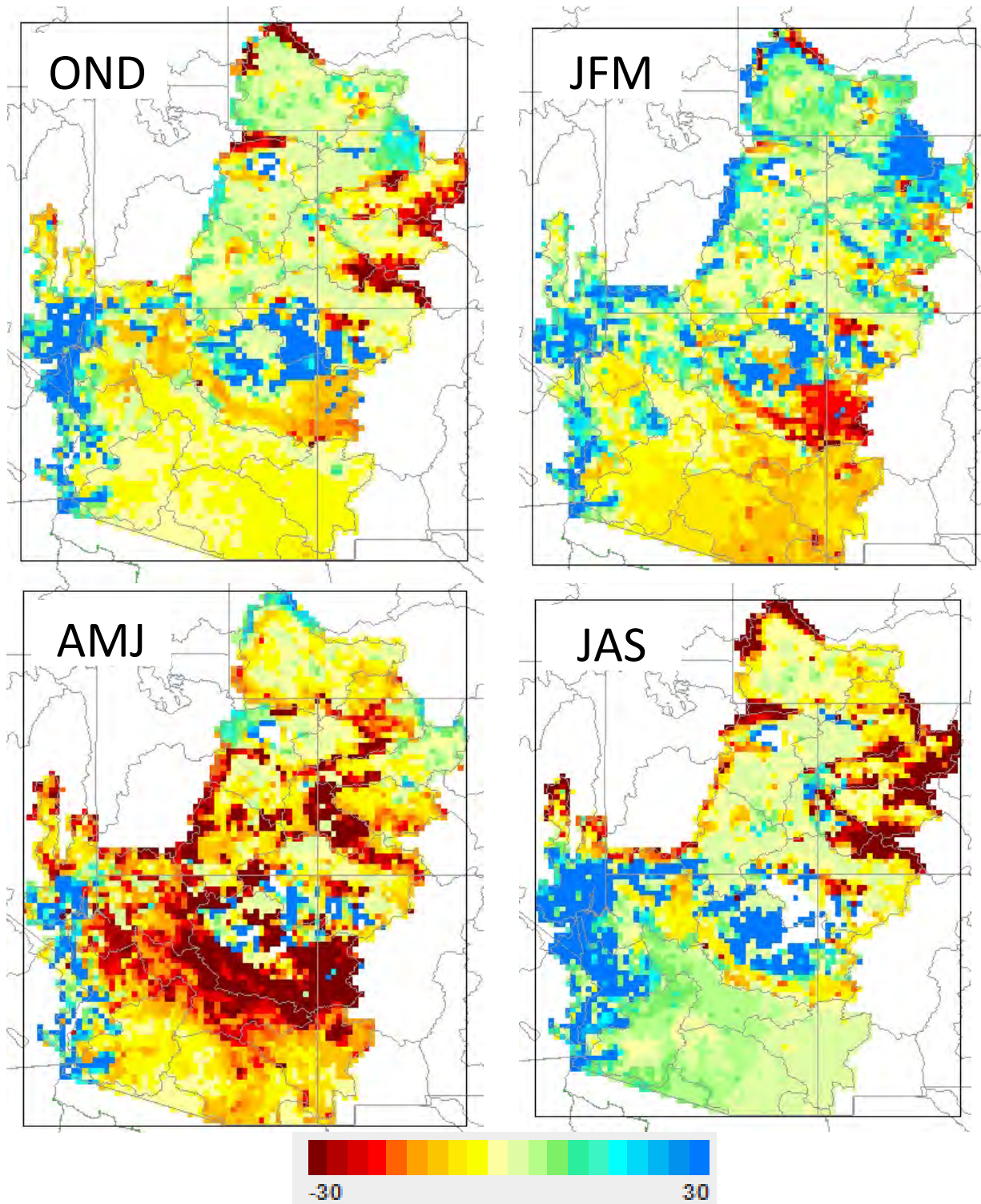


**FIGURE B6-18**  
 Projected Percent Change in Mean Seasonal Precipitation  
 2080 (2066–2095) versus 1985 (1971–2000).

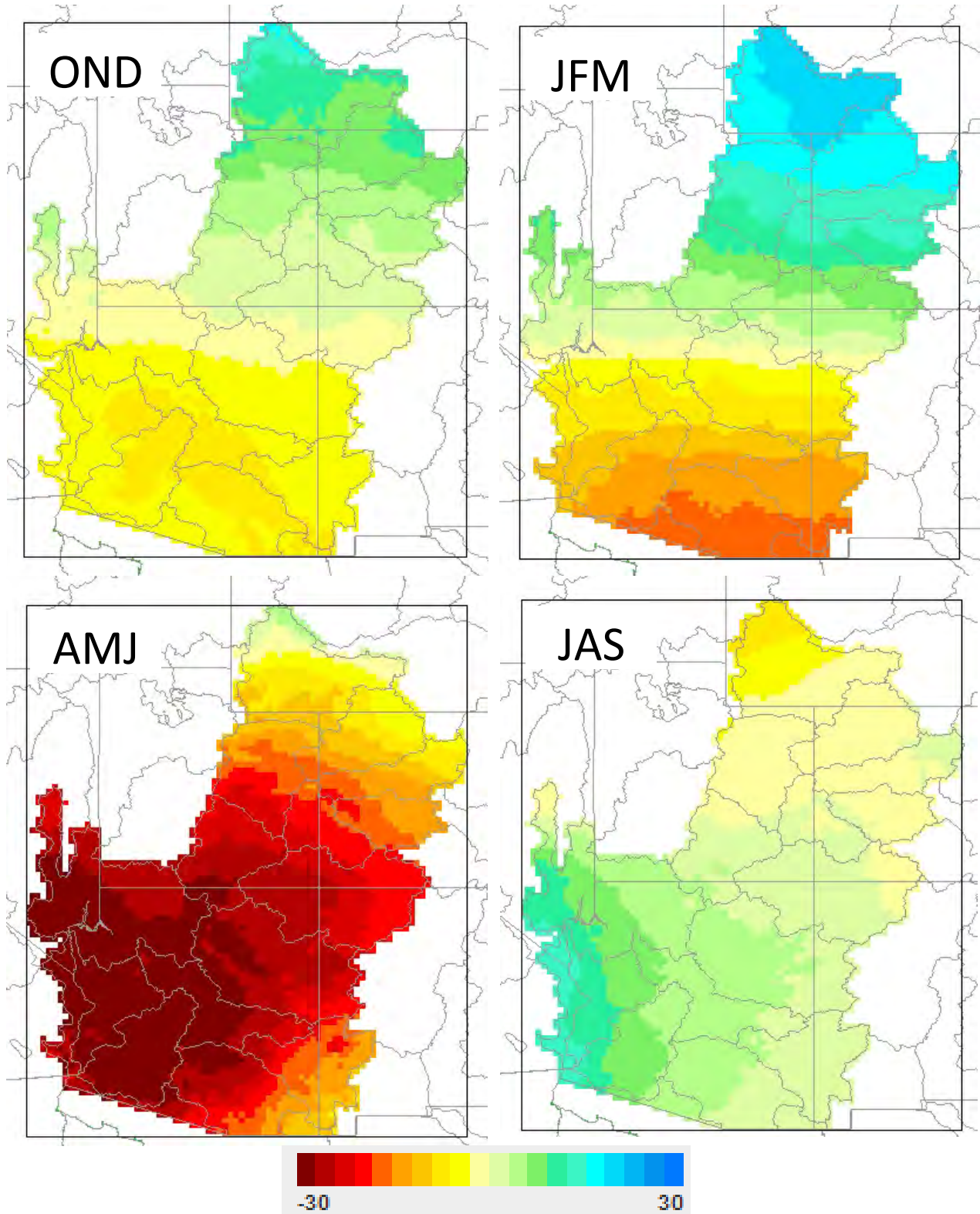


**FIGURE B6-19**  
Projected Change (°C) in Mean Seasonal Air Temperature  
2080 (2066–2095) versus 1985 (1971–2000).

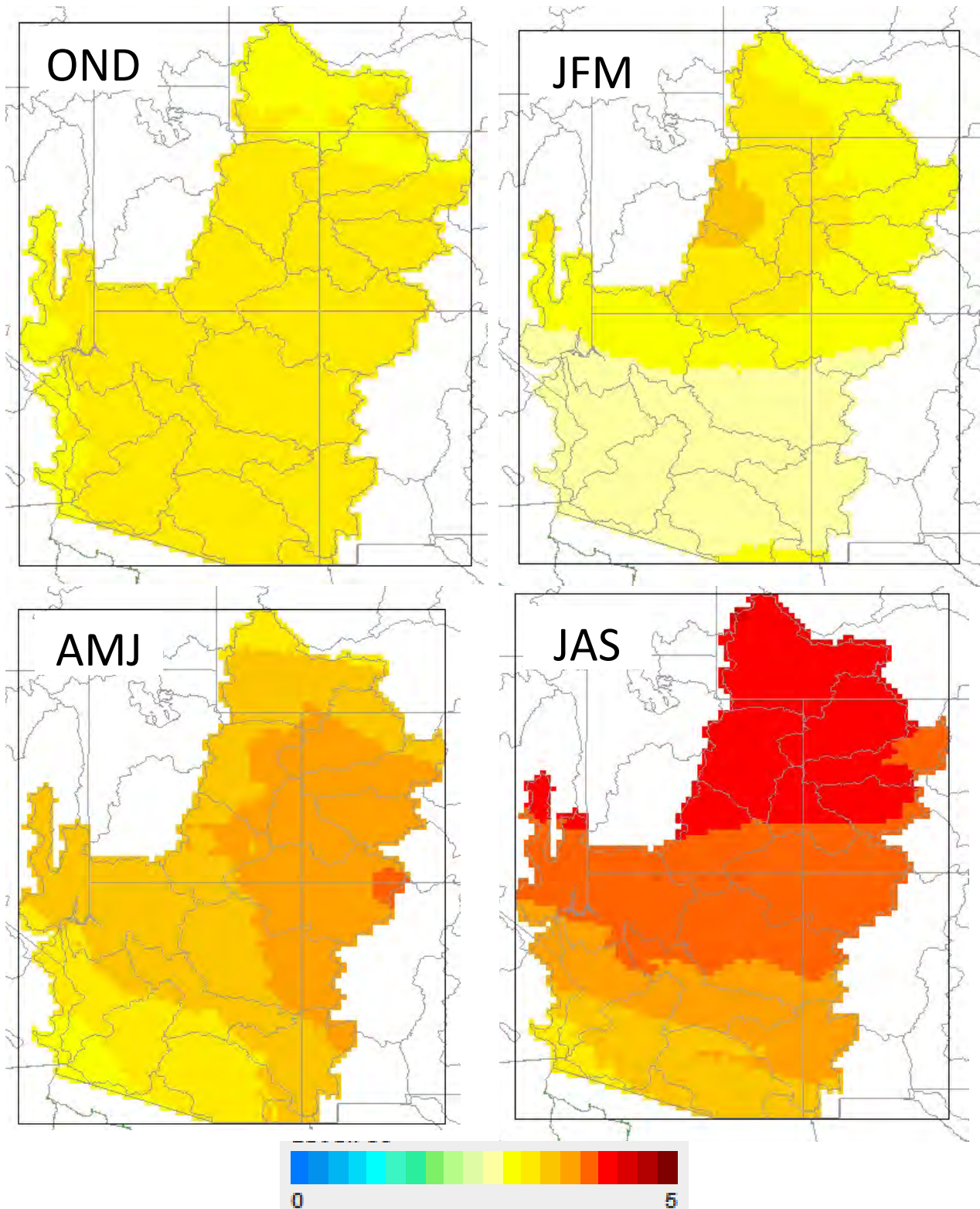


**FIGURE B6-20**  
 Projected Percent Change in Mean Seasonal Evapotranspiration  
 2080 (2066–2095) versus 1985 (1971–2000).

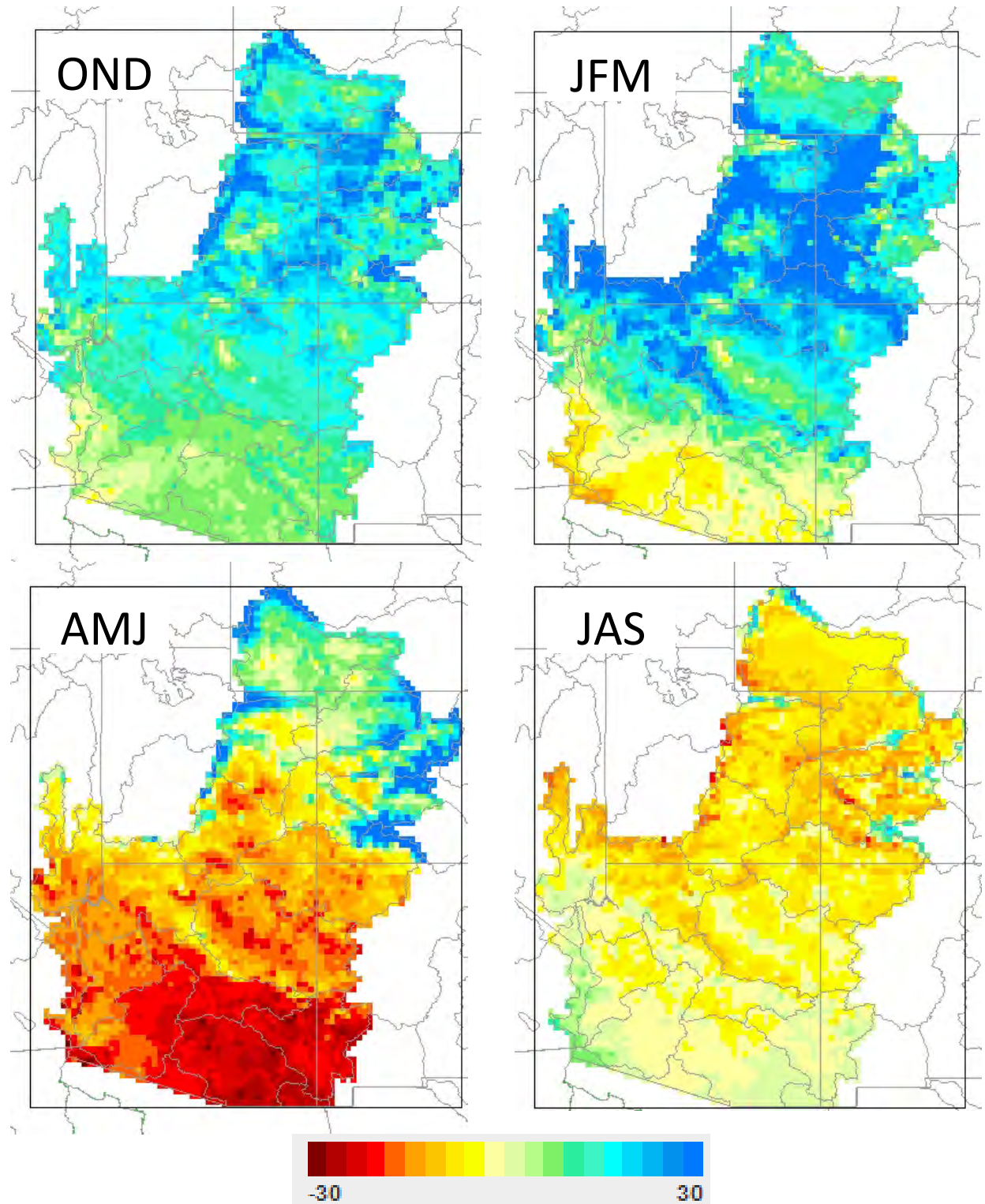


**FIGURE B6-21**  
Projected Percent Change in Mean Seasonal Runoff  
2080 (2066–2095) versus 1985 (1971–2000).

